In presenting the dissertation as a partial fulfillment of the requirements for an advanced degree from the Georgia Institute of Technology, I agree that the Library of the Institute shall make it available for inspection and circulation in accordance with its regulations governing materials of this type. I agree that permission to copy from, or to publish from, this dissertation may be granted by the professor under whose direction it was written, or, in his absence, by the Dean of the Graduate Division when such copying or publication is solely for scholarly purposes and does not involve potential financial gain. It is understood that any copying from, or publication of, this dissertation which involves potential financial gain will not be allowed without written permission.

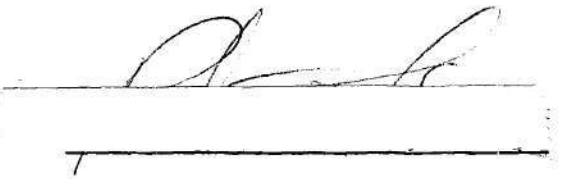

7/25/68

SIMULATED BOILING EFFECTS IN A SUBCRITICAL ASSEMBLY

A THESIS

Presented to

The Faculty of the Graduate Division

by

Robert John Lord, Jr.

In Partial Fulfillment

of the Requirements for the Degree

Doctor of Philosophy

in the School of Nuclear Engineering

Georgia Institute of Technology

March, 1972

SIMULATED BOILING EFFECTS IN A SUBCRITICAL ASSEMBLY

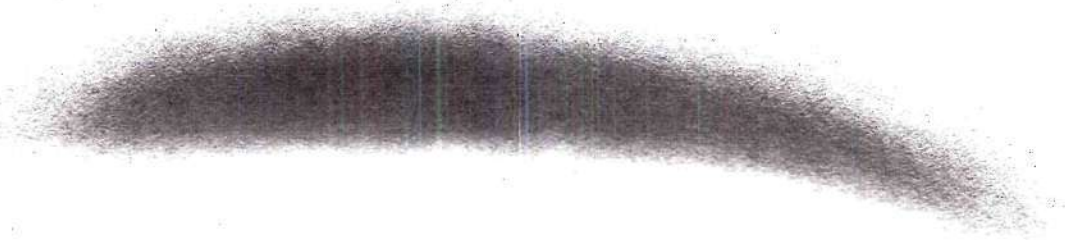

Approved:

Chairm

Date approved by Chairman: 2/25/72

ACKNOWLEDGMENTS

I wish to take this opportunity to acknowledge some of the many people who have helped make this thesis a reality. In particular, I would like to thank Dr. W. W. Graham, III, my thesis advisor, who suggested the topic and provided invaluable advice and generous assistance over the years of our association. Dr. J. D. Clement and Dr. G. G. Eichholz served on my reading committee and provided many helpful suggestions during the experimental, analytical, and writing stages of this work.

I am grateful to Dr. C. J. Roberts and the School of Nuclear Engineering for supporting this research and providing financial aid through Graduate Research Assistantships, National Science Foundation, and National Defense Education Act Traineeships.

I am indebted to Dr. W. R. Cobb for generously providing the THERMOS results. My good friend, Mr. C. W. Hodges, was instrumental in the development of the void generation system. Special thanks are due Mr. B. D. Statham of the School of Nuclear Engineering Electronics Shop for the designs of Appendix E and his assistance over the course of this work. Appreciation is extended to Mrs. Lydia Geeslin for editing and typing this thesis.

Finally, I wish to express my sincere appreciation to my parents and grandmother for their full support during the many years of my education.

TABLE OF CONTENTS

TABLE OF CONTENTS (Concluded)

LIST OF TABLES

LIST OF ILLUSTRATIONS

LIST OF ILLUSTRATIONS (Continued)

LIST OF ILLUSTRATIONS (Continued)

LIST OF ILLUSTRATIONS (Concluded)

SUMMARY

The objective of the research described in this dissertation was to predict and measure the effect of simulated boiling on the decay constants and associated lattice parameters of a heterogeneous light-water natural-uranium subcritical assembly. The ability to predict with accuracy the effect of voids on lattice parameters is vital in certain phases of safety analysis.

In order to accomplish the experimental objective the subcritical assembly was pulsed with a neutron generator and the thermal die-away spectrum was measured and analyzed with respect to the decay constant for several bucklings. Two cases were considered: dynamic voids simulating boiling in hot channels such as might result from coolant flow stoppage or excess heat production, and the non-voided case. Voids of 40, 50, and 60 percent central moderator displacement, consisting of bubbles of compressed air introduced into the central region of the assembly, were used.

The predictions were obtained through the use of the nuclear analysis programs THERMOS, TEMPEST II, FORM, and EXTERMINATOR-2. The cross section programs TEMPEST II and FORM required input parameters describing a homogenized assembly. This standard method was used to obtain one set of cross sections representative of the assembly. A second set of cross sections, which took into account to a limited extent the heterogeneity of the assembly, was derived from these same two programs. A third set of cross sections utilized THERMOS, which does not require homogenized

input. Three sets of lattice parameters and decay constants resulted from this study.

Finally, the experimental decay constants were compared to the three sets of analytical decay constants. A large thermal neutron spectrum cooling appeared for both the voided and non-voided cases. After taking this into account reasonable agreement between experiment and heterogeneous predictions was achieved.

CHAPTER I

INTRODUCTION

The first application of a pulsed neutron source to neutron research appears to have been made by Alvarez[1] in 1938. Since that time, pulsed sources have been used to study the dynamic behavior of neutrons for the purpose of measuring the reactivity of reactor systems, measuring reactor parameters, i.e., diffusion coefficient, age, absorption coefficient, infinite multiplication factor, and measuring neutron spectra by time-of-flight techniques. Extensive measurements have been made on both multiplying and non-multiplying media. Several excellent review articles[2-8] are available. For the research reported here, a pulsed source was used to investigate the effect of simulated boiling on the decay constants and associated lattice parameters of a light-water natural-uranium subcritical assembly.

Background

Multiplying Media

Numerous pulsed neutron studies have been undertaken to determine neutron diffusion parameters in multiplying media. This review will cover publications of interest since 1960.

Bach et al.[9] (1961) conducted pulsed neutron experiments in the far subcritical as well as critical region of bare and reflected multiplying hydrogenous media. The decay constants predicted by an equivalent

poison removal analytical method agreed to within ten percent of the measured values. In addition, the large diffusion cooling effect on the spectra of a small multiplying assembly was observed. Ghatak and Pearlstein[10] (1965) conducted an analysis of the pulsed neutron method in polyethylene and ^{235}U systems by numerically solving the time dependent Boltzmann equation. The time dependence of the reactor parameters was studied for both the space dependent and independent cases. Comparison with experiment was not attempted. Wells[11] (1966) measured the decay constants of reflected and bare uranium and light-water far-subcritical assemblies as a function of buckling. It was found that the decay constant is relatively insensitive to variations in buckling for a well-reflected assembly while quite sensitive for a bare assembly. In addition, the diffusion cooling effect was found to be appreciable.

Malaviya et al.[12] (1966) used the pulsed neutron technique to measure several lattice parameters of a heavy-water-moderated subcritical assembly. The agreement between the measured values of k_∞ and L^2 and those calculated by THERMOS was good. Judge and Daitch[13] (1966) used the variational method to reduce the energy-dependent Boltzmann equation to a few-group scheme, then investigated several time-dependent pulsed multiplying media problems. The measured and calculated decay constants resulting from this work agreed well. However, the bucklings used were estimated and it is pointed out that the calculated decay constants were extremely sensitive to the buckling. Bliss et al.[14] (1967) pulsed several heavy-water subcritical assemblies and compared the measured values of k_∞ to those obtained by poisoning experiments, the four factor formula, and

the two-group equation. The agreement between the four methods was quite good.

Flournoy[15] (1968) applied the pulsed neutron technique to a light-water-moderated enriched-uranium subcritical assembly. The water level was varied in order to measure the decay constant as a function of buckling. The measured diffusion parameters were in poor agreement with the predicted values as a result of large-buckling flat-geometry effects on the neutron background. Chow and Bierman[16] (1970) experimentally determined k_{eff} and deduced the neutron age to thermal for a homogeneous subcritical assembly. Good agreement was found with values predicted by two-group theory; age theory predictions were not good.

In summary, a variety of pulsed neutron experiments have been carried out on subcritical assemblies for the purposes of 1) providing lattice parameters for reactor design and 2) providing experimental parameter values against which theory may be checked. The agreement between experimentally determined lattice parameters and predictions appears mixed according to the particular parameters involved. It seems that k_{eff} can be accurately predicted, but the average neutron velocity in a pulsed neutron experiment is quite difficult to predict due to the effect of diffusion cooling. As will be subsequently developed in the current work, this difficulty is of central importance in relating calculated lattice parameters to measured decay constants in pulsed assemblies.

Voided Media

In gas-cooled reactors large cooling channels pass through the reactor core. Since these channels influence the neutron mobility in the core, research has been done on the effect of void passages on the diffusion

parameters of various media. Graves et al.[17] (1963) measured the effects of voided fuel rod housing tubes in a critical heavy-water natural-uranium oxide assembly on the axial migration area. The calculated results, based on Benoist's theory, agreed reasonably well with the measured values. Copic et al.[18] (1964) measured, using a pulsed source, the anisotropy of the diffusion parameters in Plexiglas with empty channels. The values of the anisotropic diffusion parameters were compared to the theory of Behrens with only moderate success. Utzinger et al.[19] (1965) measured the axial diffusion constants of heavy-water assemblies containing empty tubes. The experimental values of the diffusion constants were always smaller than the theoretical values.

Bennett[20] (1967) measured the effect of empty channels on the neutron diffusion coefficient in graphite using a combination of static and dynamic (pulsed neutron) techniques. The use of a static technique in void measurements tends to yield dubious results as steady state exponential experiments are susceptible to systematic errors due to direct streaming of the source neutrons along the channels, yielding too large a value for the diffusion length parallel to the channels. Page[21] (1967) used the pulsed neutron technique to determine the value of the radial diffusion coefficient of light water with constant void fraction. The radial dimensions were varied and the decay of the fundamental mode was measured to obtain the $\alpha_o(B^2)$ data. The experiment established that, for 1.3 inch diameter cylindrical voids on a 3.68 inch pitch in water, the diffusion coefficient for the radial direction was increased 25 percent above that for water alone. The theories of Leslie and Behrens predicted

21 and 51 percent increases, respectively. Khan and Kabir[22] (1968) pulsed a light-water assembly with cylindrical voids to determine the anisotropy of the diffusion coefficient. The experimental results were compared with predictions based on Benoist's theory and gave fair agreement.

Bull et al.[23] (1968) investigated the effect of cylindrical void channels on the anisotropy of the diffusion and diffusion cooling coefficients in graphite using a pulsed source. The experimental results for the diffusion coefficient were larger than those predicted by homogenizing the voids and were in good agreement with the analytical predictions of Benoist and Carter. Deniz et al.[24] (1968) studied lattices of graphite with empty channels by means of the pulsed neutron technique. The anisotropic diffusion coefficients and diffusion cooling coefficients were measured. In addition, the presence of air (instead of a vacuum) in the void channels was shown to be non-negligible for large channels in graphite. Kikuchi et al.[25] (1969) measured the effect of elongated void channels on the local flux distribution and neutron spectrum in a light-water critical assembly. It was found that the spatial variation of the neutron spectrum needed to be taken into account in order to predict thermal group constants for a given void volume fraction.

Again, as part of gas-cooled reactor development, theoretical work[26-31] has been done on the effect of voids on the diffusion parameters. The voids considered in this work were of the cooling channel type and the theory is probably not applicable to the situation in boiling water. However, a common conclusion is that the diffusion coefficient in a voided medium is larger than would be predicted by treating the void simply as a reduction in density of the medium.

Objective of This Research

The objective of the research described in this dissertation was to measure the effect of dynamic voids on the decay constants and associated lattice parameters of a heterogeneous light-water natural-uranium subcritical assembly using the pulsed neutron technique. The voids, bubbles of compressed air introduced into the central region of the assembly, simulated boiling in hot channels such as might result from coolant flow stoppage or excess heat production. In addition, the programs FORM, TEMPEST II, THERMOS, and EXTERMINATOR-2 were used to predict the measured effect. This served as a test of the applicability of these commonly used reactor design programs to the problem, with special attention given to whether the effect of boiling on the lattice parameters is adequately represented by the theory on which these programs are based.

CHAPTER II

THEORETICAL CONSIDERATIONS

During the course of this work, the decay constants of a light-water sample and of a light-water natural-uranium subcritical assembly were measured utilizing the pulsed neutron method. In this chapter, the pulsed neutron method, as applied to both multiplying and non-multiplying media, is discussed and two methods of obtaining diffusion parameters from decay constants are developed.

The Pulsed Neutron Method

The pulsed neutron method was applied in this work because of the good success it has produced in determining basic information about nuclear reactor systems. This technique is capable of providing accurate values of cross sections, diffusion coefficients, neutron ages, multiplication factors, and other lattice parameters. The pulsed neutron method incorporates a neutron generator, a thermal neutron detector, electronic analysis equipment, and the medium of interest. A burst of monoenergetic fast neutrons is injected into the medium and the time response of the thermal neutron detector at a given point in the medium is analyzed. Upon entering the medium the monoenergetic fast neutrons slow down, thermalize, and finally diffuse through the medium. After sufficient time, dependent on the thermalization properties of the medium, the diffusing neutrons achieve an equilibrium condition in both energy and space.

These neutrons continue to diffuse until they escape the medium through leakage or are absorbed. The time-dependent die-away of this equilibrium spectrum can be characterized by a single decaying exponential, referred to as the fundamental mode, whose decay constant is designated the fundamental decay constant, α_o.

The typical time response of a thermal neutron detector to a burst of fast neutrons is shown in Figure 1.[32] The transient region exists until space and energy equilibrium is achieved by the thermalizing neutrons. Depending on the source strength, the fundamental mode region will exist for one to two milliseconds for light-water. The neutron detector and analysis equipment should be capable of utilizing high count rates in order to process as much data as possible following a burst.

The neutron detector is normally connected to a preamplifier, an amplifier, and a multichannel analyzer operating as a multiscaler. The analyzer is triggered simultaneously with the neutron generator and records pulses from the detector over a preset time duration (typically 20 μsec for light-water), stores the number of pulses received during that time interval (channel) in the memory location associated with that channel, and repeats the count and store procedure until all analyzer channels have been used. The result is a series of channels, each containing a portion of the time spectrum. The pulsing procedure is repeated with successive burst results accumulated in the analyzer memory until sufficient (i.e., statistically sound) data are stored. A least squares fit of a single exponential to the data points in the fundamental mode region yields the fundamental decay constant. It is often difficult to determine the first and last channels of the fundamental mode region. To insure

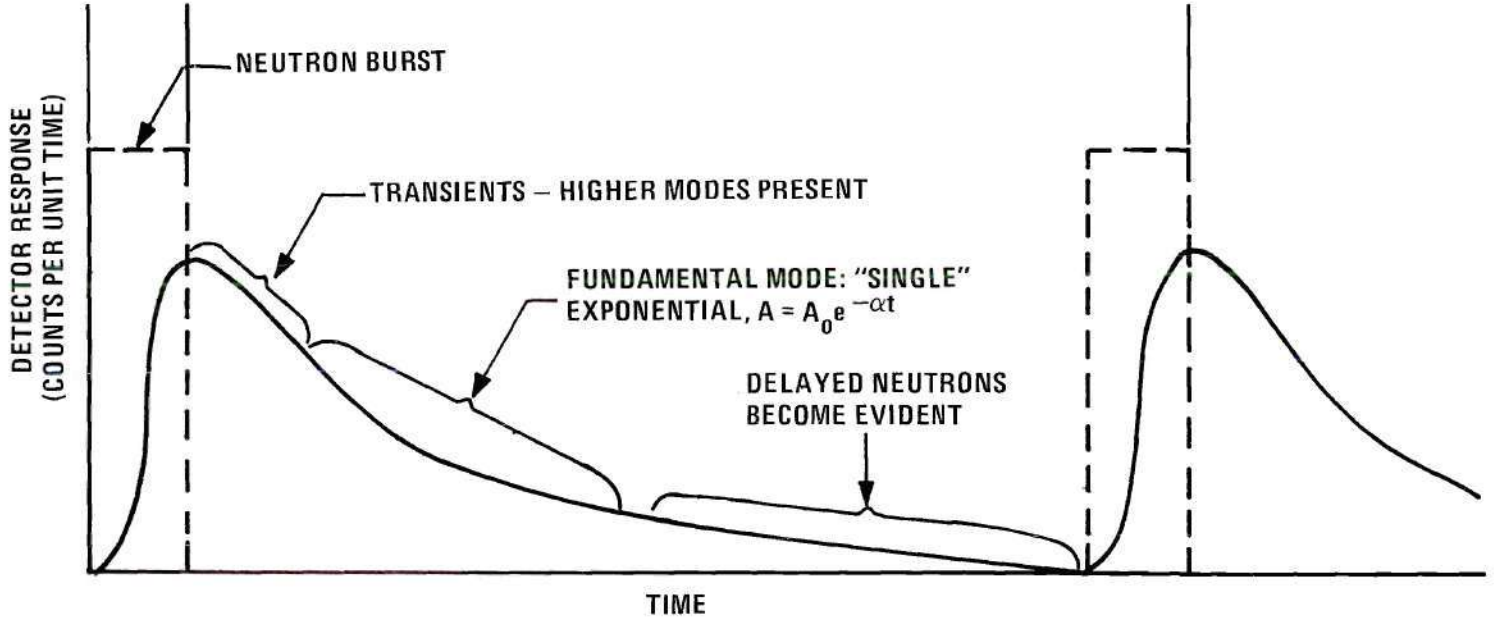

Figure 1. Time Dependent Response of a Detector to Neutron Die-Away in a Multiplying Medium.

that the fitted points are not in the transient or delayed neutron region of the curve, a least squares fit of a single exponential is made over what appears to be the fundamental mode region, then an endpoint is dropped and another fit made. This channel-dropping procedure continues until the fitted parameter α_o, the fundamental decay constant, becomes independent of the channels over which it is fit.

The total elapsed time required for a pulsed neutron experiment is determined by a combination of factors which include the nature of the materials to be pulsed, the characteristics of the detection system, and the performance specifications for the pulse generator itself. This latter factor was not insignificant in the present work, since the pulsing rate, neutron burst yield, and total available bursts for the sealed-tube generator probe are characteristically less than corresponding values obtainable from larger-scale machines.

Non-Multiplying Media

The relationship between the space-time dependent flux and the decay constant will first be discussed for a non-multiplying medium.

The simple one-group model commonly used to define the time dependent thermal neutron flux for a pulsed neutron experiment is

$$\overline{vD}\ \nabla^2\ \phi(\vec{r},t)\ -\ \overline{v\Sigma}_a\ \phi(\vec{r},t)\ =\ \frac{\partial\phi(\vec{r},t)}{\partial t} \qquad (1)$$

which is applicable after the burst (source = 0). In this equation

$\overline{v}$ = average neutron velocity

$\overline{D}$ = average diffusion coefficient

$\overline{\Sigma}_a$ = average macroscopic absorption coefficient

$\phi(\vec{r},t)$ = space and time-dependent neutron flux.

In addition, Appendix C demonstrates that

$$\overline{v\Sigma}_a = \overline{v} \cdot \overline{\Sigma}_a \tag{2}$$

$$\overline{vD} = \overline{v} \cdot \overline{D} \ . \tag{3}$$

Assuming space and time independence

$$\phi(\vec{r},t) = R(\vec{r}) \cdot T(t) \tag{4}$$

where $R(\vec{r})$ is the eigenfunction satisfying

$$\nabla^2 R_{lmn}(\vec{r}) + B^2_{lmn} \, R_{lmn}(\vec{r}) = 0 \ . \tag{5}$$

The time dependent solution becomes

$$\frac{1}{T_{lmn}(t)} \cdot \frac{dT_{lmn}}{dT} = - \, (\overline{vD} \, B^2_{lmn} + \overline{v\Sigma}_a) \tag{6}$$

or

$$T_{lmn}(t) = \exp \, [- \, (\overline{vD} \, B^2_{lmn} + \overline{v\Sigma}_a)t] \ . \tag{7}$$

Thus, the solution of equation (1) is

$$\phi(\vec{r},t) = \sum_{lmn} A_{lmn} \, R_{lmn}(\vec{r}) \, \exp \, [- \, (\overline{vD} \, B^2_{lmn} + \overline{v\Sigma}_a)t] \tag{8}$$

where $R_{lmn}(\vec{r})$ are the solutions of equation (5) and A_{lmn} are constants dependent on the boundary conditions. Often, the product $\overline{vD}$ is written as $\overline{D}_o$. The eigenvalue B^2_{lmn} is the geometrical buckling of the lmn^{th} mode and will range from a minimum value B^2_o to a maximum value at B^2_∞. The higher modes die away more rapidly than the lower ones until the B^2_o mode dominates. This is called the fundamental mode. The fundamental mode decay is then given by:

$$\phi(\vec{r},t) = A_{ooo}\, R_{ooo}(\vec{r})\, \exp\,(-\alpha_o t) \tag{9}$$

where the fundamental decay constant is:

$$\alpha_o(B^2) = \overline{v\Sigma}_a + \overline{D}_o\, B^2_{ooo}\ . \tag{10}$$

By measuring this decay constant α_o for several different moderator sizes or bucklings, $\overline{v\Sigma}_a$ can be determined along with $\overline{D}_o$ and neutron lifetime, $\ell = 1/\overline{v\Sigma}_a$. The diffusion length $L = \sqrt{\overline{D}_o/\overline{v\Sigma}_a}$ and transport mean free path $\lambda_{tr} = 3\overline{D}_o/\overline{v}$ can also be determined.

When experiments of this nature were performed, it was found that the $\alpha_o(B^2)$ vs. B^2 plots for small systems were not linear as equation (10) predicts. This is shown in Figure 2.[33] For small systems the asymptotic decay constant becomes:

$$\alpha_o(B^2) = \overline{v\Sigma}_a + \overline{D}_o\, B^2 - C\, B^4 + \ldots \tag{11}$$

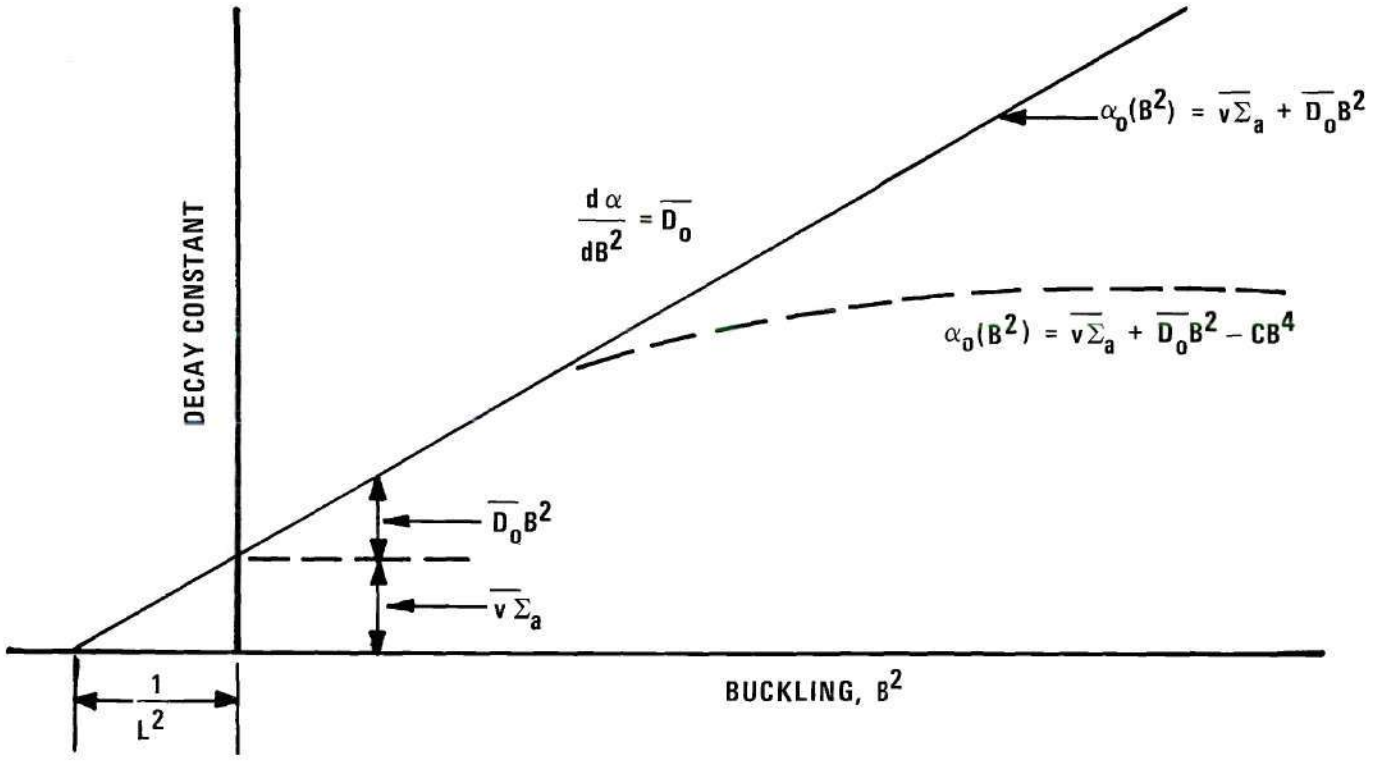

Figure 2. Decay Constant as a Function of Buckling for a Non-Multiplying Medium.

with more terms required for smaller systems. The term C is usually called the diffusion cooling coefficient and allows for the preferential leakage of high energy neutrons. It corrects for the neutron energy spectrum not being a thermalized Maxwellian during the entire asymptotic time decay period. However, with the application of transport theory, C is found to be the sum of C_D and C_T where C_D is the diffusion cooling coefficient and C_T is the purely transport theoretical correction to the results of elementary diffusion theory.[34] The majority of pulsed neutron experiments have been based on equation (11) with values of the three parameters $\overline{v\Sigma}_a$, $\overline{D}_o$, and C being obtained by least-squares fitting to the observed α_o-variation as a function of buckling.[35]

Transport theory also predicts a maximum buckling beyond which asymptotic decay is no longer possible. The one dimensional transport equation in a source-free isotropically scattering medium in plane geometry is[36]:

$$\frac{1}{v}\frac{\partial F(E,u,x,t)}{\partial t} = -\Sigma_t(E)\cdot F - u\frac{\partial F}{\partial x} \qquad (12)$$

$$+\frac{1}{2}\int_0^{\infty}\int_{-1}^{+1}\Sigma_s(E'\rightarrow E)F(E',u',x,t)\,dE'du'$$

where F is the vector flux. Using separation of variables:

$$F(E,u,x,t) = F(E,u,x)\exp(-\alpha t) \qquad (13)$$

and substituting this into equation (12):

$$\left(\Sigma_t(E) - \frac{\alpha}{v}\right)F(E,u,x) = u\,\frac{\partial F}{\partial x} + \frac{1}{2}\int_0^{\infty}\int_{-1}^{+1}\Sigma_s(E'\rightarrow E)F(E',u',x)\,dE'du' \quad . \quad (14)$$

$F(E,u,x)$ is always ≥ 0, as is the inscattering integral $\int\int\Sigma_s(E'\rightarrow E)F(E',u',x)\,dE'du'$. For space independence, $\partial F/\partial x = 0$, and thus:

$$\Sigma_t(E) - \frac{\alpha}{v} \geq 0 \qquad (15)$$

or

$$\alpha \leq v\Sigma_t(E)_{min} \qquad (16)$$

for an asymptotic decay. This also means that there exists a maximum value of B^2, denoted B^2_{max}, such that for all $B^2 > B^2_{max}$ there is no asymptotic decay, i.e., no discrete eigenvalues.

A physical explanation for this is that leakage tends to distort the energy spectrum due to preferential leakage of higher energy neutrons while collisions tend to reestablish the energy spectrum. The equilibrium energy spectrum exists when the leakage and energy transfer rates are equal. The neutron collision rate is $v\Sigma_t(E)$. If an assembly has a $B^2 > B^2_{max}$ the leakage rate becomes greater than the energy transfer rate (limited by $v\Sigma_t(E)_{min}$), the energy spectrum becomes time dependent, and a discrete decay constant is never established.[37] As a result, to obtain the neutron transport parameters by the pulsed neutron method, the B^2 of the assembly must be less than B^2_{max}.

Multiplying Media

The equation governing the time decay of the fundamental mode in a multiplying assembly is identical with that for the non-multiplying assem-

bly except that an additional term appears to represent the effects due to neutrons produced in the fissile material. The equation governing the thermal die-away is[38] (see Appendix D)

$$\alpha_o(B^2) = \overline{v\Sigma}_a^M + \bar{D}_o B^2 + \overline{v\Sigma}_a^F \left[1 - (1-\bar{\beta})\eta\epsilon p_{th} L_f\right] . \tag{17}$$

The representative $\alpha_o(B^2)$ vs. B^2 plot is shown in Figure 3.[39] From Figure 3, the critical size of the assembly can be predicted by determining where $\alpha_o(B^2) = 0$; this means that the time-dependent part of the solution to the space-time equation is unity. In addition, the diffusion coefficient and the absorption cross section of the fuel-moderator mixture can be determined by letting $B^2 \to \infty$ and then

$$\alpha_o(B^2) \cong \overline{v\Sigma}_a^T + \bar{D}_o B^2 . \tag{18}$$

It we set

$$f = \frac{\overline{\Sigma}_a^F}{\overline{\Sigma}_a^T} \tag{19}$$

$$k_\infty = \eta\epsilon f p_{th} \tag{20}$$

$$L_f = \exp(-B^2\tau) \tag{21}$$

$$\overline{\Sigma}_a^T = \overline{\Sigma}_a^F + \overline{\Sigma}_a^M \tag{22}$$

equation (17) becomes

$$\alpha_o(B^2) = \overline{v\Sigma}_a^T + \bar{D}_o B^2 + \overline{v\Sigma}_a^T (1-\bar{\beta}) k_\infty \exp(-B^2\tau) . \tag{23}$$

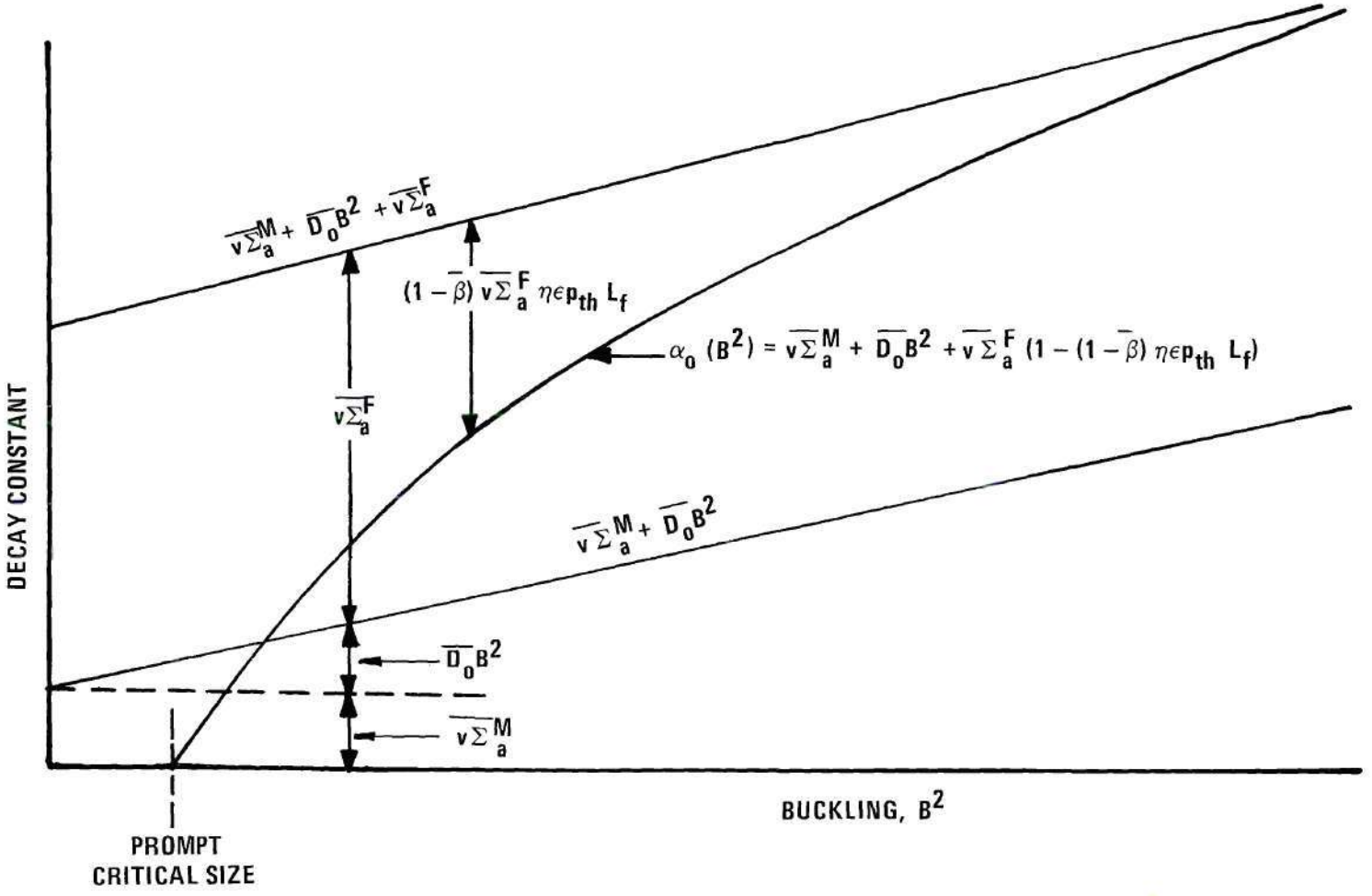

Figure 3. Decay Constant as a Function of Buckling for a Multiplying Medium.

For the general case, B^2 and α are energy- and space-mode dependent.

Time Scale

To determine the lattice parameters of a given assembly, α_o can be measured as a function of the assembly buckling, B^2, by inserting a neutron transient into the system and observing the thermal neutron die-away. In order to assemble such an experiment, a pulsable neutron source and a detector capable of responding in a sufficiently sensitive fashion and rapidly enough to reproduce the die-away conditions are needed. In addition, an analyzer is required that can record counts in various channels representing short, even time intervals after pulse insertion. To select such a system we need an estimate of the die-away time and the number and width of the analyzer channels.

The die-away of thermal neutrons in a sample is dependent on its size and composition. As an example of the time involved, the results of a laboratory report from Argonne National Laboratory, ANL-6990,[40] will be quoted. For a cubical assembly of light water 9 x 9 x 9 inches, the fundamental decay constant was measured as $\alpha = 6500\ \text{sec}^{-1}$. In our research, due to the low source strength of the neutron generator used, the fundamental mode was observable for about one decade of decay before the background interfered. For the light-water cube, the time required to follow the fundamental decay for one decade is $\ln(10)/\alpha$, 354 microseconds in the example given. This is a relatively short time and presents the problem of how wide (in time) to make the analyzer channels. Channels too wide yield few time points, making it difficult to accurately fit the single exponential to the data; channels too narrow yield few counts in each channel, thus, poor statistical accuracy.

Harmonic Analysis

It is desirable to make the time interval over which useful data are collected as large as possible. One technique of increasing this interval would be to extract data from the transient region. Lopez and Beyster[41] did this using water as the medium. It is the method used in this thesis to analyze the data of the light-water test case.

This data collection and reduction method is based on a Fourier analysis of the time-dependent spatial distribution of the thermalized neutrons. Using one-group diffusion theory, the neutron distribution is

$$\bar{D}\ \nabla^2\ \phi(\vec{r},t)\ -\ \bar{\Sigma}_a\ \phi(\vec{r},t)\ =\ \frac{1}{\bar{v}}\ \frac{\partial\phi(\vec{r},t)}{\partial t} \tag{24}$$

which has

$$\phi(x,y,z,t)\ =\ \sum_{lmn} A_{lmn}(0)\ R_{lmn}(x,y,z)\ \exp\ [-\ (\overline{v\Sigma}_a\ +\ \bar{D}_o\ B^2_{lmn})t] \tag{25}$$

as a general solution. $R_{lmn}(x,y,z)$ and B_{lmn} are, respectively, the eigenfunctions and eigenvalues of the Helmholtz equation:

$$\nabla^2 R\ +\ B^2 R\ =\ 0 \tag{26}$$

with the boundary conditions that the $R_{lmn}(x,y,z)$ are zero at the extrapolated boundaries of the medium.

For a rectangular geometry of dimensions a x b x c:

$$R_{lmn}(x,y,z)\ =\ \cos\ \frac{\ell\pi x}{a+2\epsilon}\ \cdot\ \cos\ \frac{m\pi y}{b+2\epsilon}\ \cdot\ \sin\ \frac{n\pi z}{c+2\epsilon} \tag{27}$$

where the origin of the coordinate system is at the center of one end of the rectangle. B^2_{lmn} is defined as:

$$B^2_{lmn} = \left(\frac{\ell\pi}{a+2\epsilon}\right)^2 + \left(\frac{m\pi}{b+2\epsilon}\right)^2 + \left(\frac{n\pi}{c+2\epsilon}\right)^2 \tag{28}$$

where ϵ is the extrapolated end point. The coefficients $A_{lmn}(0)$ of the various terms of equation (25) depend on the initial distribution of thermalized neutrons.

If the source position is such that the lateral incident flux has nearly a cosine distribution, the fundamental mode in the x-y plane will quickly be attained while the axial mode will still be rich in harmonics. In addition, if the detectors are situated along the z axis at x = y = 0, we have

$$B^2_{11n} = \left(\frac{\pi}{a+2\epsilon}\right)^2 + \left(\frac{\pi}{b+2\epsilon}\right)^2 + \left(\frac{n\pi}{c+2\epsilon}\right)^2 \tag{29}$$

$$R_{11n}(0,0,z) = \sin\left(\frac{n\pi z}{c+2\epsilon}\right) \tag{30}$$

$$\phi(0,0,z,t) = \sum_n^{\infty} A_{11n}(0) \sin\left(\frac{n\pi z}{c+2\epsilon}\right) \exp(-\alpha_n t) \tag{31}$$

where $\alpha_n = \overline{v\Sigma}_a + \overline{D}_o B^2_{11n}$. (32)

Substituting

$$b_n(t) = A_n(0)\exp(-\alpha_n t) \tag{33}$$

equation (31) becomes:

$$\phi(0,0,z,t) = \sum_{n}^{\infty} b_n(t) \sin\left(\frac{n\pi z}{c+2\epsilon}\right) \tag{34}$$

which is a Fourier sine series.

If, for example, we use four detectors along the z axis and multichannel analyze the time spectrum, equation (34) would become (for any time t_i):

$$\phi(z_1,t_i) = b_1(t_i) \sin\left(\frac{\pi z_1}{c+2\epsilon}\right) + b_2(t_i) \sin\left(\frac{2\pi z_1}{c+2\epsilon}\right) + \tag{35}$$

$$b_3(t_i) \sin\left(\frac{3\pi z_1}{c+2\epsilon}\right) + b_4(t_i) \sin\left(\frac{4\pi z_1}{c+2\epsilon}\right)$$

$$\phi(z_2,t_i) = b_1(t_i) \sin\left(\frac{\pi z_2}{c+2\epsilon}\right) + b_2(t_i) \sin\left(\frac{2\pi z_2}{c+2\epsilon}\right) + \tag{36}$$

$$b_3(t_i) \sin\left(\frac{3\pi z_2}{c+2\epsilon}\right) + b_4(t_i) \sin\left(\frac{4\pi z_2}{c+2\epsilon}\right)$$

$$\phi(z_3,t_i) = b_1(t_i) \sin\left(\frac{\pi z_3}{c+2\epsilon}\right) + b_2(t_i) \sin\left(\frac{2\pi z_3}{c+2\epsilon}\right) + \tag{37}$$

$$b_3(t_i) \sin\left(\frac{3\pi z_3}{c+2\epsilon}\right) + b_4(t_i) \sin\left(\frac{4\pi z_3}{c+2\epsilon}\right)$$

$$\phi(z_4,t_i) = b_1(t_i) \sin\left(\frac{\pi z_4}{c+2\epsilon}\right) + b_2(t_i) \sin\left(\frac{2\pi z_4}{c+2\epsilon}\right) + \tag{38}$$

$$b_3(t_i) \sin\left(\frac{3\pi z_4}{c+2\epsilon}\right) + b_4(t_i) \sin\left(\frac{4\pi z_4}{c+2\epsilon}\right) .$$

We have four simultaneous equations with four unknowns: $b_n(t_i)$. If we solve for the b_n terms for several different t_i, we can determine α_n by

differentiating $b_n(t_i)$, equation (33), with respect to time:

$$\alpha_n = - \frac{d}{dt} \ln [b_n(t_i)] . \tag{39}$$

For this case we would get α_1, α_2, α_3, and α_4. These four decay constants could be plotted against the B_n^2 and would produce the standard $\alpha(B^2)$ vs. B^2 curve. Thus, one experiment using the analysis of transient time data yields as much information as several of the classical type experiments where the physical dimensions of the assembly were changed for each α_o measurement. This, however, assumes that sufficient experimental equipment is available to run several detection channels simultaneously.

In conclusion, the pulsed neutron method is seen to be a technique whereby diffusion and lattice parameters may be experimentally determined. Two basic methods are used to obtain the parameters of interest:

1. vary the geometry of the system, and
2. Fourier analyze the decay of a fixed geometry system.

CHAPTER III

INSTRUMENTATION AND EQUIPMENT

This chapter describes the subcritical assembly, which was used as the multiplying medium in this work, the void generation system employed to simulate boiling, the pulse-producing neutron generator, and the composition and operation of the detection and data recording instrumentation.

The Subcritical Assembly

The light-water-moderated natural-uranium subcritical assembly used in this research was located in the School of Nuclear Engineering at the Georgia Institute of Technology. A triangular lattice consisting of 137 fuel rods on a 1.70 inch spacing was used to create a core with variable height. A cadmium box, 19.14 X 18.70 X 33.50 inches, centered within the water tank defined the four side and bottom boundaries. Each fuel rod consisted of an aluminum tube sealed at one end in which 8 3/8-inch long, 1 inch diameter natural-uranium fuel slugs could be loaded end-to-end. The core height was determined by the number of fuel slugs in the fuel rod and the height of the moderator level in the water tank. Figure 4 shows a vertical cross-section of the subcritical assembly. The neutron generator positioning tube allowed the target to lie along the vertical center line of the core, eight inches below the cadmium box. The purpose of the Styrofoam block was to displace water, thus minimizing

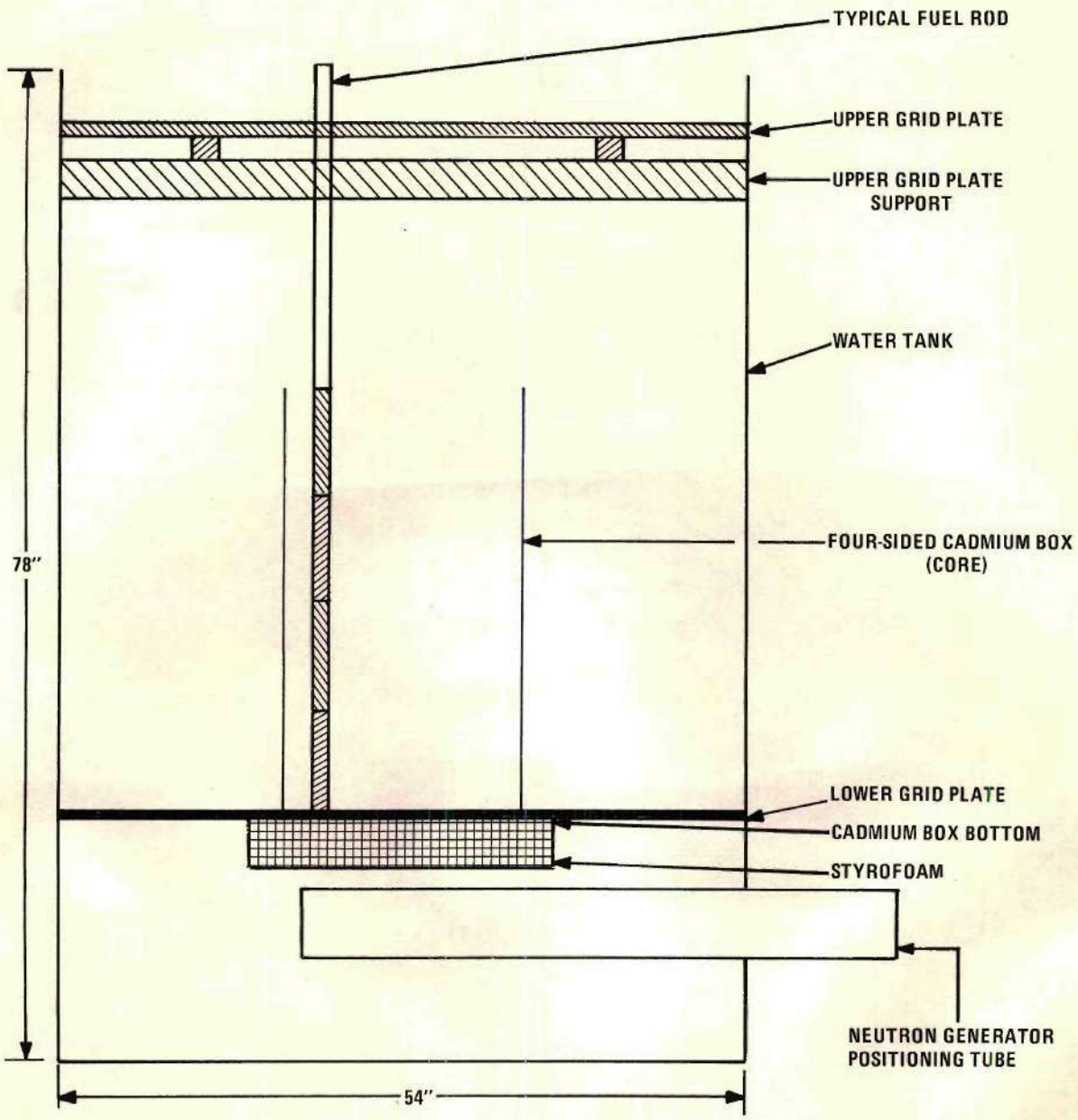

Figure 4. Vertical Section of the Subcritical Assembly.

the attenuation of fast neutrons from the neutron generator. The fuel rods passed through holes in the upper grid plate and fitted into holes in the lower grid plate, thereby assuring the exact positioning of the fuel. Figure 5 is a side view of the subcritical assembly with the neutron generator positioning tube at the bottom center. The water surrounding the four sides and bottom of the core serves as a shield from room return neutrons. The ceiling of the room housing this assembly is approximately twenty-four feet high, minimizing the effect of room return neutrons from above. McDaniel and Elliott[42] have given a detailed description of this assembly.

The Void Generation System

The void generation system consisted of the building compressed air supply, a flow meter, a plenum, gas hoses, valves, and 22 modified fuel tubes. Its purpose was to provide bubbles to simulate large scale boiling involving 22 central fuel elements. Compressed air at 20 psig flowed through a control valve, through a 1 1/4 inch I. D. rubber hose, past a fine control valve, and into a Fischer and Porter Co. Model 10 A 1027A flow meter. The flow meter could measure flow rates up to 11.1 scfm. From the flow meter the compressed air entered a plenum which distributed the gas through 3/8 inch I. D. Tygon tubes to 22 fuel elements, each stoppered at the top and with four equally-spaced 1/4 inch holes drilled around the tube one inch from the bottom. The compressed air entered the fuel tubes at the top, flowed downward between the fuel slugs and the tube walls and exited into the water through the 1/4 inch holes. The resulting bubbles then rose, creating a dynamic void. Figure 6 shows the air hose,

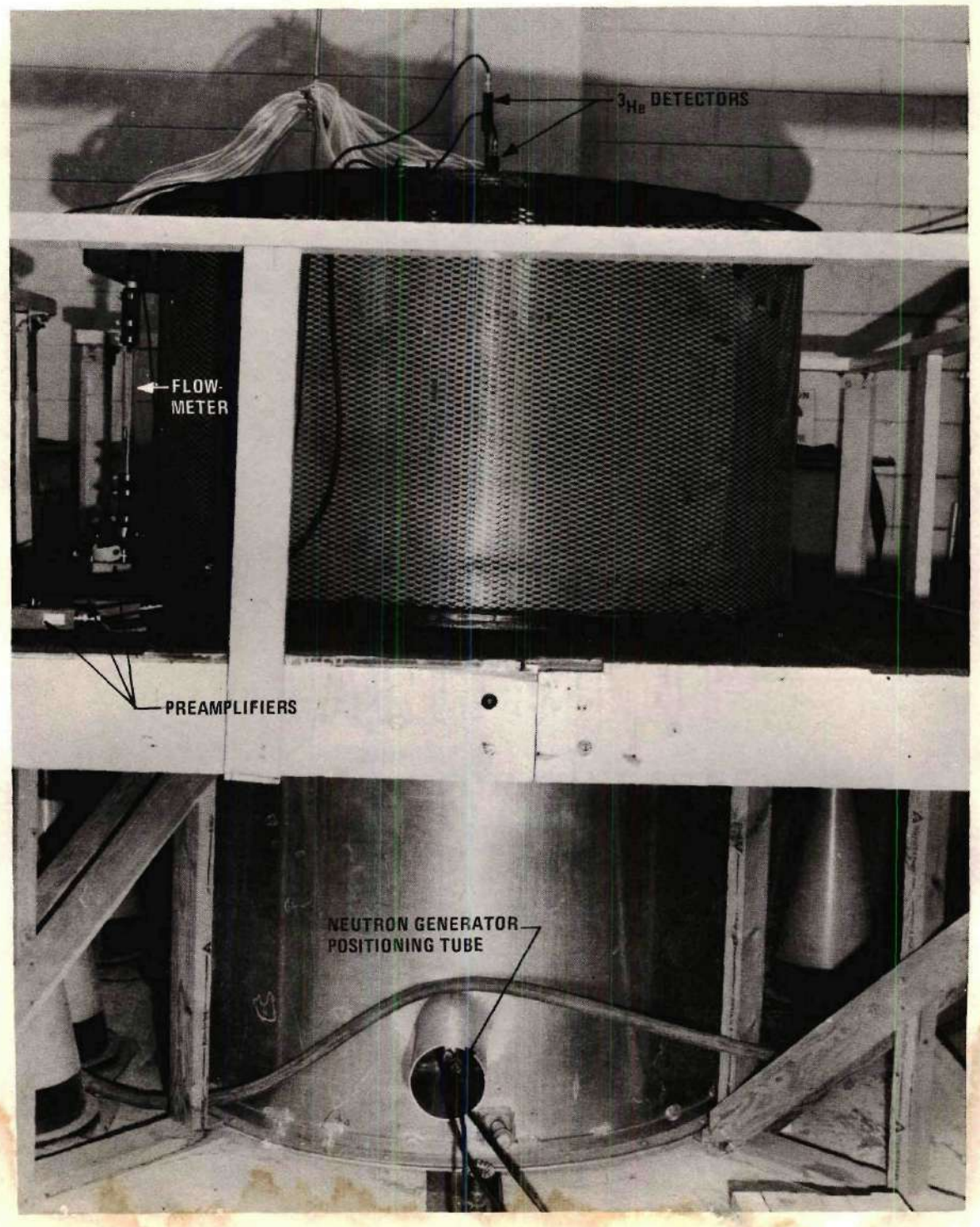

Figure 5. Side View of the Subcritical Assembly.

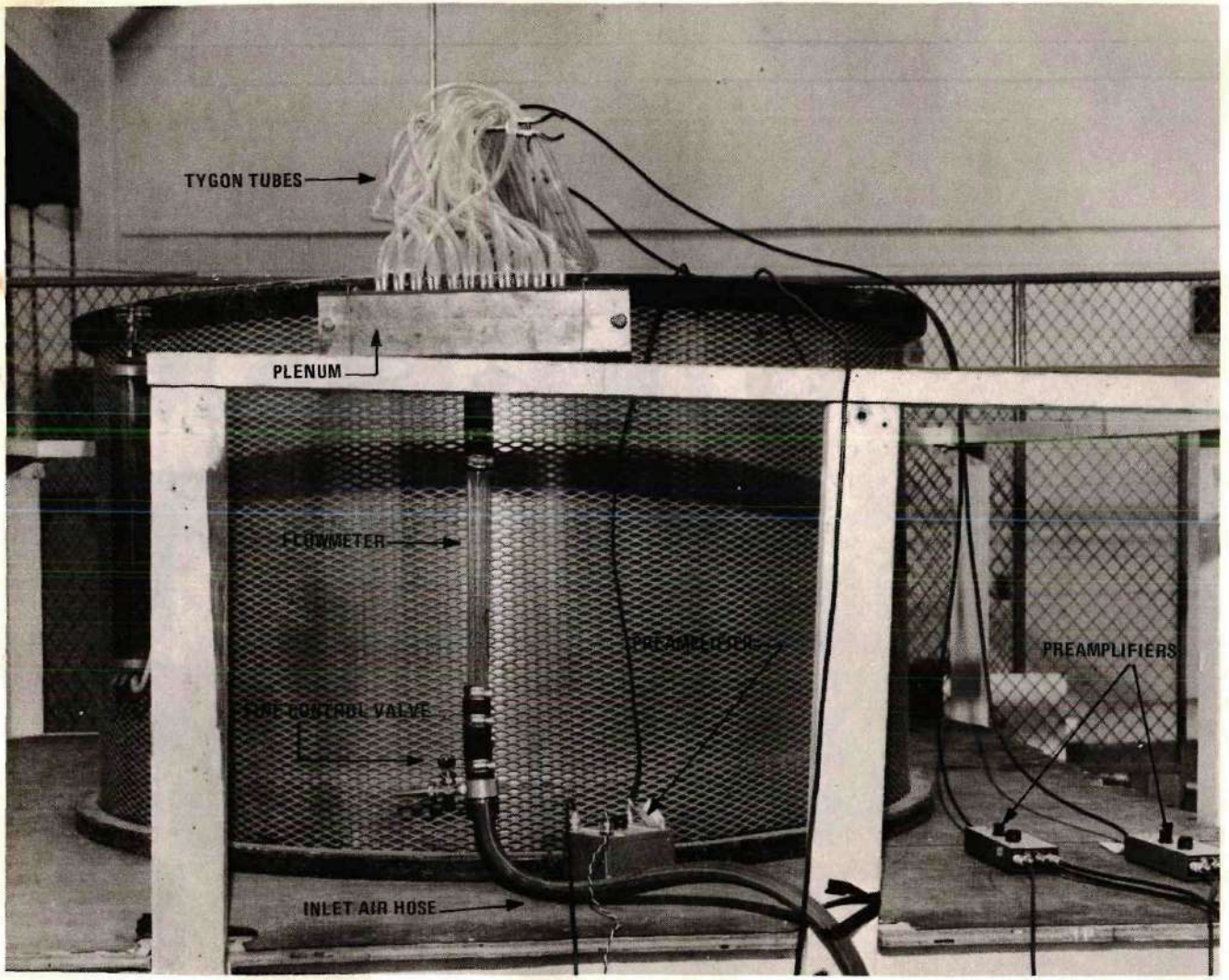

Figure 6. Void Generation System.

fine control valve, flow meter, and plenum. Figure 7 shows the top of the subcritical assembly with the void distribution system in place.

The Neutron Generator

A Kaman Nuclear Model A-800 neutron generator provided the neutrons for this research. The generator consisted of two separate units, pictured in Figure 8. The accelerator unit, on the left, contained the basic neutron generating equipment. The console unit, on the right, contained all the instrumentation and controls necessary for the remote operation of the accelerator unit. During use the two units were connected by 30-foot electrical cables. Only neutron pulses of 2.5 μs half-width were available from this generator. Pulsing was accomplished by applying a high voltage pulse to the anode of the ion source. No continuous mode of operation existed. The life expectancy of the accelerator unit was 200,000 pulses.

Within the accelerator unit during a pulse, deuterium ions were accelerated through a 120 kV potential into a tritium-impregnated titanium target. The resulting $H^3(d,n)He^4$ reaction produced 14.3 MeV neutrons with a yield of 6.6×10^7 neutrons per pulse. The pulse rate for extended pulsing operations of more than a few minutes was externally adjustable up to 5 pulses per second; short-term rates up to 10 pulses per second are possible.

Detection and Data Recording System

The detection and data recording system was assembled according to Figures 9 and 10. This system is actually composed of two subsystems, the

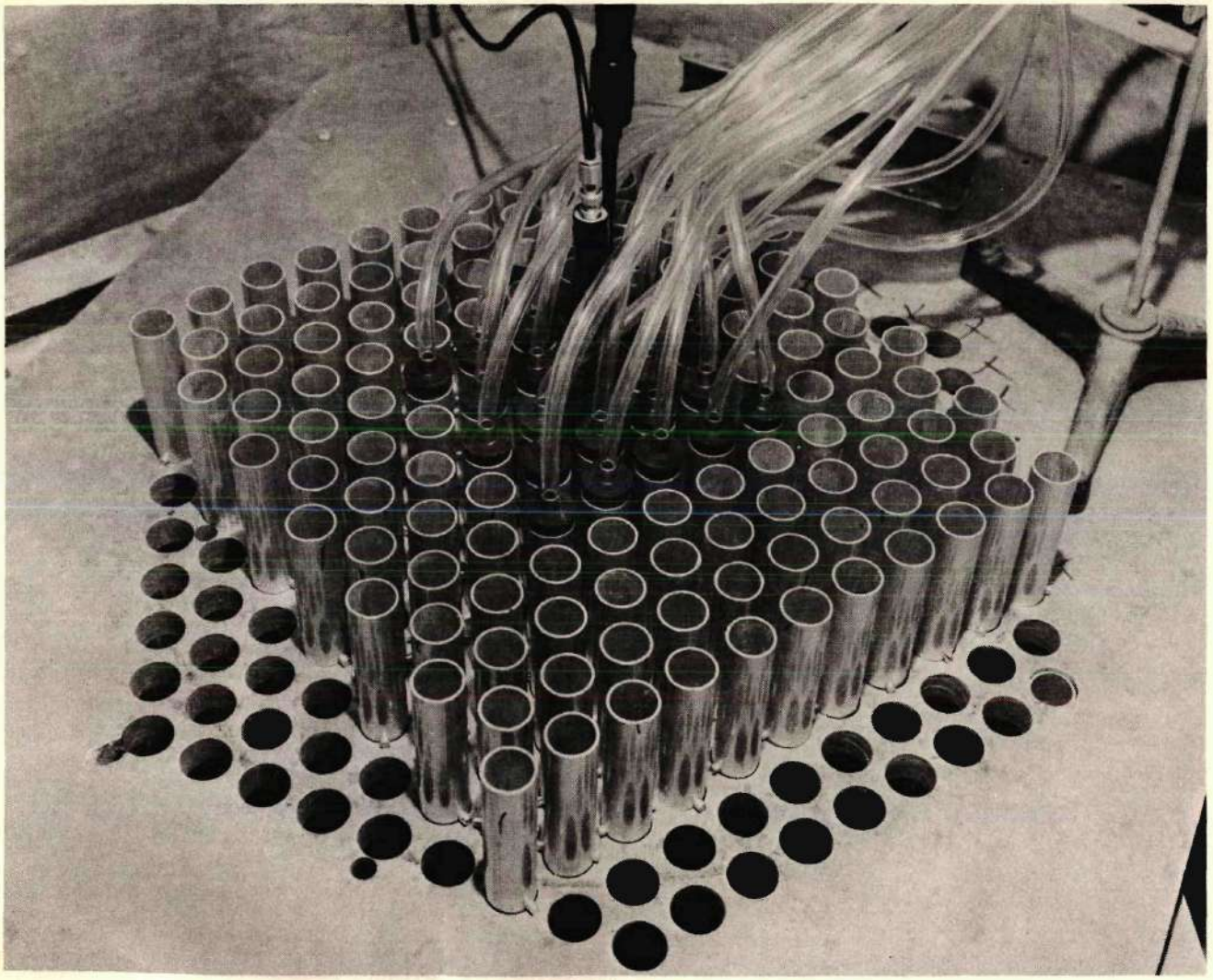

Figure 7. Top View of the Subcritical Assembly With Void Generation System and Detectors in Place.

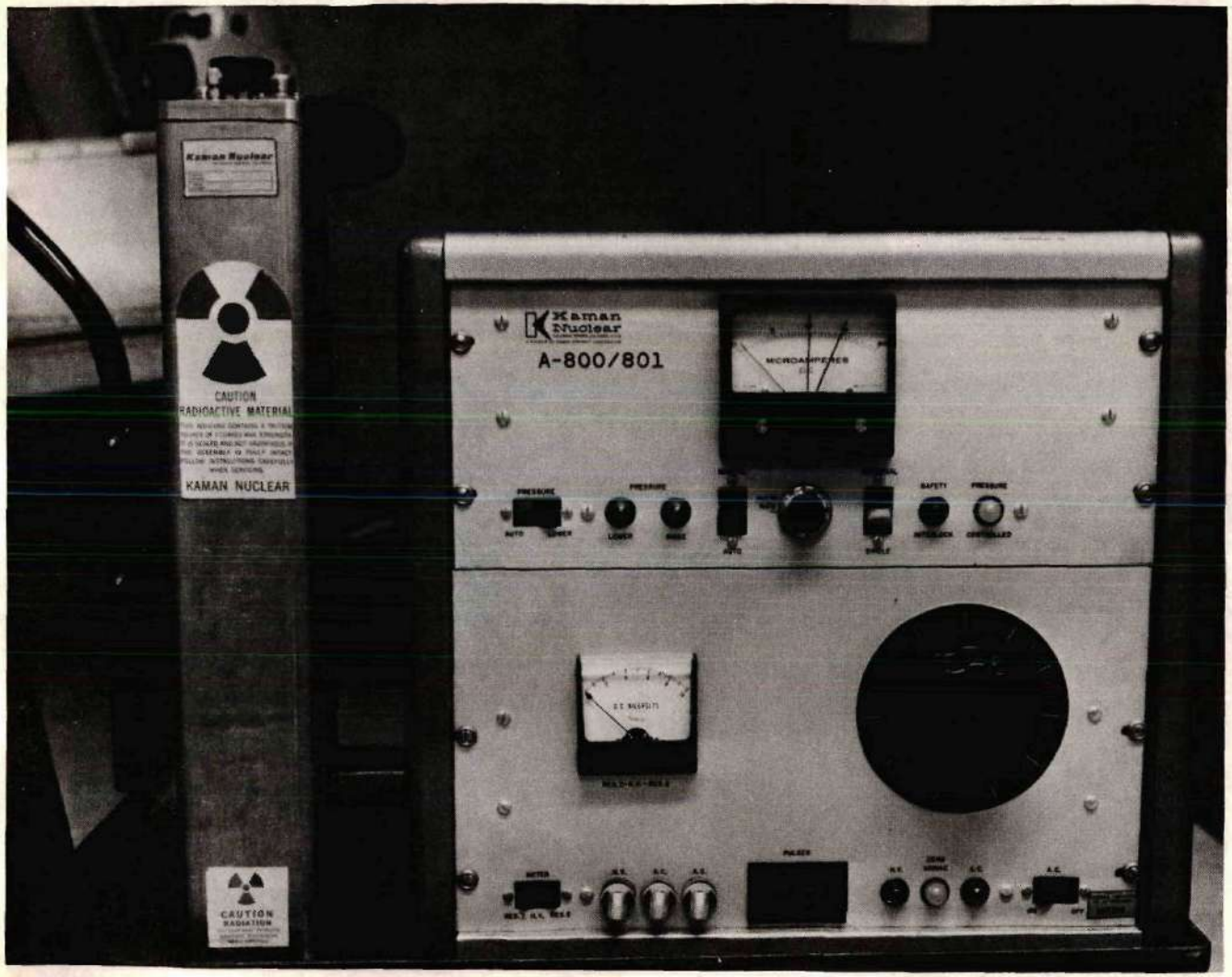

Figure 8. Neutron Generator Accelerator Unit and Console.

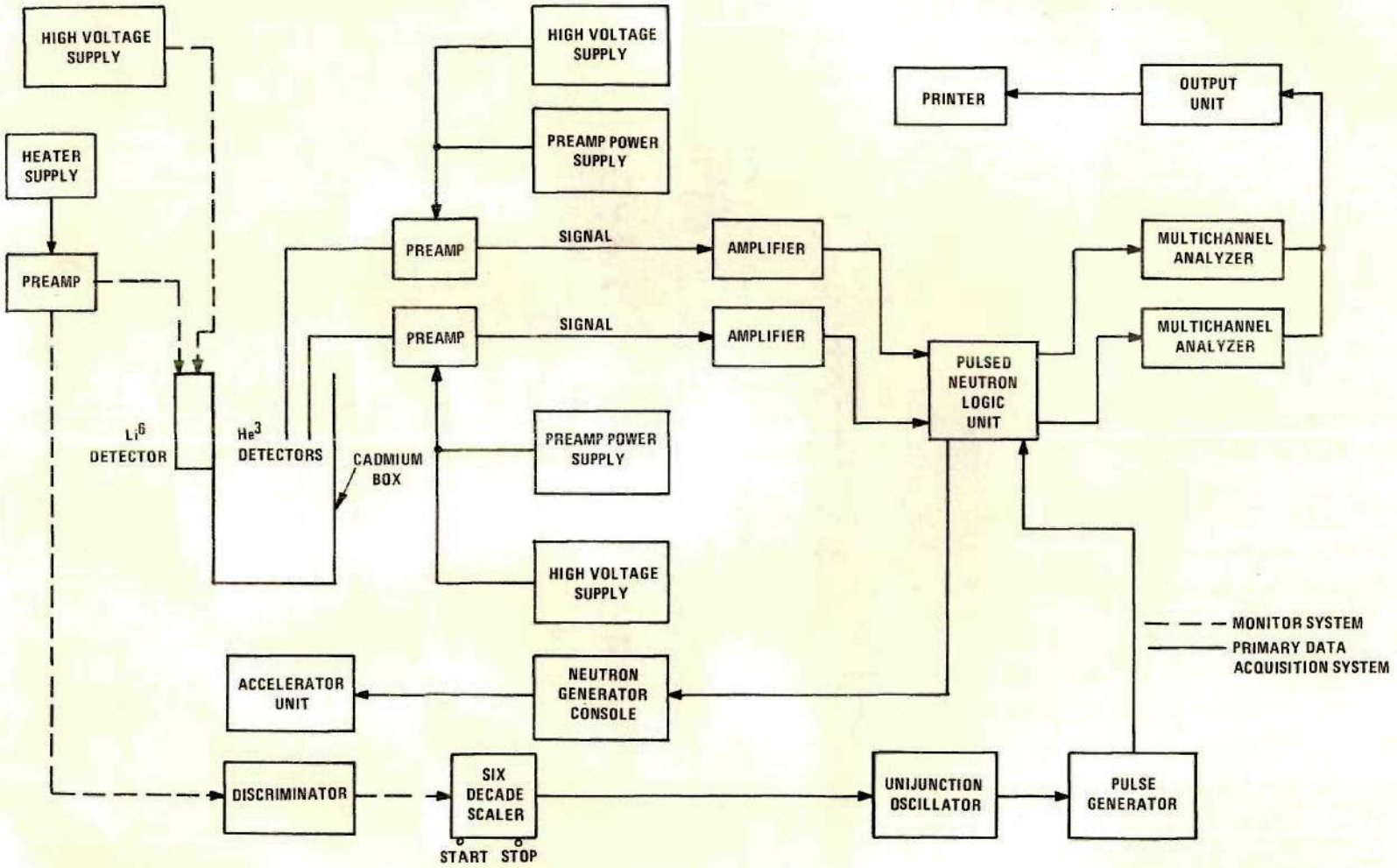

Figure 9. Block Diagram of the Detection and Data Recording System.

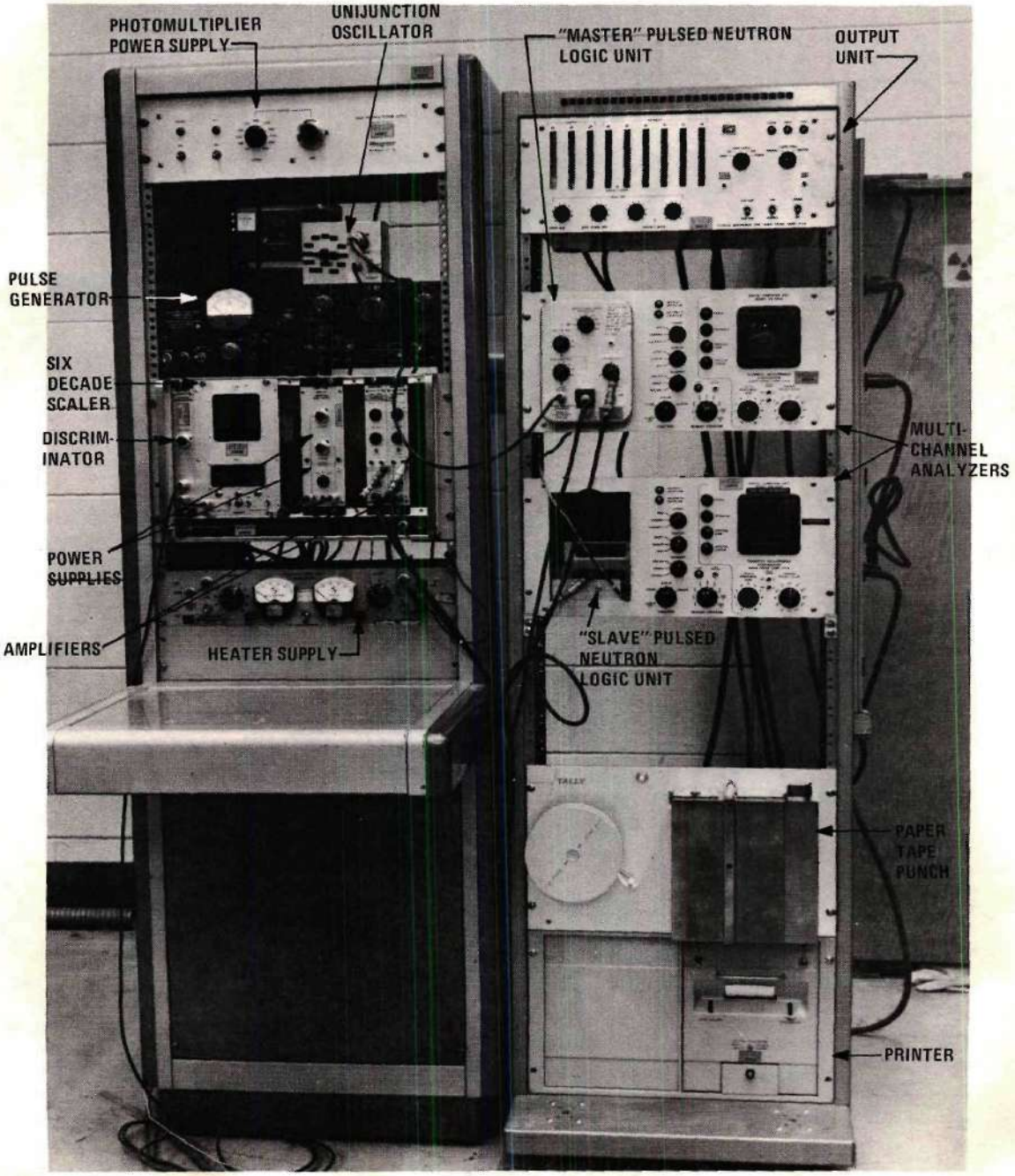

Figure 10. Detection and Data Recording Equipment.

monitor system and the primary data acquisition system. The purpose of the monitor system was to provide a number directly proportional to the total neutron output of the generator during a particular experiment. This permitted comparison of all experimental data even though the generator output changed from one experiment to another because of varying gas pressure in the accelerator tube and target burnout. The purpose of the primary data acquisition system was to measure and record the thermal neutron die-away in the subcritical assembly.

The Monitor System

A two-inch Nuclear Enterprises, Inc. Model NE 421 slow neutron detector, utilizing 96 percent enriched Li^6 dispersed in a ZnS(Ag) matrix, was mounted on an Amperex Electronic Corporation model PA 56 universal photomultiplier base assembly. The output from the anode of the photomultiplier was connected to a variable input-sensitivity preamplifier whose circuit was identical to a Nuclear Chicago Model 8765 preamplifier. The preamplifier output was a square 5.2 volt positive pulse of 1.2 μsec width. The Ortec Model 421 integral discriminator was set at 1 volt; this reduced the noise background to less than one count per hour. The discriminator output drove a Hamner Model NS-11-10E scaler, which tallied the monitor system counts. A remote-control power supply, diagrammed in Figure 37, was built into the scaler start-stop circuit for the purpose of linking the monitor system to the primary data acquisition system. Thus, the scaler was the master unit whose start-stop buttons controlled the entire experiment. A Hamner Model N-4035 high voltage power supply provided -1800 volts to the photomultiplier base; an Electronic Measurement

Co. Model 212 AM transistor power supply furnished -15 volts to the preamplifier.

The Primary Data Acquisition System

The primary data acquisition system utilized two identical detection channels. Neutrons were detected by Reuter-Stokes Model RSN-1055-M9 proportional counters. These detectors, shown in Figure 11, were filled to a pressure of 304 cm mercury with 98 percent He^3, were built as probes 52 1/4 inches in length and 5/16 inch in diameter, and had a sensitive length of one inch. A dual unit Ortec Model 428 detector bias supply provided 650 volts to operate these detectors near the center of their 150 volt wide plateaus. The preamplifiers were charge-sensitive Hewlett-Packard model 5554A units which had variable charge sensitivity, gain, and pulse output shape. Two Ortec Model 485 amplifiers were adjusted to yield unipolar output pulses of at least one volt amplitude. In addition, these amplifiers powered the preamplifiers with +24 volts. Two TMC Model CN-1024 digital computer units were used to record the primary data acquisition system results. A TMC Model 212 pulsed neutron logic unit was modified so that it was capable of controlling both computer units with a "master-slave" relationship. This modification included an additional module containing input and discriminator circuits for use with the second detection channel. This unit is shown in Figure 12. The circuit diagram for this modification appears in Figures 38 and 39. The pulsed neutron logic unit discriminators were set at 1/2 volt, providing noise background of less than one count per 5000 bursts. The source trigger output pulse from this logic unit was of sufficient height to drive the neutron generator. The TMC Model 220 data output unit was connected to the master

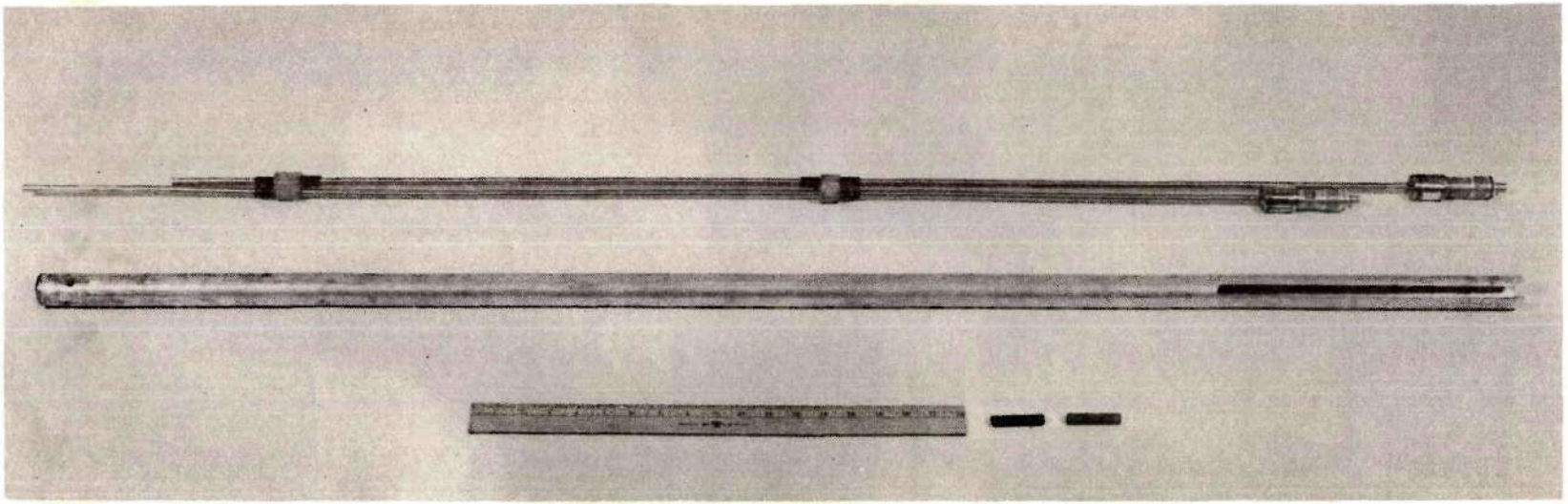

Figure 11. ^{3}He Detectors with Spacers, Cadmium Covers, and Guide Tube.

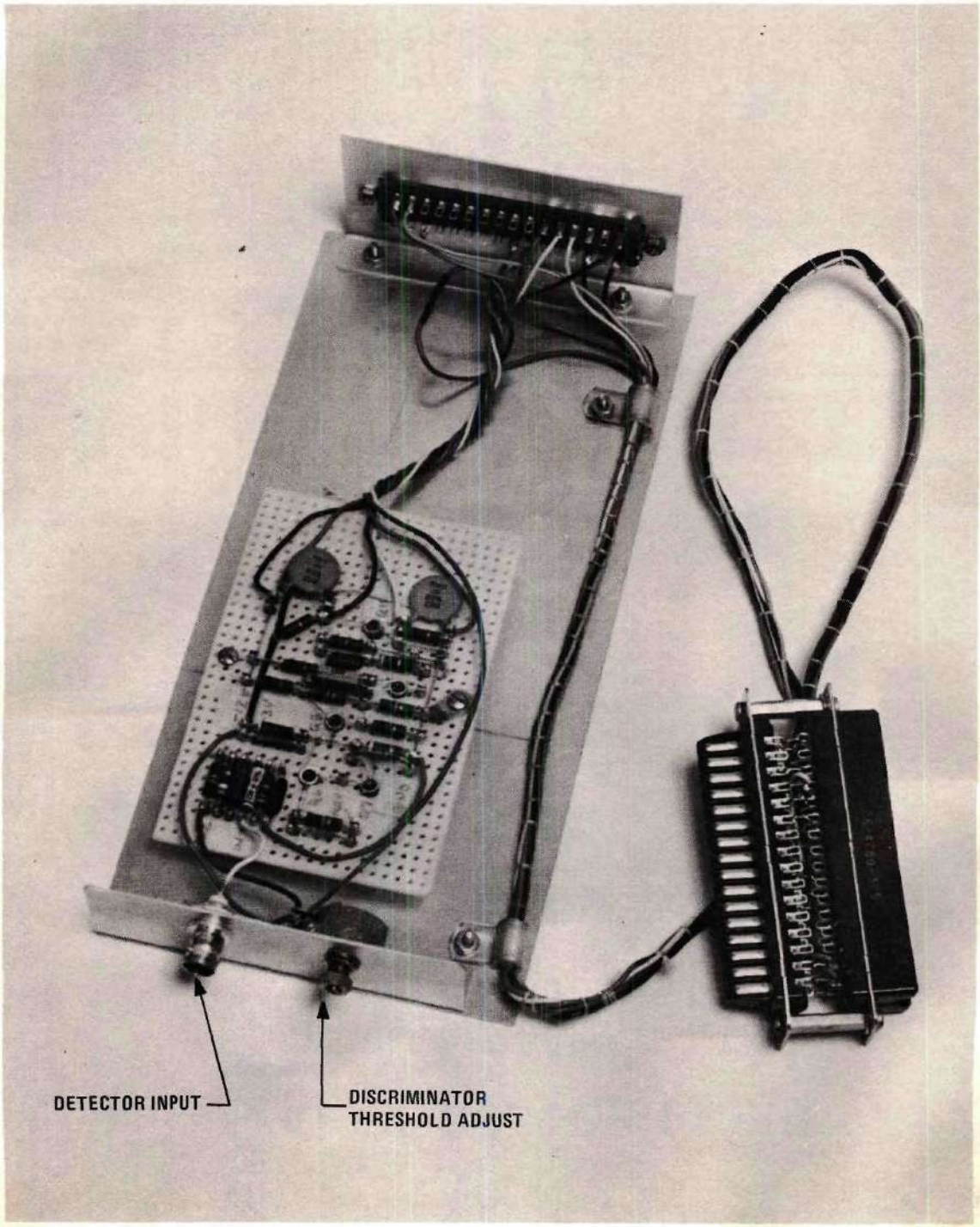

Figure 12. "Slave" Module for Use With Second Detection Channel.

computer unit and was utilized to count the number of neutron generator bursts and then to control the output of data from either computer unit to the Hewlett-Packard J44561B digital recorder. Each computer unit memory was interrogated individually and its output was recorded on 4 inch printer tape listing channel number and counts.

Due to the low rate at which the generator could be pulsed, a unijunction oscillator, shown in Figure 40, was built to provide switch-selectable pulse rates between 1/2 and 10 pulses per second. This pulser was powered by the start-stop circuit of the Hamner scaler. An externally driven General Radio Company pulse generator, type 1217-B, converted pulses from the unijunction oscillator into pulses capable of driving the pulsed neutron logic unit.

Operation of the Detection and Data Recording System

Pressing the start button on the Hamner scaler enabled the monitor system to commence recording events and simultaneously started the unijunction oscillator which ultimately provided the system trigger input pulse to the pulsed neutron logic unit, initiating a data collection cycle of the primary data acquisition system. Eighty microseconds after the system trigger pulse, during which time backgrounds from both detectors were recorded, the logic unit provided a source trigger output pulse which triggered the neutron generator. A 90 μsec delay followed the 5 μsec neutron generator burst to allow some of the transients following the generator burst to die out. The logic unit then initiated 255 successive data measurements during each of which pulses from the amplifiers were counted for 40 μseconds, then stored in the appropriate memory channels

during a 10 μsec storage time. The entire data collection cycle was repeated at a rate determined by the unijunction oscillator until sufficient data was recorded. Pressing the stop button on the Hamner scaler terminated the recording of events by the monitor system and interrupted the production of system trigger pulses by the unijunction oscillator.

CHAPTER IV

EXPERIMENTAL PROCEDURES AND RESULTS

This chapter describes the calibration of the equipment, details the preliminary and final experiments, and presents the measured decay constants.

System Calibration

The two primary data acquisition channels were calibrated for dead time and relative counting efficiency. Dead time was measured by the method of Bierman et al.[43] This approach was based on the fact that the system was limited as to the maximum number of events it could count in a given time interval, the time between each count in this non-paralyzable system being the dead time. This parameter is an important one since the count rate following the neutron generator burst is often as high as 100,000 counts per second.

The Georgia Tech Research Reactor operating at 1 megawatt was the source of thermal neutrons for the dead time calibration. The two detectors and preamplifiers were set up inside the biomedical facility; all other instrumentation was outside. With the instrumentation operated under actual experimental conditions the data collection system was cycled 1000 times. The average of the first 100 data channels in each analyzer yielded a maximum count rate of 125,000 counts per second with a corresponding dead time of 8 μsec.

The relative counting efficiency of the two channels was measured using a 70.7 μgm ^{252}Cf source inside a paraffin-filled 55 gallon drum. The detectors were placed side-by-side, one inch apart, tangent to the drum at the mid-plane. The data collection system was cycled 1000 times with the instrumentation operated under actual experimental conditions at very low count rates and the average of the first 100 data channels in each analyzer was used to measure the relative counting efficiency. One detection channel was found to be 1.006 times more efficient than the other. Because of the accessibility of the ^{252}Cf source this efficiency calibration was checked after every other experiment. The relative efficiency remained constant.

Bubble Transit Time Measurement

One parameter necessary for the determination of the void fraction of the central core region was the time required for a bubble to transit the height of the core. A bubble detector circuit, shown in Figure 41, was constructed and used in conjunction with a Hewlett-Packard Model 5216A 12.5 MHz electronic counter in the time interval measurement mode to measure the transit time. The first bubble to leave a selected 1/4-inch hole in the bottom of a fuel tube provided a start pulse to the one MHz oscillator internal to the counter. Upon breaking the surface of the water the bubble supplied a stop pulse. The value displayed by the counter was the bubble transit time for that depth of water. A 5 7/16 inch I. D. Plexiglas cylinder sealed at one end formed a water tank which permitted careful observation of the bubbles' behavior during the timing experiment. Two parallel, thin, 1/2 X 3/8 inch sheet-metal plates mounted on fiber

board 1/4 inch apart served as the detector. Two detectors were used, one mounted above the hole and the other just above the surface of the water positioned where the "average" bubble would appear. The application of compressed air to the fuel tube caused bubbles to emerge from the hole in the bottom of the fuel tube. The first one out of the hole passed between the parallel plates of the lower detector, changed the resistance of the path between the plates, and provided the start pulse. Upon reaching the surface, the bubble raised the local surface level enough to wet the upper detector plates and provided a stop pulse. The air was then turned off, the counter reading recorded, and the counter reset. For each water level this was repeated ten times. Three water levels were used: 9, 13.5, and 18 inches (measured as the height of water above the center of the hole). The results of the bubble transit time measurements are given in Table 1. The equation relating bubble transit time to water level was found to be

$$T = 0.069 \times H \tag{40}$$

where

T = transit time in seconds

H = height of water above hole in inches.

The size of the bubbles emerging from the 1/4 inch hole was essentially constant as determined by visual observations.

Light-Water Test Case

As a final check on the performance of the data collection system the diffusion parameters, $\overline{v\Sigma}_a$ and $\overline{D}_o$, were measured for light-water. The

Table 1. Measured Transit Times for 9, 13.5, and 18 inch Water Levels

Measurement	Transit Time (Seconds) 9 inch Level	13.5 inch Level	18 inch Level
1	0.613	0.931	1.249
2	0.621	0.912	1.238
3	0.628	0.924	1.206
4	0.623	0.926	1.228
5	0.615	0.937	1.217
6	0.628	0.925	1.260
7	0.620	0.923	1.259
8	0.624	0.932	1.222
9	0.627	0.914	1.234
10	0.628	0.935	1.218
Total	6.227	9.259	12.331
Average	0.63	0.93	1.23

experiment consisted of measuring the time-dependent neutron flux at four detector locations in a light-water sample. Harmonic analysis and curve fitting procedures were used to obtain the diffusion parameters from the experimental data.

The Experiment

The cadmium box used for this measurement was 19 1/2 × 20 1/4 × 24 inches high. In order to minimize the number of neutron generator bursts the experimental method used was that of Lopez and Beyster.[44] This method, discussed in Chapter II, permitted the harmonic analysis of the time-dependent axial flux. Four detector positions, equispaced along the vertical center line of the core, were used. For this 24 inch high core the first detector location was 4.85 inches from the bottom of the box with the next detector location 4.85 inches above it and so on. These detector spacings actually sum to 24.25 inches as a result of adding twice the assumed extrapolation distance of 0.13 inches to the core height. It is assumed that the neutron flux goes to zero at the boundaries of this enlarged core.

The detectors were bound together as shown in Figure 11 with their active volumes 4.85 inches apart. They were then inserted into the guide tube and positioned so that the centers of their active volumes were at the two lower detector locations when the guide tube was inserted along the vertical centerline of the core. Then, by moving the detectors together 9.70 inches upward, the remaining two detector locations could be accessed. The monitor detector, whose purpose was to measure the time-integrated neutron generator output, was bagged in polyethylene and

fastened to the outside of the top of the cadmium box with the NE 421 detector 16 inches below the surface of the water.

With the two detectors in the lower position the assembly was pulsed 4000 times. The resulting data were then printed out, the monitor reading recorded and reset, and the detectors were moved to the upper position. The assembly was then pulsed again until the monitor reading was approximately the same as it had been previously (requiring only 2200 bursts), at which time the generator was stopped and the data printed out. The tank was drained after every experiment.

Data Reduction

The raw data from the experiment were the result of measuring the neutron population as a function of time at four locations. Equations (34), (35), (36), and (37) in matrix notation became

$$\phi = AB \tag{41}$$

where

$$\phi = \begin{bmatrix} \phi(z_1, t_i) \\ \phi(z_2, t_i) \\ \phi(z_3, t_i) \\ \phi(z_4, t_i) \end{bmatrix}$$

$$A = \begin{bmatrix} 0.58779 & 0.95106 & 0.95106 & 0.58779 \\ 0.95106 & 0.58779 & -0.58779 & -0.95106 \\ 0.95106 & -0.58779 & -0.58779 & 0.95106 \\ 0.58779 & -0.95106 & 0.95106 & -0.58779 \end{bmatrix}$$

$$B = \begin{bmatrix} b_1(t_i) \\ b_2(t_i) \\ b_3(t_i) \\ b_4(t_i) \end{bmatrix} .$$

Solving for B

$$B = A^{-1}\phi \tag{42}$$

where

$$A^{-1} = \begin{bmatrix} 0.23511 & 0.38042 & 0.38042 & 0.23511 \\ 0.38042 & 0.23511 & -0.23511 & -0.38042 \\ 0.38042 & -0.23511 & -0.23511 & 0.38042 \\ 0.23511 & -0.38049 & 0.38042 & -0.23511 \end{bmatrix} .$$

Finally, the elements of B are related to the decay constants by the equation

$$b_n(t_i) = A(0)\ \exp(-\alpha_n t_i) . \tag{43}$$

A FORTRAN program for the Univac-1108 was written to obtain the decay constant from the raw data. This program corrected the data for background, dead time losses, differences in detector efficiency, and for monitor differences, yielding ϕ of equation (41). Appendix A discusses these corrections. The matrix multiplication operation of equation (42) was then performed. At this point the $b_n(t_i)$ and the corresponding t_i were ready to be least squares fit to equation (43). This was done following the method of Bevington,[45] taking the logarithms of both sides of equation (43) and fitting the results to a straight line. Appendix B discusses the curve fitting procedures. This was done to each of the four

sets of $b_n(t_i)$, with the values of the four α_n as the end result. In addition, the technique of channel-dropping was employed to insure that each decay constant was free from modal contamination. With this, all input data points were used in the determination of the α_n, then the earliest time channel was dropped and the remaining points were used to determine the α_n. This dropping procedure was continued until only five channels remained in the fitting procedure. The program then output the α_n and A(0) and their standard deviations for each fit.

A second FORTRAN program accomplished a least squares fit of equation (32) to the α_n determined above and with the B^2_{11n} determined from equation (29) with ϵ assumed equal to 0.13 inches as before. The results are depicted in Figure 13. The values of $\overline{v\Sigma}_a$ and $\overline{D}_o$ appear quite reasonable. The values $\overline{v\Sigma}_a = 4924 \pm 109$ sec^{-1} and $\overline{D}_o = 37955 \pm 4740$ cm^2/sec agree fairly well with the experimental values of Lopez and Beyster[46]: $\overline{v\Sigma}_a = 4761 \pm 24$ sec^{-1} and $\overline{D}_o = 37240 \pm 400$ cm^2/sec, and with the theoretical values of Clendenin[47]: $\overline{v\Sigma}_a = 4886$ sec^{-1} and $\overline{D}_o = 37970$ cm^2/sec. Our large error ($\pm 1\ \sigma$) resulted from limited statistical accuracy due to minimizing the number of neutron generator bursts. If a $\overline{v}$ of 2.48×10^5 cm sec^{-1} was assumed, $\overline{D}$ was found to be 0.0603 inches. Since the extrapolation length, ϵ, is approximately $0.7104 \times 3\overline{D}$, the previously assumed value of 0.13 inches was correct. The above results indicated that the data collection system was functioning properly.

Multiplying Medium and Void Experiments

Upon satisfactorily completing the testing of the data collection system, the measurement of the multiplying medium parameters was begun.

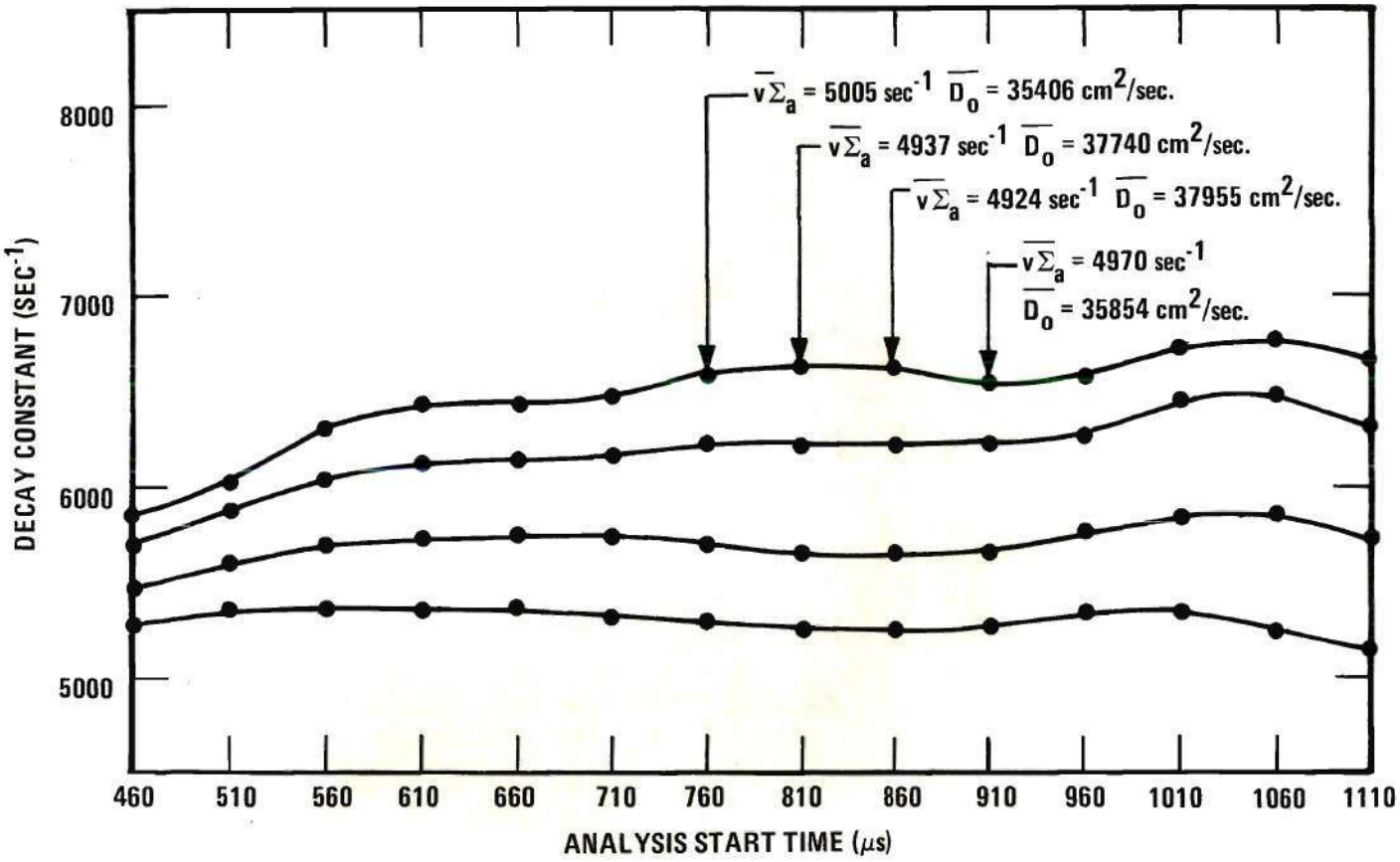

Figure 13. Decay Constants of the Light-Water Test Assembly as a Function of Starting Channel.

First, however, the void fraction of the central region had to be known accurately if the assembly was to be successfully modeled at a later date.

Determination of Void Fraction

The central region consisted of twenty-two fuel tubes plus the central detector guide tube. For the maximum core height of 33 1/2 inches (4 fuel slugs) the maximum fluid volume of the central region was 0.569 ft^3. The volume of the void, when the compressed air was flowing, was given by

$$\text{Void Volume } (ft^3) = \text{Flow Rate } (ft^3/min) \times \text{Bubble Transit Time (min)} \quad (44)$$

where the flow rate was registered by the flow meter and the bubble transit time was, from equation (40), .0373 min. Dividing the void volume by the maximum fluid volume of the region, the void fraction of the region was arrived at:

$$\text{Void Fraction} = 6.558 \times 10^{-2} \times \text{Flow Rate } (ft^3/min) \quad (45)$$

The void fraction defined in this way was simply the fraction of moderator removed from the region. The flow rate could be easily calculated from equation (45) to produce the desired void fraction. This flow rate was, in addition, independent of core height because the numerator (through bubble transit time) and the denominator (through volume) both contain the height as a common factor. However, since bubbles increase in volume upon rising it was important to have the desired flow rate be the average flow rate; which was the flow rate measured at the horizontal mid-plane of the core. Thus, the flow rate of equation (45) was the flow rate at the pressure of the core midplane. Through the relationship

$$P_2 - P_1 = w(h_2 - h_1) \ , \tag{46}$$

where

P_i = pressure at height i

h_i = fluid height i

w = specific weight of fluid (62.4 lb/ft^3) ,

the mid-plane pressure was calculated. Then using

$$\overset{o}{V}_1 = \frac{\overset{o}{V}_2 P_2}{P_1} \ , \tag{47}$$

where

$\overset{o}{V}_1$ = volumetric flow rate at atmospheric pressure

$\overset{o}{V}_2$ = volumetric flow rate at pressure P_2

P_1 = atmospheric pressure (14.7 psia)

P_2 = midplane pressure ,

the flow rate of equation (45) was converted into a standard flow rate in units of standard cubic feet per minute, assuming negligible temperature effect.

The flow meter was calibrated at 14.7 psia and 70 °F, i.e., at standard conditions. Since the flow meter was upstream from the exit holes at the bottom of the fuel rods, the pressure at which the compressed air was metered was approximately that of the bottom of the core. Equation (46) was used to determine the pressure of the metered gas and the appropriate correction factor[48] was used to determine the correct flow meter reading. The results of these calculations are shown in Table 2.

Table 2. Corrected Flow Rate as a Function of Core Height and Void Fraction

Core Height (inches)	Void Fraction	Flow Rate From Eq. (45) (ft^3/min)	Midcore Pressure (psia)	Standard Flow Rate (scfm)	Bottom Pressure (psia)	Meter Correction Factor (Divide By)	Flow Rate At Meter (scfm)	Flow Rate At Meter (Percent)
32.5	0.40	6.100	15.30	6.349	15.9	1.04	6.06	54.5
32.5	0.50	7.624	15.30	7.935	15.9	1.04	7.60	68.5
32.5	0.60	9.149	15.30	9.522	15.9	1.04	9.13	82.2
24.125	0.50	7.624	15.15	7.857	15.6	1.03	7.60	68.5
15.75	0.50	7.624	15.00	7.780	15.3	1.02	7.60	68.5

Preliminary Experiments

In order to gain some experience with multiplying media, two core configurations were pulsed. The x-y dimensions were fixed as described in Chapter II, and z was varied by the addition of one fuel slug and corresponding moderator height from 16 3/4 to 25 1/8 inches. Detectors were equally spaced along the z axis (see Figure 14). For each configuration both central-voided and non-voided assemblies were pulsed 5000 times at a rate of two pulses per second. The results, corrected for background, dead time, and relative detector efficiency, are shown in Figures 15-18. One feature consistently demonstrated by these four figures is that early in time the lower detector measures a flux greater than the upper detector, then quickly drops off to a lower flux level. Ideally, detectors symmetrically placed about the center of the core should measure the same flux level during asymptotic decay. Figure 18 is the only one to demonstrate this. Another feature is that there is very little harmonic content present; the fundamental appears in less than 1 msec. The fundamental decay constants which resulted from the fitting of a single exponential to each of the decay curves in Figures 15-18, utilizing channel dropping, are shown in Figures 19 and 20. The fundamental decay constant is determined from the graphs in Figures 19 and 20 as being the value of the decay constant that is approximately constant over a number of starting channels. The absence of a constant region on a graph indicates that the fundamental decay mode was not attained before the neutron population measured by the detector decayed to the background level. From Figures 19 and 20 it appears that the upper detector realized fundamental decay before the lower

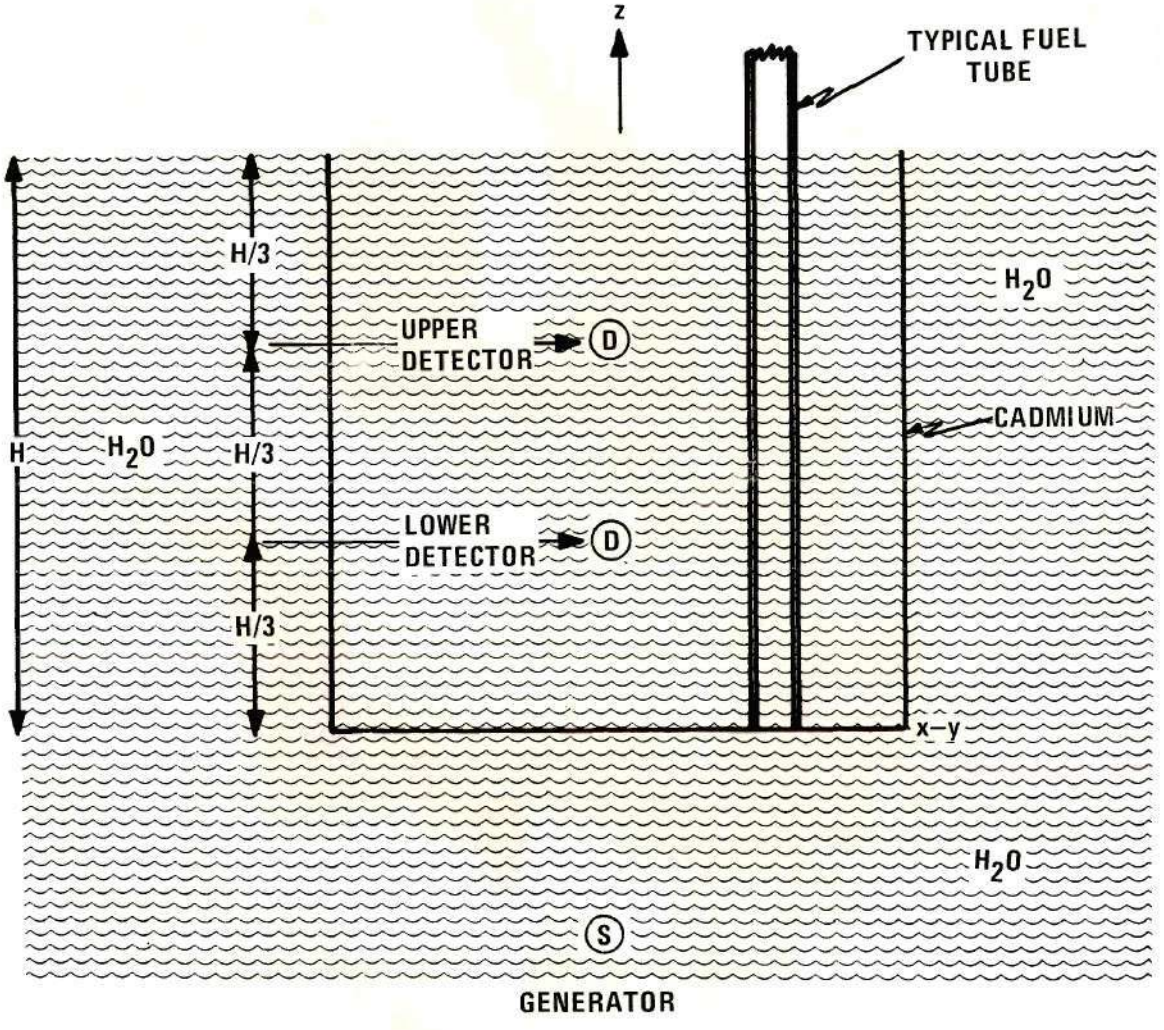

Figure 14. Detector Arrangement During Preliminary Multiplying Medium Experiments.

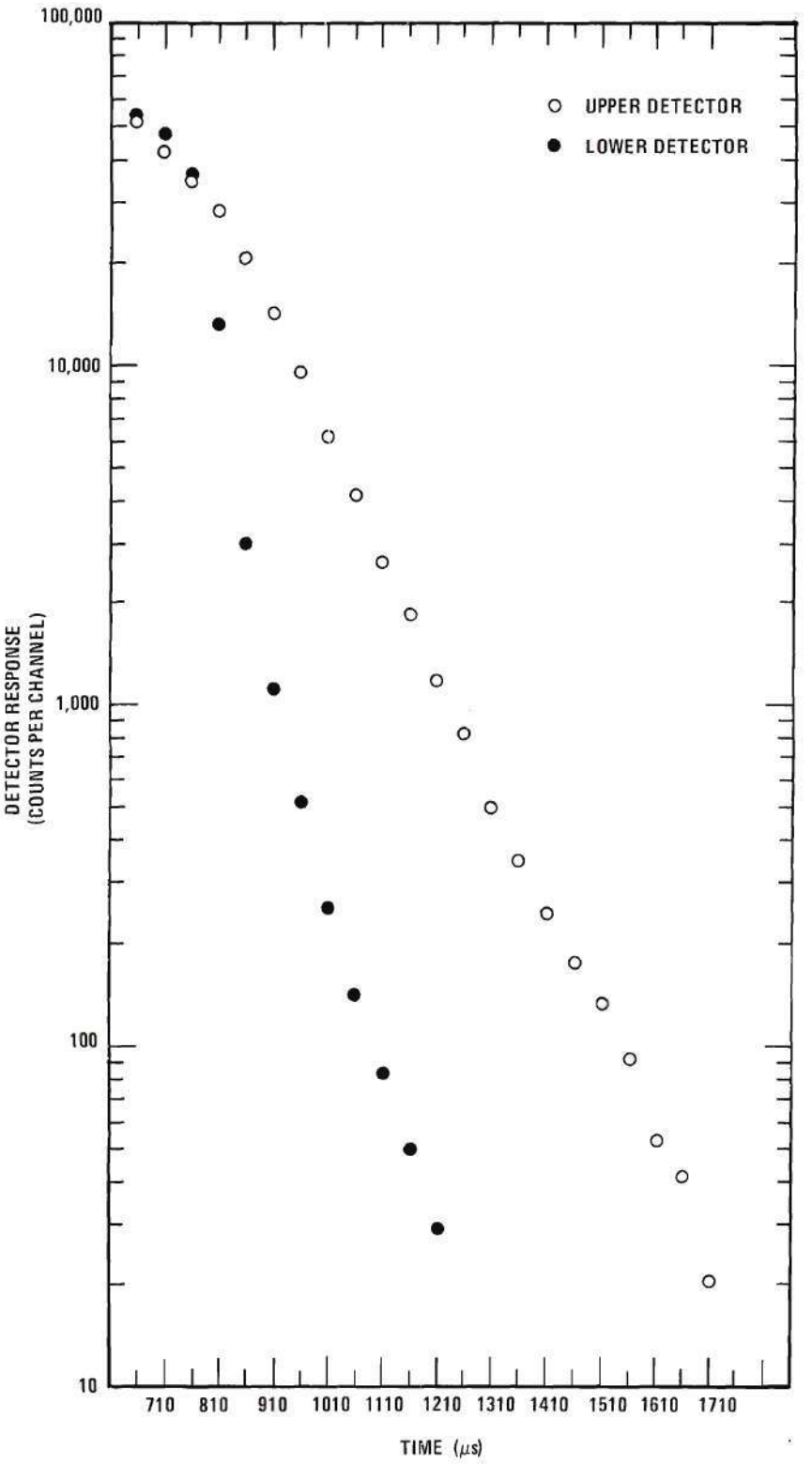

Figure 15. Time Spectra for the Non-Voided 16 3/4 Inch Core.

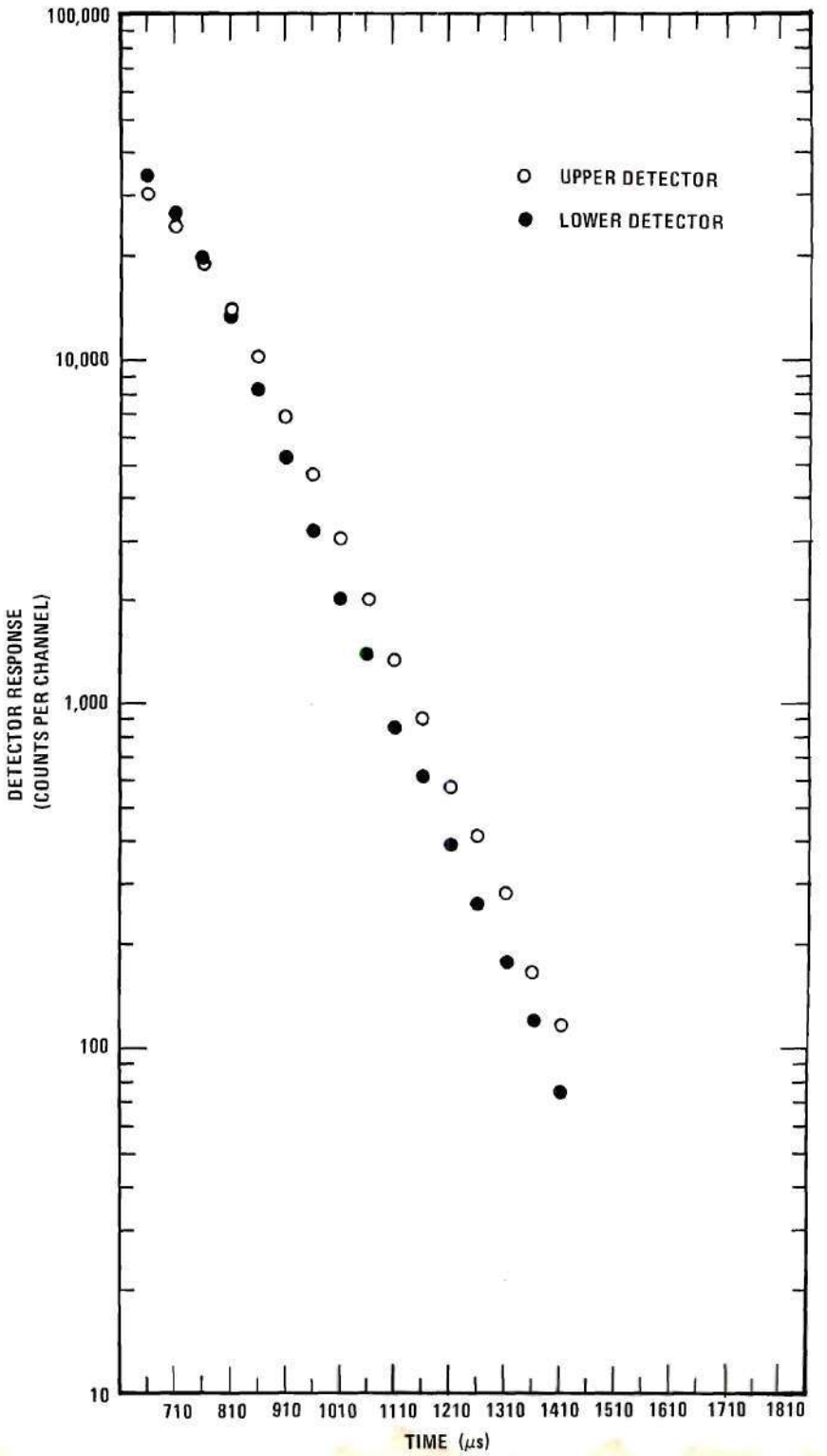

Figure 16. Time Spectra for the Voided 16 3/4 Inch Core.

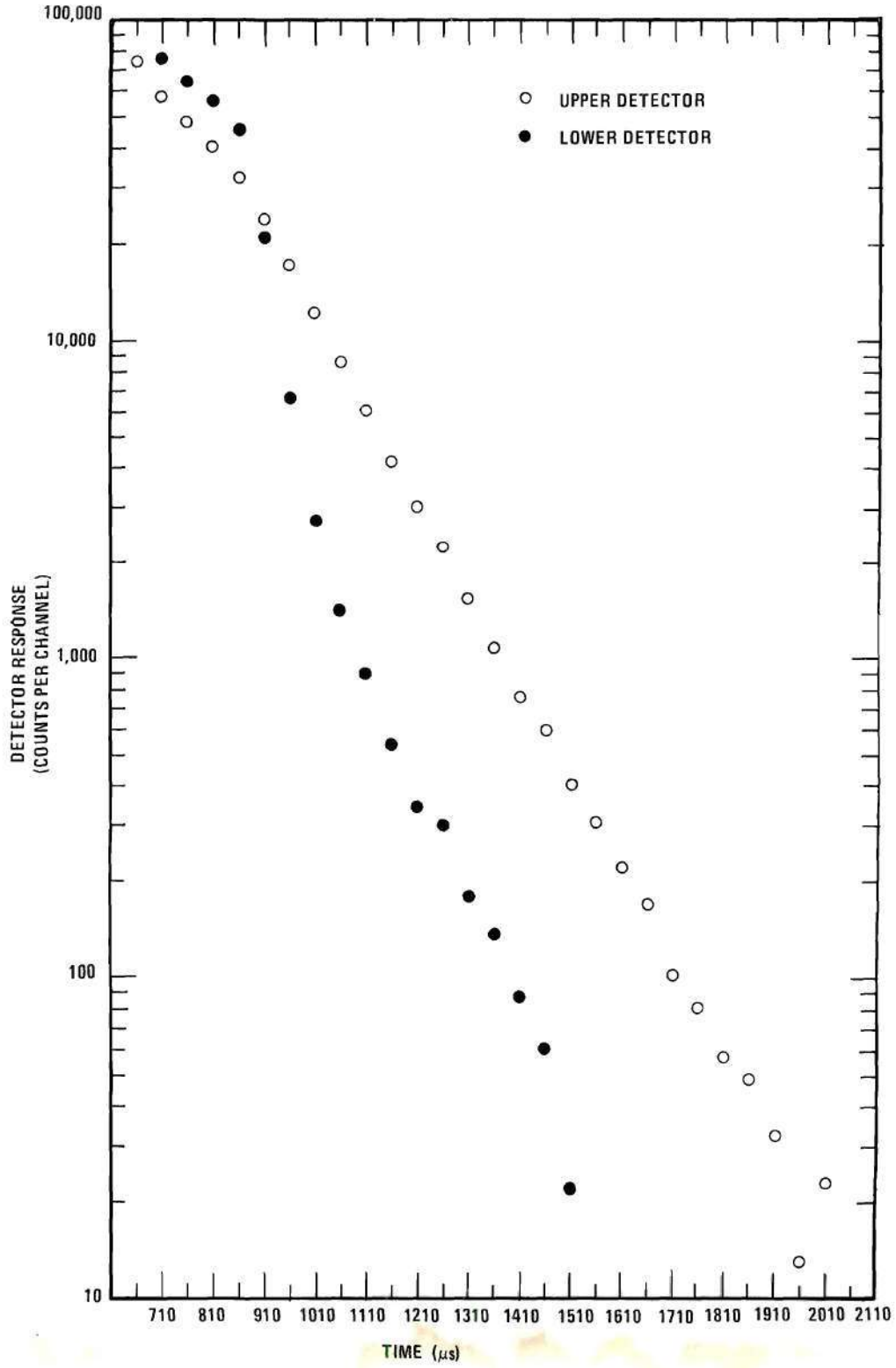

Figure 17. Time Spectra for the Non-Voided 25 1/8 Inch Core.

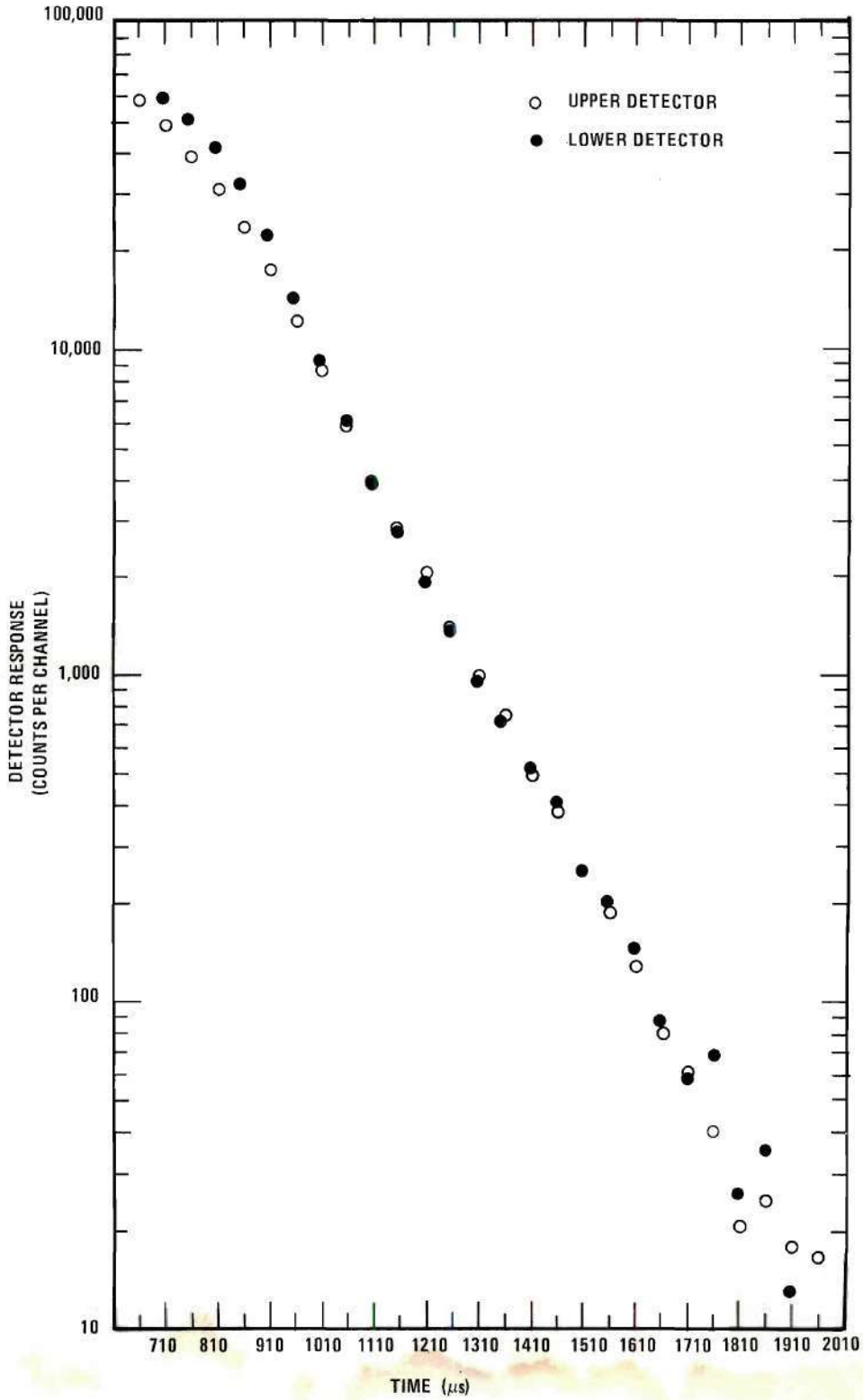

Figure 18. Time Spectra for the Voided 25 1/8 Inch Core.

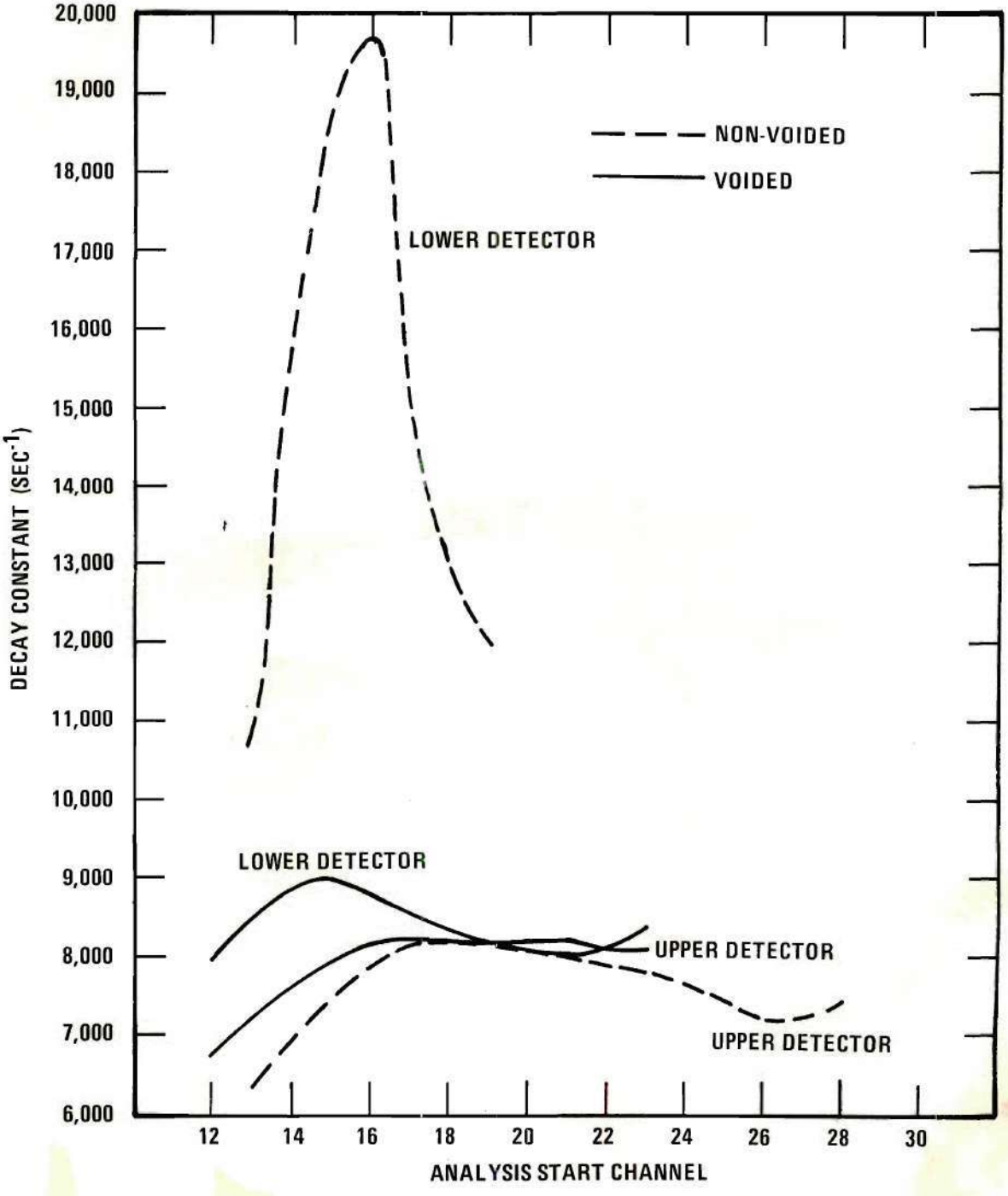

Figure 19. Decay Constant of the 16 3/4 Inch Core as a Function of Starting Channel for the 50 Percent Voided and Non-Voided Cases.

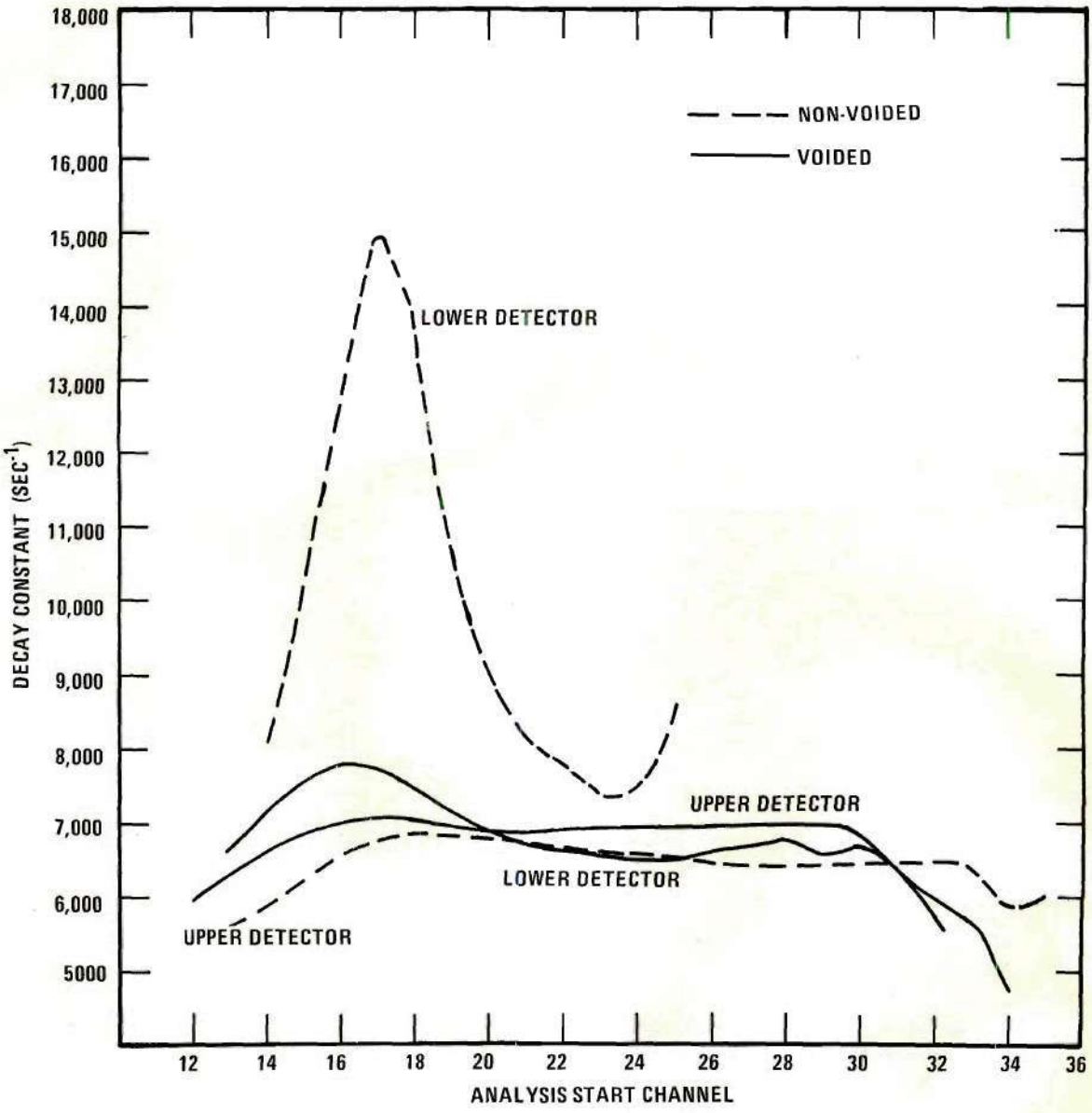

Figure 20. Decay Constant of the 25 1/8 Inch Core as a Function of Starting Channel for the 50 Percent Voided and Non-Voided Cases.

detector and that even with the statistical precision which resulted from minimizing the number of neutron generator bursts the fundamental decay constant can be measured to within five percent for the worst case. However, it was decided to further investigate the flux behavior in the core.

Time-, Space-, and Energy-Dependent Flux Measurements

To investigate the flux behavior, the four fuel slug core was used. It was filled with water to a height of 33 inches. An axial flux transverse was made with ten detector locations three inches apart, starting three inches from the bottom of the core. The two ^{3}He detectors were connected, as in the light-water case, 15 inches apart. In this manner, the lower detector could measure the flux at one of the five lower core detector positions while the upper detector could measure the flux at one of the five corresponding upper core detector positions depending upon the positioning of this detector unit in the guide tube. Two axial traverses were made: one with the detectors bare, the second with the active volume of the detectors cadmium covered. For each detector unit position the core was pulsed 500 times; no voids were used. The resulting data were corrected for background, dead time, relative detector efficiency, and normalized to the maximum monitor value. Figure 21 shows the bare detector count rate as a function of position and time after the neutron generator pulse, Figure 22 shows the cadmium covered detector results, and Figure 23 shows the difference between the two. Statistical fluctuations in the data resulting from the low number of pulses are evident. However, Figures 21 and 23 show well-behaved asymptotic flux decay in the upper half of the core while the lower core appears to be in a transient state.

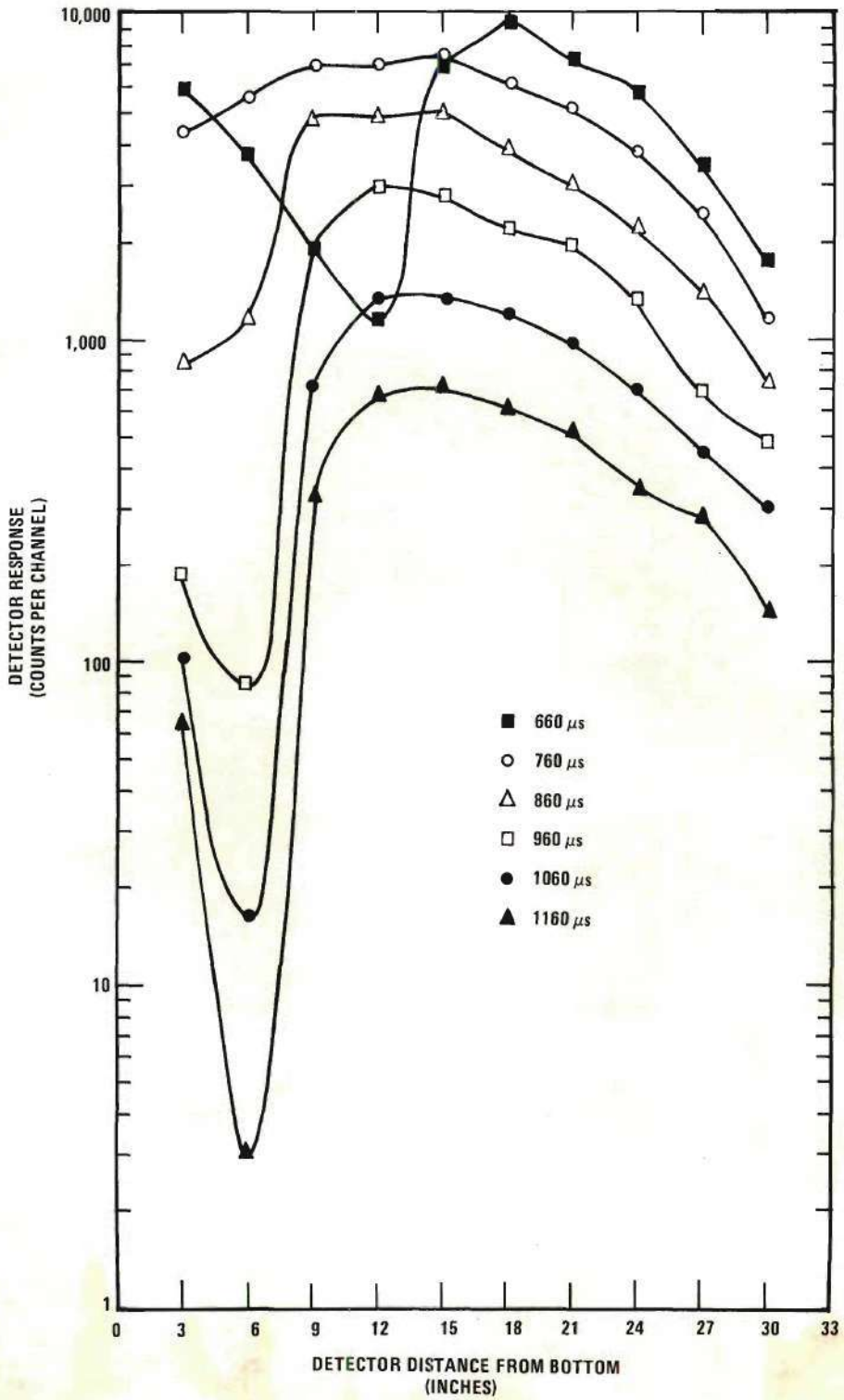

Figure 21. Bare Detector Response as a Function of Time and Position Along the Z Axis of the 33 Inch Core.

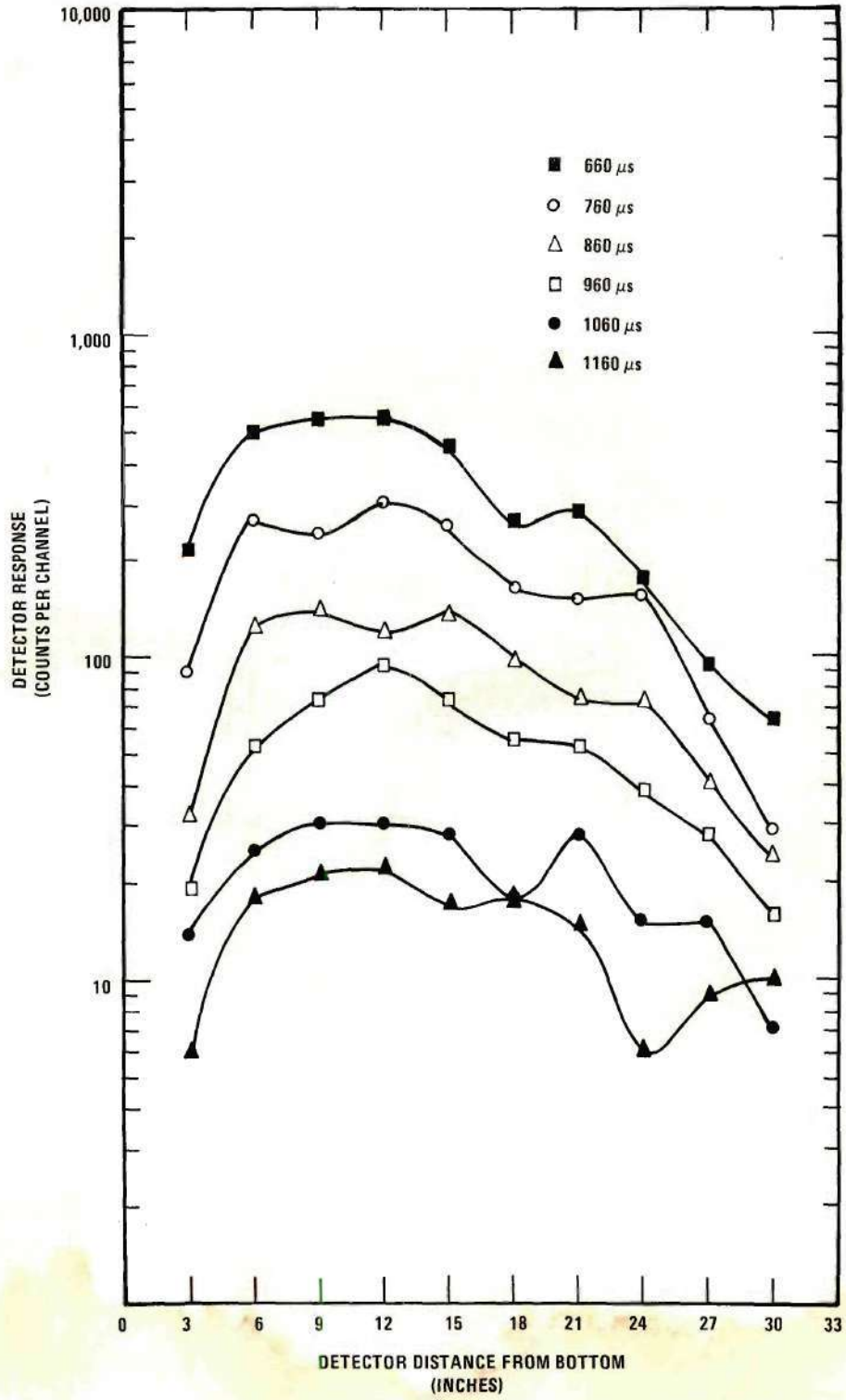

Figure 22. Cadmium Covered Detector Response as a Function of Time and Position Along the Z Axis of the 33 Inch Core.

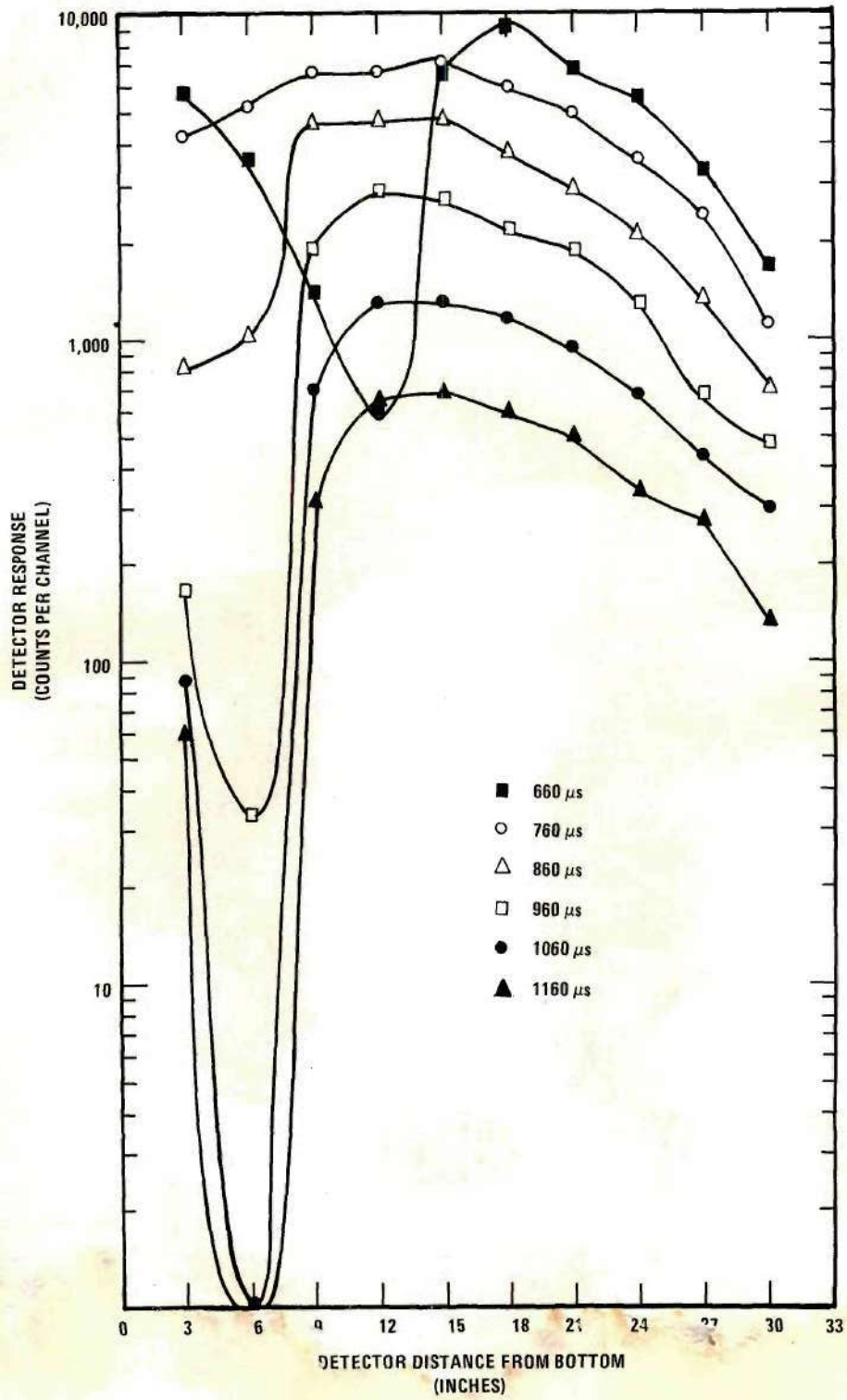

Figure 23. Difference Between Bare and Cadmium Covered Detector Responses as a Function of Time and Position Along the Z Axis of the 33 Inch Core.

Since this was not expected, it was decided to reexamine the flux behavior in the lower half of the core. The ^{3}He detectors were bound together six inches apart and the four lower detection positions were used. Again, two axial traverses were made; this time on the first traverse the lower detector was bare and the upper covered and vice-versa on the second traverse. This procedure minimized the amount of cadmium in this region with so close a detector spacing. In addition, this axial four position measurement was repeated outside the cadmium box core, in what has been referred to as the room return shield. It was anticipated that the cadmium box would decouple the core from this shield as far as the thermal flux was concerned. Each measurement was the result of 250 neutron generator bursts. Figure 24 shows the corrected bare detector count rate in the core as a function of position and time after the neutron generator pulse, Figure 25 shows the corrected cadmium covered detector results for the core, and Figure 26 shows the difference between the two. Similarly, Figures 27-29 show the corrected results of the measurements made in the shield. Figures 24 and 26 still exhibit the rapid die-away of the thermal and total flux in this region. Figures 28 and 29 show epicadmium and thermal peaking in the lower half of the reflector.

As a result of these measurements it was decided to use the flux in the upper half of the core to characterize the neutron die-away. Judge and Daitch[49] calculated the time-, energy-, and space-dependent flux in a pulsed multiplying water-moderated system and observed a similar spatial flux asymmetry. It is attributed to the fact that the pulsed neutron source is not symmetric within the system, thereby giving rise to spatial transients and the resulting asymmetry.

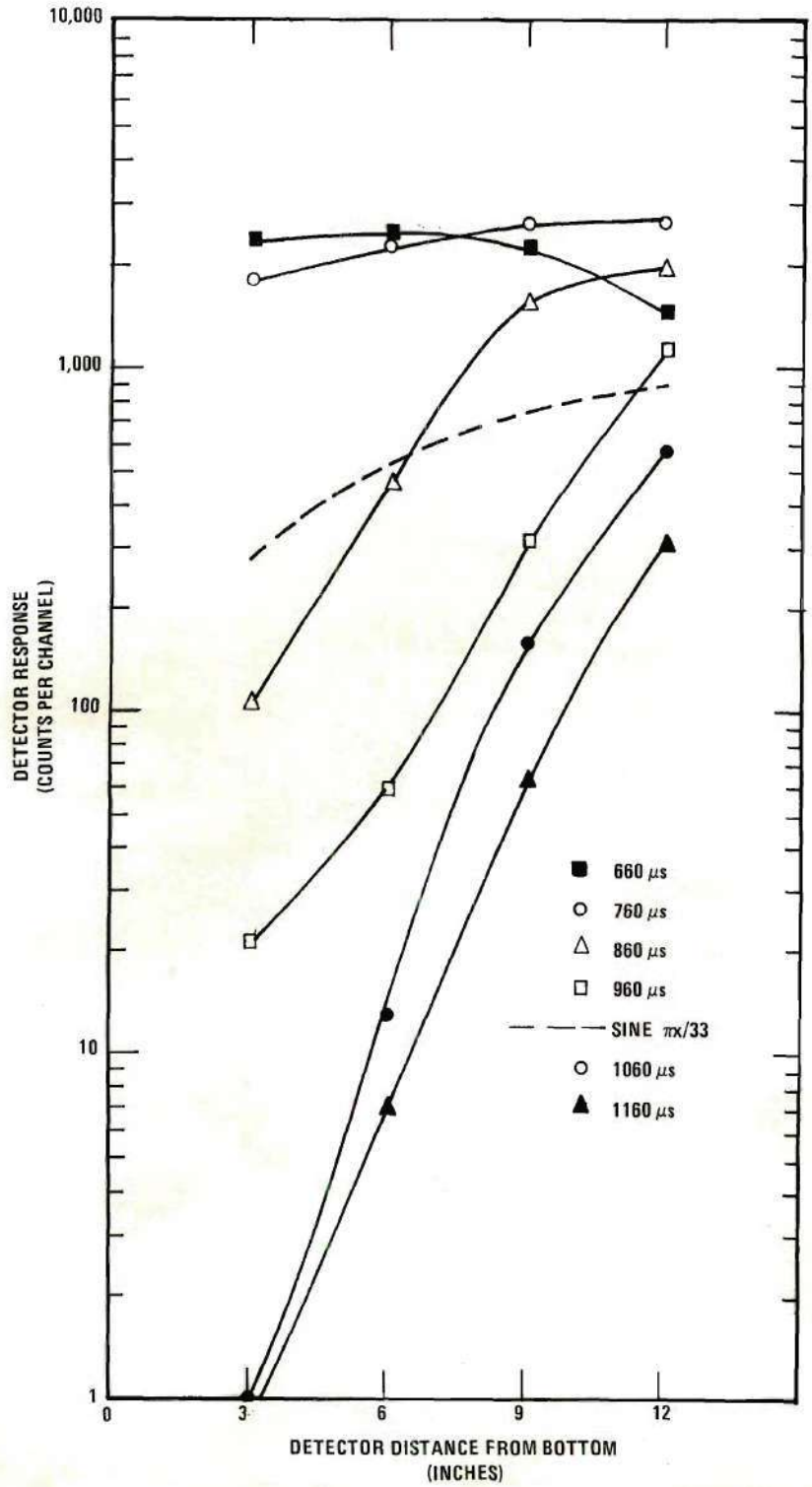

Figure 24. Bare Detector Response as a Function of Time and Position Along the Z Axis of the 33 Inch Core.

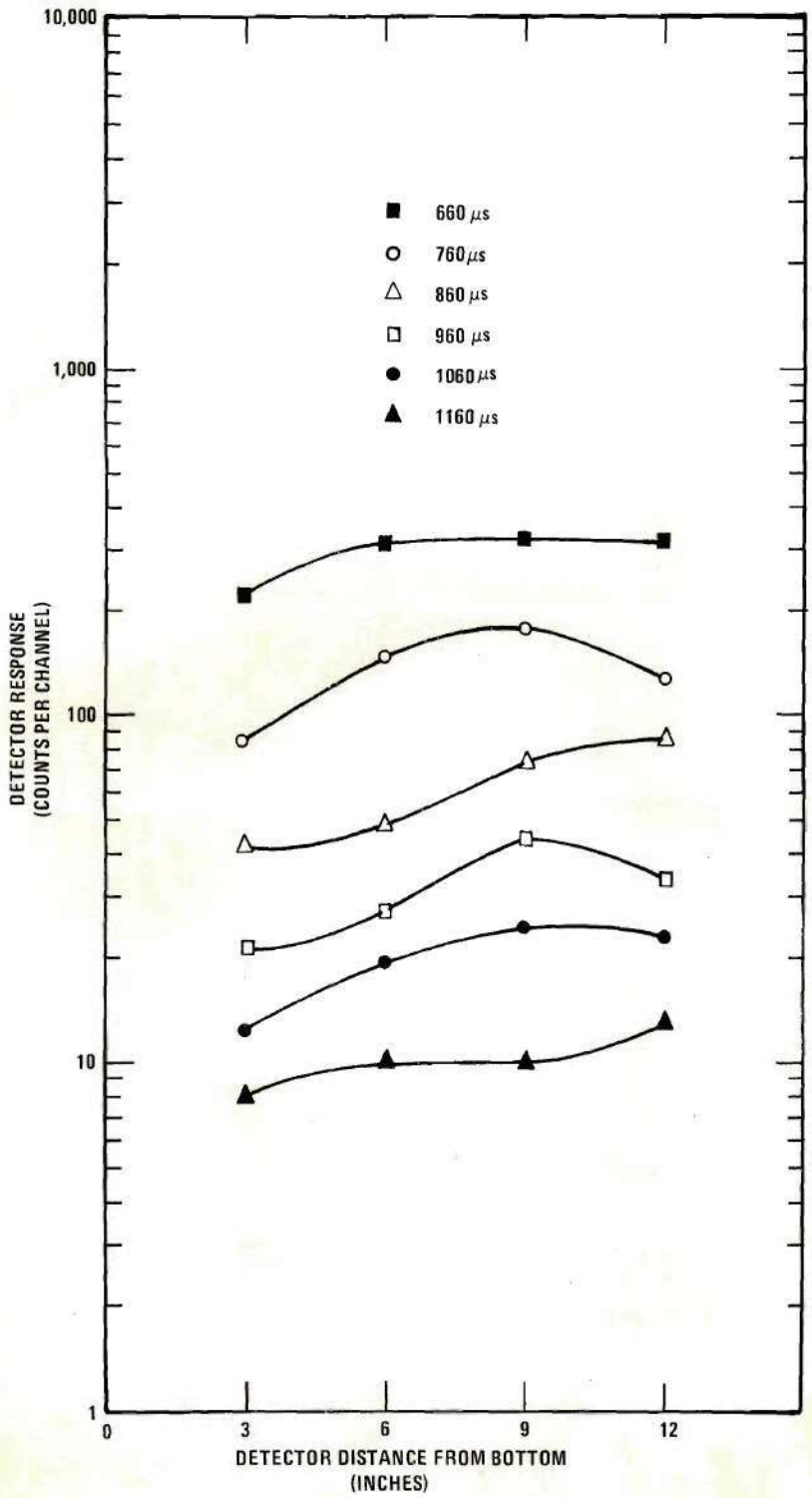

Figure 25. Cadmium Covered Detector Response as a Function of Time and Position Along the Z Axis of the 33 Inch Core.

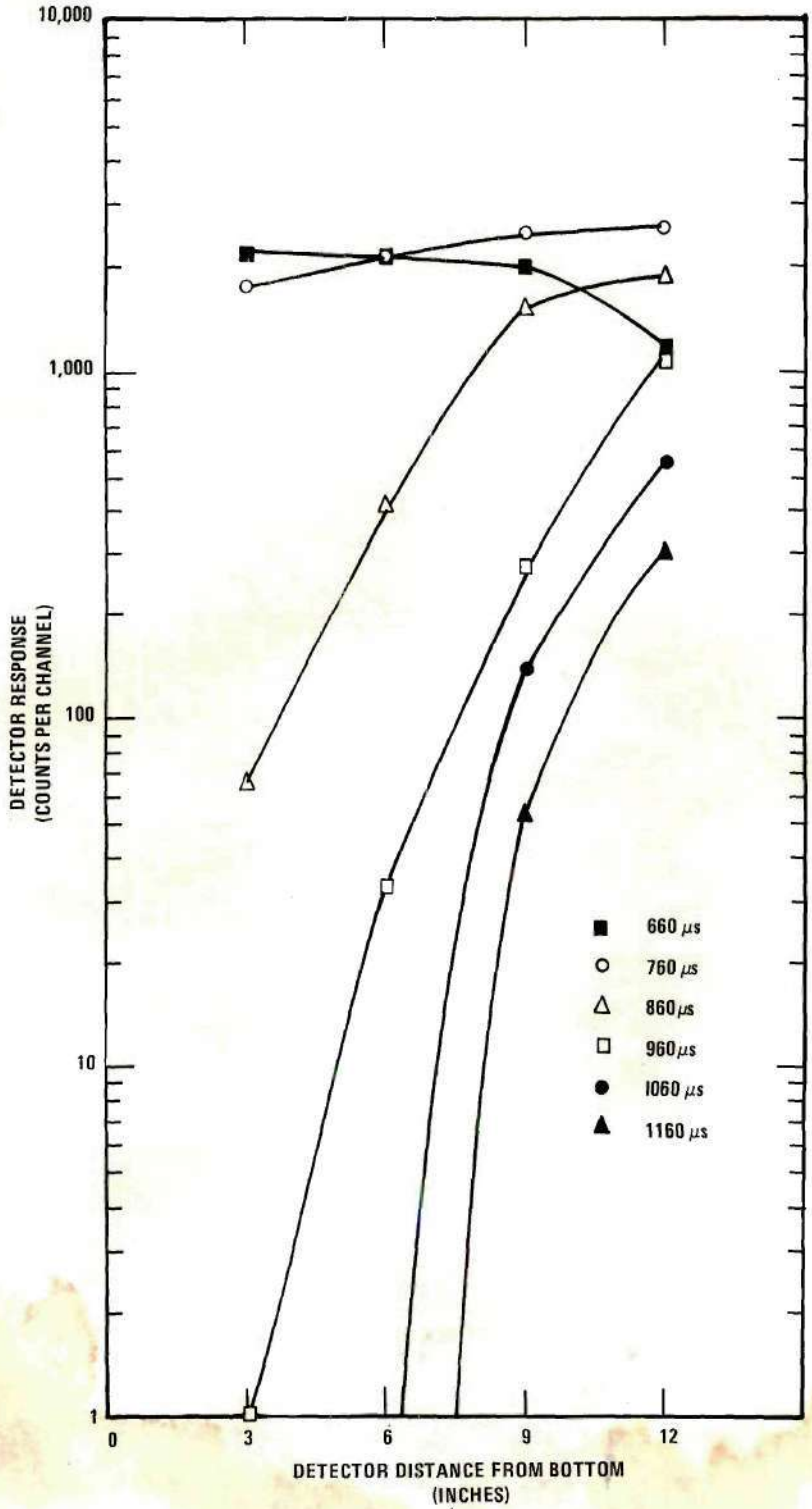

Figure 26. Difference Between Bare and Cadmium Covered Detector Responses as a Function of Time and Position Along the Z Axis of the 33 Inch Core.

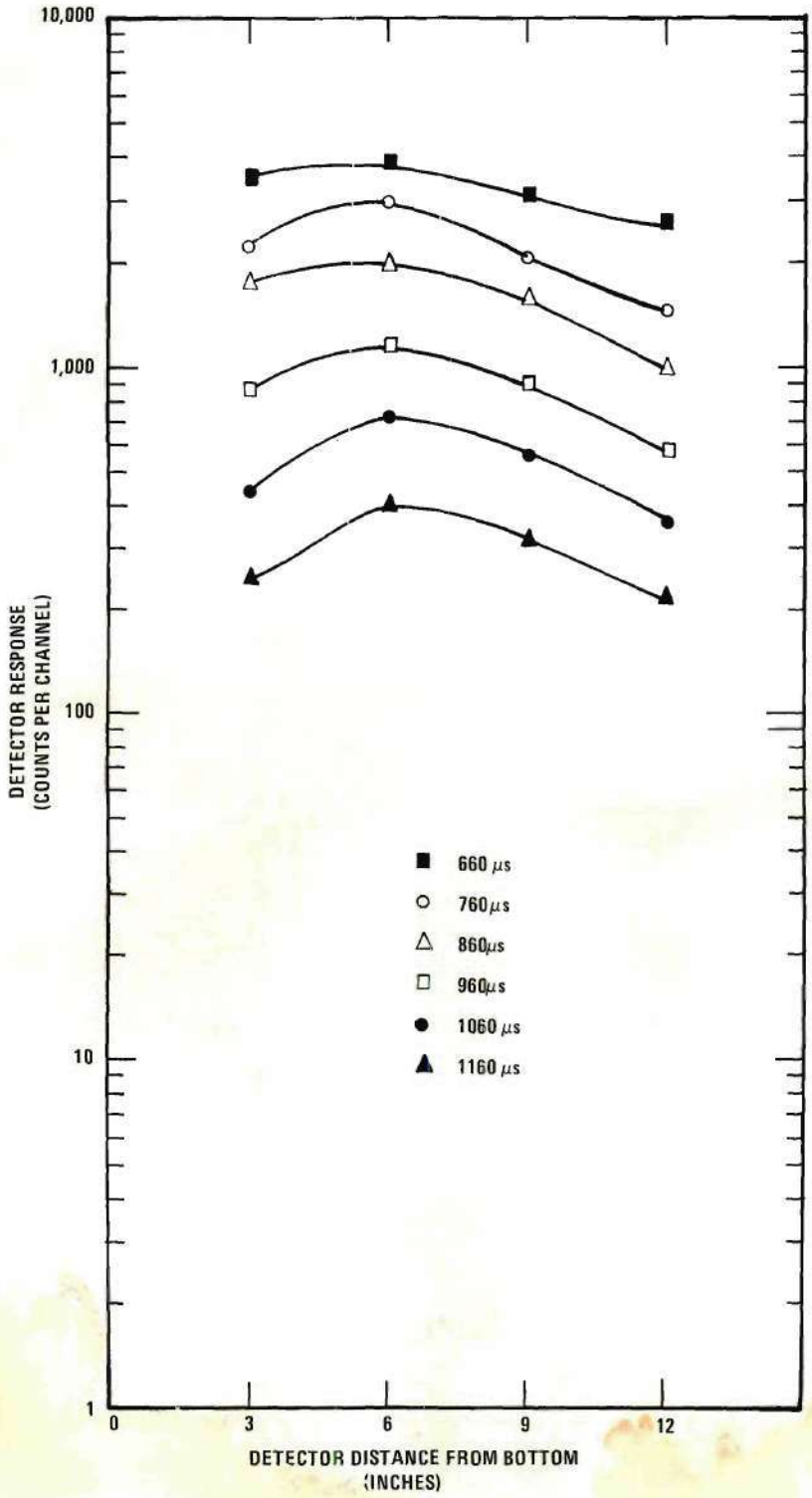

Figure 27. Bare Detector Response as a Function of Time and Position in the Shield of the 33 Inch Core.

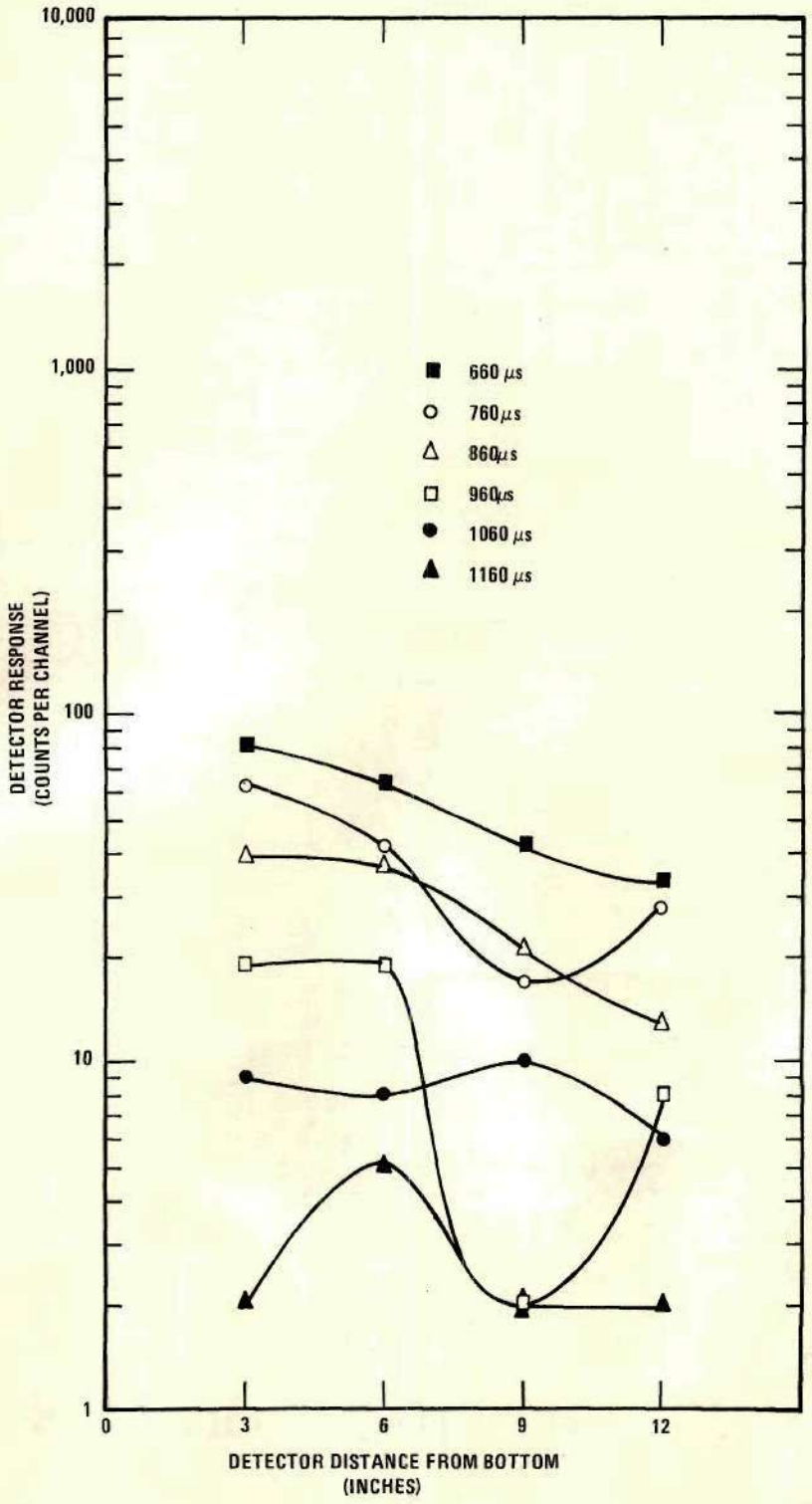

Figure 28. Cadmium Covered Detector Response as a Function of Time and Position in the Shield of the 33 Inch Core.

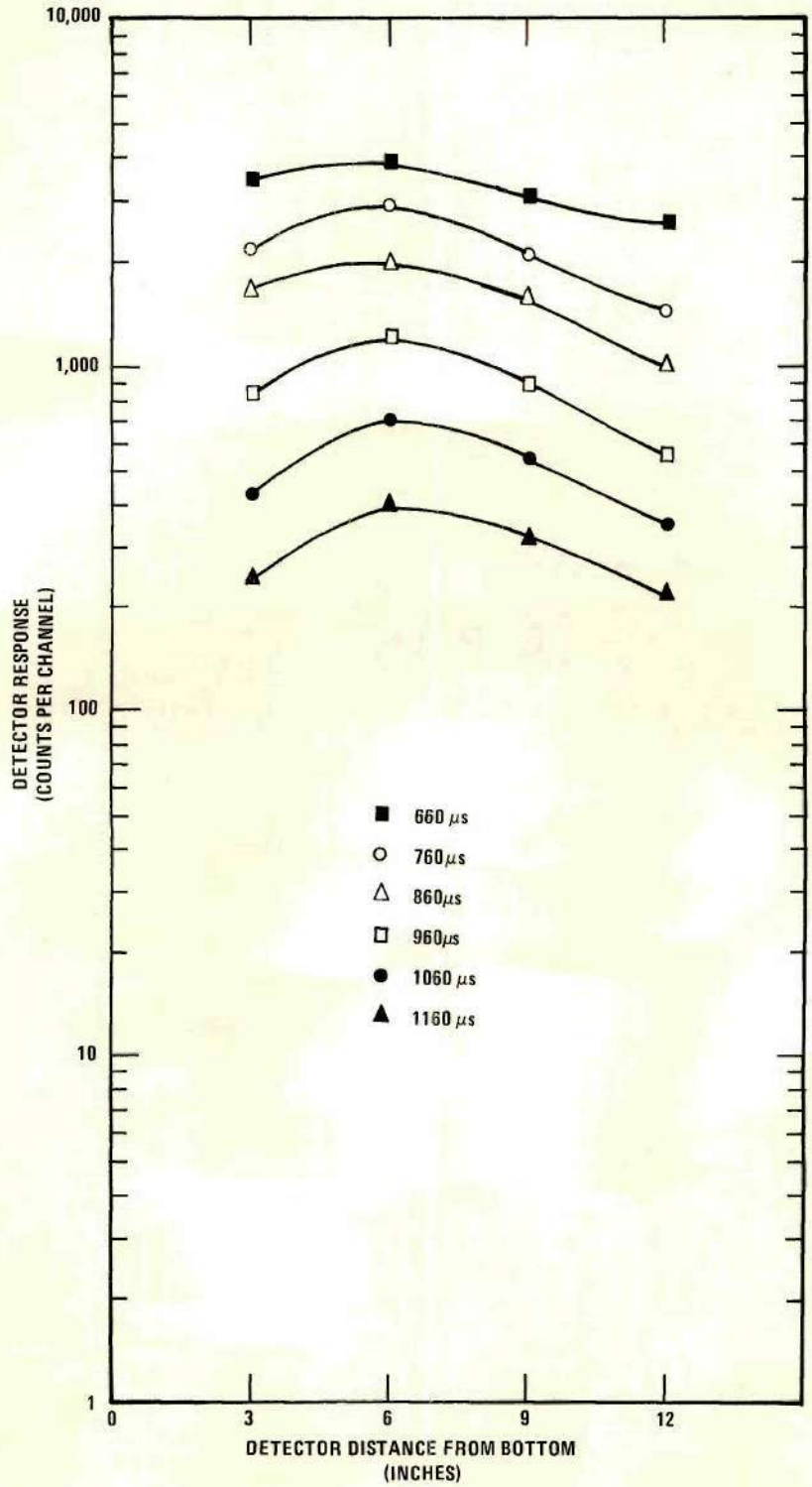

Figure 29. Difference Between Bare and Cadmium Covered Detector Responses as a Function of Time and Position in the Shield of the 33 Inch Core.

The Concluding Experiments

The previous experiments demonstrated that the technique of harmonically analyzing the axial flux was unfeasible due to the absence of a well-defined traveling wave. This resulted in the decision to use the classical technique of pulsed neutron data analysis. The resulting experimental plan was to measure the decay constants as a function of core height, then to void fifty percent of the water in the central fuel region and to remeasure the decay constants as a function of core height. In addition, the decay constants at the maximum core height were to be measured for forty and sixty percent centrally voided moderator. These measurements would permit comparison with predictions of the decay constants as a function of buckling and as a function of void fraction.

The core heights used in these experiments were 21, 29, and 33 1/2 inches. The 21 and 29 inch cores consisted of three and four fuel slugs, respectively, with the moderator level defining the core height. The ^{3}He detectors were placed 14 and 17 inches from the bottom of the core for these experiments. The void fractions were determined by the flow rates of Table 2. Each decay constant measurement used 2500 neutron generator bursts. The resulting data were corrected for background and dead time, the two detector results summed to improve statistical accuracy, and the results least squares fit to a single exponential by channel dropping. The results of this series of experiments are shown in Figures 30-33. These figures reflect the effect of minimizing neutron generator bursts through their wavy appearance. Nevertheless, portions of each curve appear flat and representative of the fundamental decay constant.

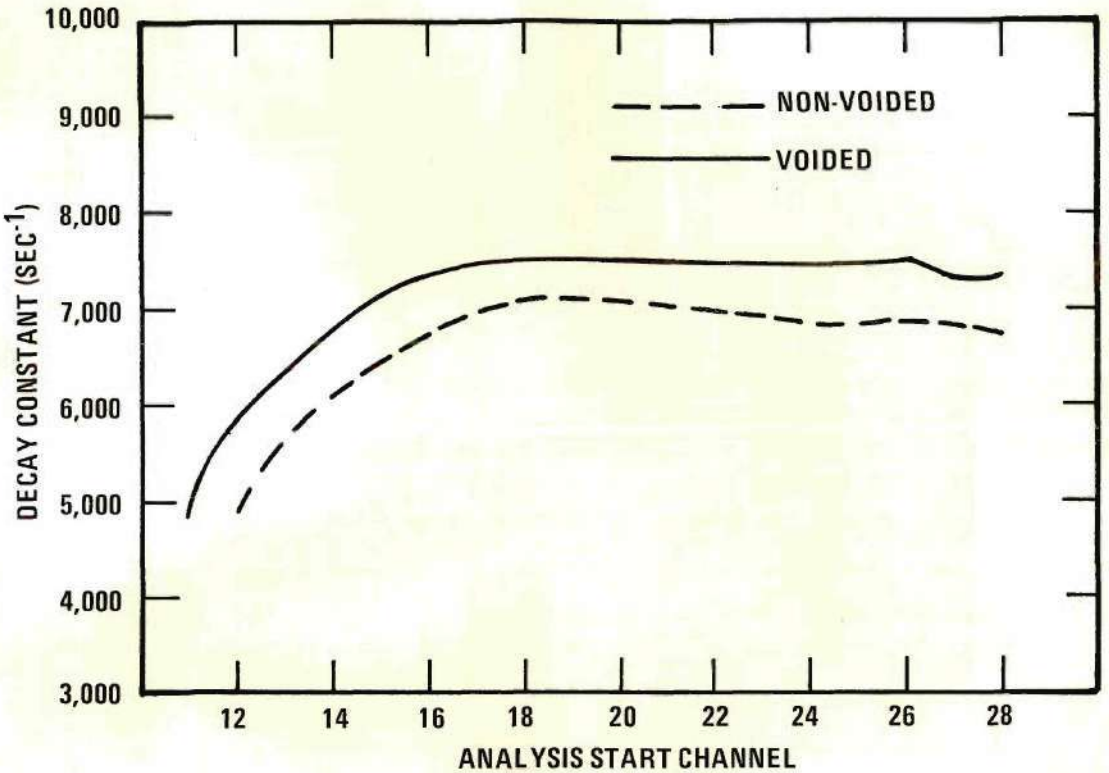

Figure 30. Decay Constant of the 21 Inch Core as a Function of Starting Channel for the 50 Percent Voided and Non-Voided Cases.

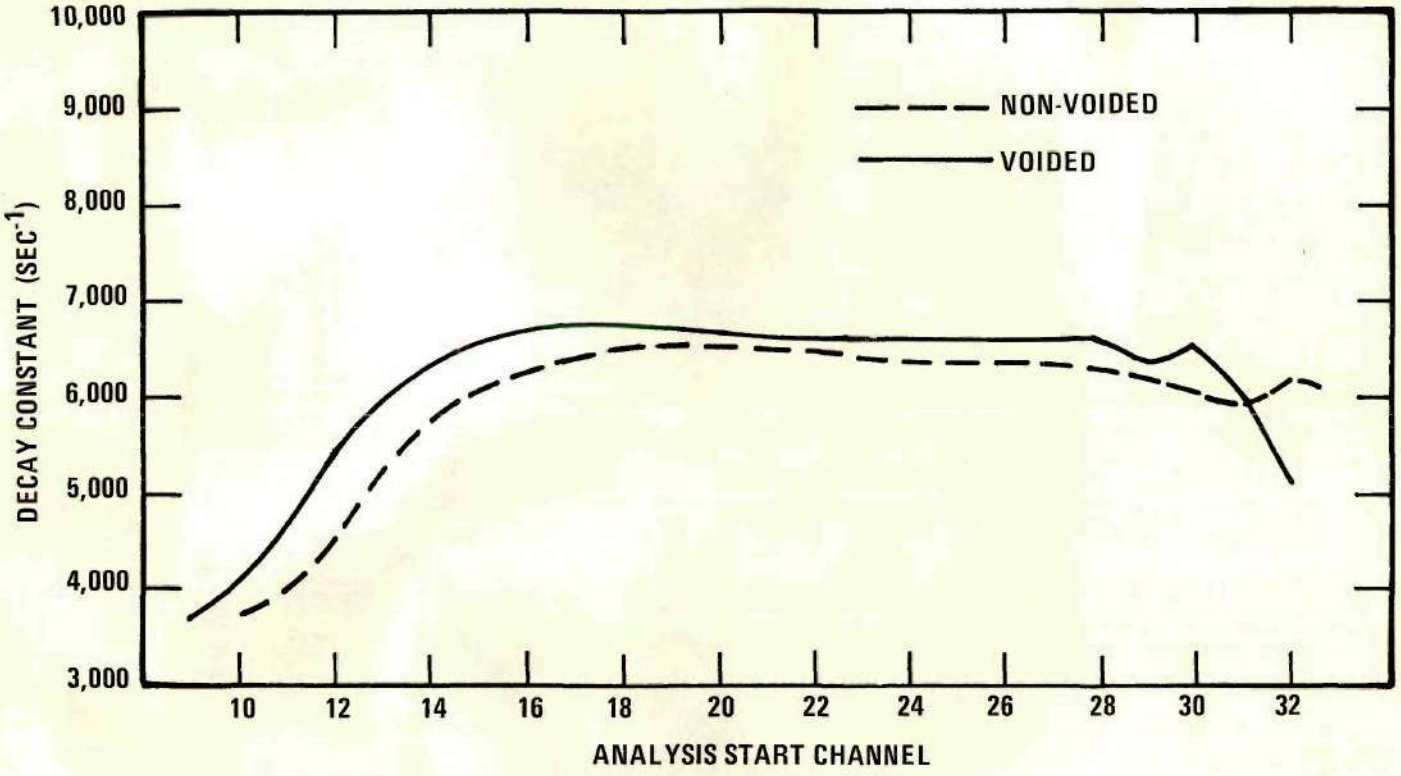

Figure 31. Decay Constant of the 29 Inch Core as a Function of Starting Channel for the 50 Percent Voided and Non-Voided Cases.

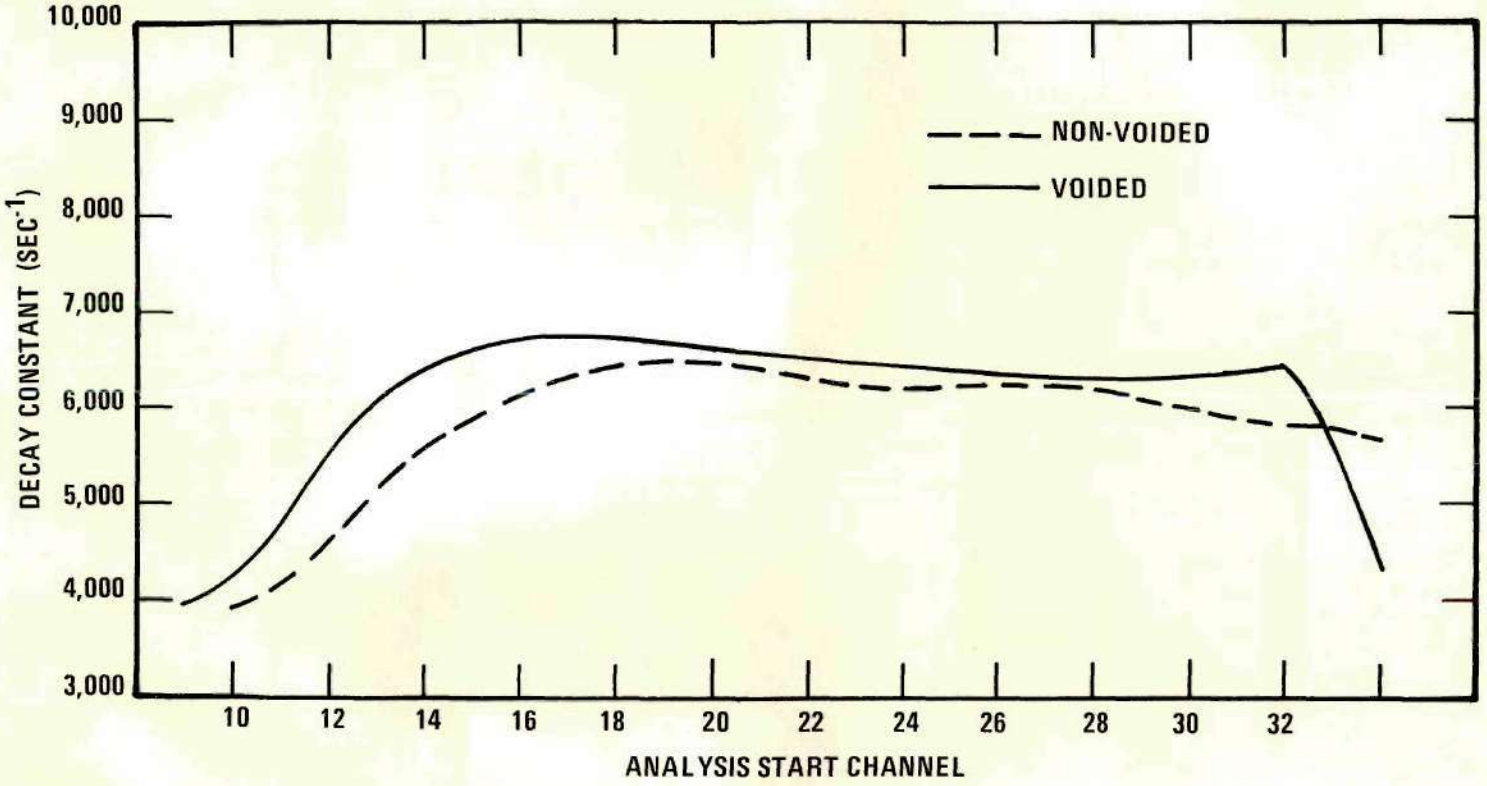

Figure 32. Decay Constant of the 33 1/2 Inch Core as a Function of Starting Channel for the 50 Percent Voided and Non-Voided Cases.

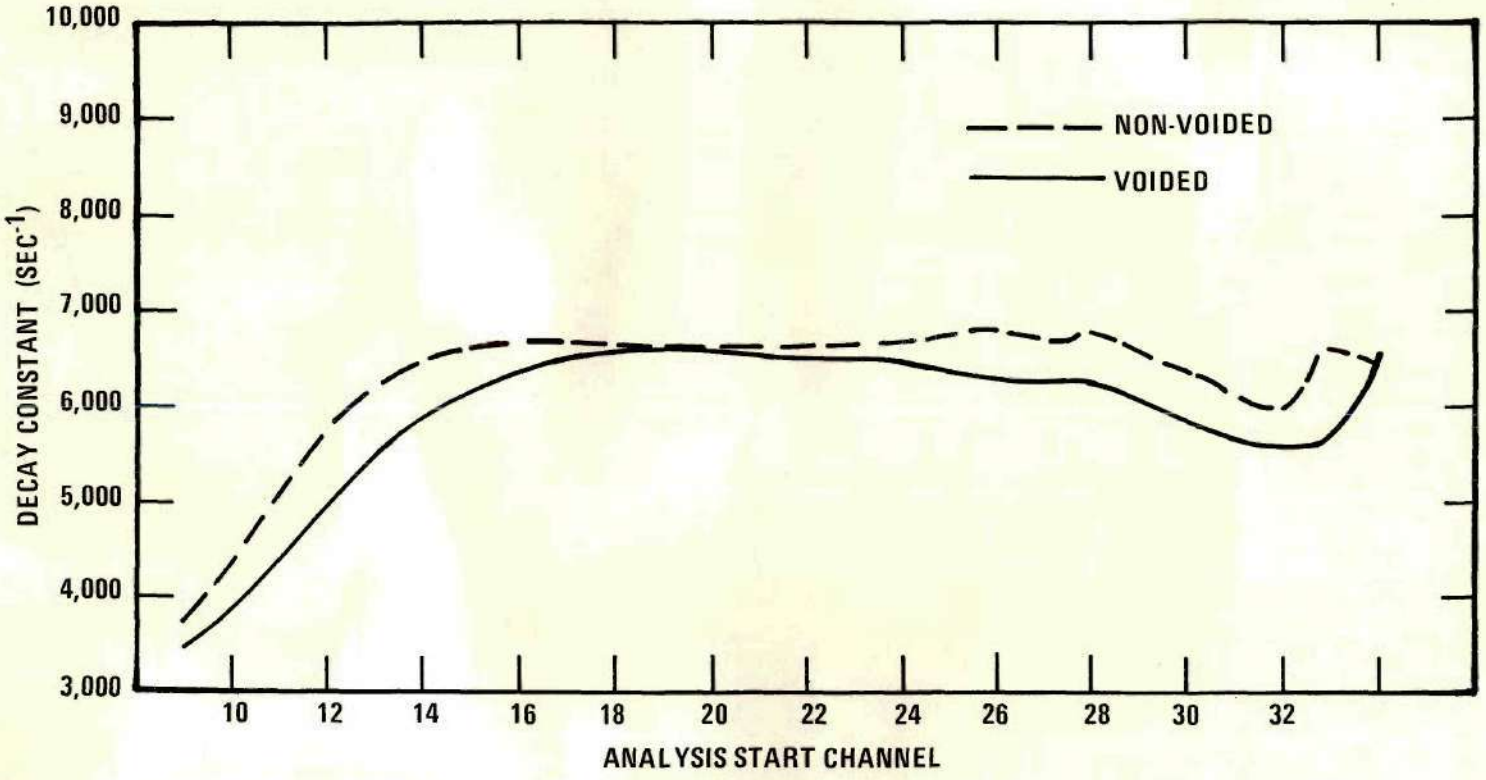

Figure 33. Decay Constant of the 33 1/2 Inch Core as a Function of Starting Channel for the 40 and 60 Percent Voided Cases.

Summary of Results

Figures 19, 20, 30, 31, 32, and 33, together with the computer printout containing the standard deviation of each decay constant for each starting channel, were used to determine the decay constant representative of each experiment. The criterion for choosing the decay constant was to select that decay constant whose standard deviation was sufficient to represent all decay constants lying along the asymptotic portion of the curve. This technique led to a large "error bar" associated with the decay constant, but one could be reasonably sure that the true decay constant lay within that error bar. The only exception to this was the 16 3/4 inch core with no voids (Figure 19) where a lack of a well-defined asymptotic region required the averaging of decay constants over channels 22-28. The error associated with this decay constant was chosen to be sufficiently large to encompass all reasonable experimental values. The results of the experiments are summarized in Table 3.

Table 3. Summary of Experimental Results

Core Height (inches)	Decay Constant Non-Voided Case (sec^{-1})	Voided Case Void Fraction	Decay Constant Voided Case (sec^{-1})
16.75	7532 ± 300	0.50	8101 ± 144
21.00	6883 ± 127	0.50	7460 ± 121
25.125	6361 ± 144	0.50	7014 ± 155
29.00	6093 ± 183	0.50	6603 ± 140
33.50	5975 ± 158	0.40	6254 ± 125
33.50	5975 ± 158	0.50	6300 ± 152
33.50	5975 ± 158	0.60	6796 ± 147

All measurements made at 21-22°C.

CHAPTER V

ANALYTICAL PROCEDURES AND RESULTS

To compare the measured effects with their calculations, it was necessary to obtain the lattice parameters that accurately characterized the subcritical assembly. These parameters are influenced by the space- and energy-dependent neutron spectrum. Cell calculations were performed to obtain energy spectrum weighted cross sections; core calculations were made to obtain cross sections spatially weighted over the core.

Cell Parameters

The computer programs TEMPEST II, THERMOS, and EXTERMINATOR-2 were used to create thermal cell parameters; FORM and EXTERMINATOR-2 were used to obtain the fast cell parameters. Four cells, corresponding to 0, 40, 50, and 60 percent voiding of moderator, were used. The hexagonal cell, which was the actual lattice geometry, was converted to a cylindrical cell having the same volume. Input requirements for TEMPEST II,[50] which calculates the thermal neutron flux spectra in the cell using several different scattering kernels and then provides microscopic and macroscopic cross sections averaged over those spectra, required that the cell be homogenized. The homogeneous problem was run and both the macroscopic and microscopic cross sections, weighted by the spectrum of the Wilkins heavy moderator kernel, were the output obtained. One parameter required for input was buckling, a somewhat ill-defined quantity. The following

method was used to determine buckling. The height of the cell was chosen to be the average of those used experimentally, 25 1/8 inches. No net leakage across a cell side boundary was assumed; only end leakage was permitted. Therefore:

$$B^2 = \left(\frac{\pi}{H+2\epsilon}\right)^2 . \tag{48}$$

Initially, a guess was made of $\bar{D}$, the diffusion coefficient. Then, the following relations were used

$$\lambda_{tr} = 3 \cdot \bar{D} \tag{49}$$

$$\epsilon = 0.7104\ \lambda_{tr} \tag{50}$$

where

λ_{tr} = transport mean free path

ϵ = extrapolation distance.

Finally B^2 was determined, TEMPEST II run, and the output parameter $\bar{D}$ was compared to the one used to determine the buckling. An iteration process was used until the initial and final $\bar{D}$'s agreed. This technique was applied to each of the four cases and yielded parameters that were consistent with the leakage.

Two sets of thermal cell parameters were developed from the output of TEMPEST II. The first set was the macroscopic parameters directly calculated by TEMPEST II, representing the homogeneous cell. The second set utilized the microscopic cross sections in an attempt to account for the

spatial variation of the flux across the actual heterogeneous cell.

The thermal microscopic cross sections were used to simulate a two-region cell resembling a fuel rod. The inner region contained natural uranium, the outer contained homogenized cladding, fuel rod wall, water, and void. EXTERMINATOR-2,[51] a multigroup, multiregion, two dimensional diffusion program, was used to determine the spatial flux distribution in the cell. The two-group, two-region, r-z geometry problem was run for each of the four void conditions with no return-current boundary conditions for the side of the cell and the zero flux condition at the top and bottom boundaries. The regionwise average flux, calculated by EXTERMINATOR-2, was used to weight the cross sections in each region as

$$\bar{\Sigma} = \frac{\Sigma_1 \bar{\phi}_1 V_1 + \Sigma_2 \bar{\phi}_2 V_2}{\bar{\phi}_1 V_1 + \bar{\phi}_2 V_2} \tag{51}$$

where

$\bar{\Sigma}$ = flux weighted cross section

$\bar{\phi}_i$ = average flux in region i

V_i = volume of region i

Σ_i = cross section of region i.

Thus, the cross sections in this set resulted from homogenizing the cell, determining the thermal neutron spectrum, spectrum weighting the microscopic cross sections, reconstructing the heterogeneous cell using spectrum-weighted cross sections, determining the space dependent flux, and finally flux weighting the cross sections.

A third set of thermal cross sections was obtained from THERMOS.

THERMOS[52] computes the scalar thermal neutron spectrum as a function of position in a heterogeneous cell by solving the integral transport equation and provides thermal spectra and flux averaged cross sections. It was used to directly produce the cell averaged cross sections. The version used required that a three region problem be run: (1) fuel in the central region, (2) clad, void space and fuel tube homogenized, and (3) water plus bubbles homogenized. The cell averaged neutron velocity, $\bar{v}$, was directly calculated by THERMOS and calculated from TEMPEST II by

$$\bar{v} = K \frac{\int \phi(E)dE}{\int n(E)dE} \tag{52}$$

where

$\phi(E)$ = energy dependent thermal flux

$n(E)$ = energy dependent thermal neutron density

$K = 2.482 \times 10^3$, a dimensionless proportionality constant.

The three sets of thermal cell parameters appear in Table 4.

FORM,[53] which calculates the multigroup slowing down spectrum and provides fast microscopic and macroscopic few group parameters, required the cell to be homogenized. Therefore, the same approach used with TEMPEST II was used with FORM. The diffusion coefficient iteration scheme was utilized to determine a buckling consistent with output parameters and two sets of one-group fast parameters were developed. The L-factor, required as input for each resonance absorber, is defined as

$$L = \frac{(RI)_{HET}}{(RI)_{HOM}} \tag{53}$$

Table 4. Summary of Thermal Group Cell Parameters

Void Fraction	Parameter	TEMPEST II Homogeneous	TEMPEST II Heterogeneous	THERMOS
0.0	$\bar{D}$ (cm)	0.32280	0.27563	0.26679
0.0	$\bar{\Sigma}_a$ (cm^{-1})	0.08793	0.07566	0.07035
0.0	$\nu\Sigma_f$ (cm^{-1})	0.10350	0.08671	0.07752
0.0	$\bar{v}$ (m/s)	3125.	---	2997.
0.40	$\bar{D}$	0.50950	0.47163	0.42637
0.40	$\bar{\Sigma}_a$	0.07658	0.06946	0.06364
0.40	$\nu\Sigma_f$	0.09298	0.08361	0.07444
0.40	$\bar{v}$	3422.	---	3221.
0.50	$\bar{D}$	0.59140	0.56502	0.49749
0.50	$\bar{\Sigma}_a$	0.07270	0.06688	0.06130
0.50	$\nu\Sigma_f$	0.08889	0.08136	0.07271
0.50	$\bar{v}$	3576.	---	3324.
0.60	$\bar{D}$	0.70190	0.69740	0.59419
0.60	$\bar{\Sigma}_a$	0.06805	0.06350	0.05845
0.60	$\nu\Sigma_f$	0.08373	0.07796	0.07023
0.60	$\bar{v}$	3785.	---	3470.

where

$(RI)_{HET}$ = heterogeneous resonance integral

$(RI)_{HOM}$ = homogeneous resonance integral.

The homogeneous resonance integral for ^{238}U was calculated from[54]

$$(RI)_{HOM} = 2.69 \left(\frac{\Sigma_s}{N_o}\right)^{0.471} \tag{54}$$

where

Σ_s = macroscopic scattering cross section of homogeneous cell

N_o = atom density of resonance absorber.

The heterogeneous resonance integral for ^{238}U was calculated from[55]

$$(RI)_{HET} = d[5.23 + 26.6\ D_{eff}\ \sqrt{S/M}\ ] \tag{55}$$

where

d = Doppler factor

D_{eff} = effective Dancoff correction

S/M = surface to mass ratio of ^{238}U in fuel.

Reference 55 states explicitly how to calculate $(RI)_{HET}$. The L-factor for ^{238}U was calculated for the 0, 40, 50, and 60 percent voided moderator cells. The L-factor for ^{235}U was chosen as 0.995 because it was very dilute.[56] The L-factors for ^{238}U were calculated to be 0.478, 0.605, 0.652, and 0.713 for the 0, 40, 50, and 60 percent cases, respectively.

The first set of fast parameters consisted of the macroscopic parameters directly calculated by FORM representative of the homogenized cell.

The second set resulted from flux weighting the microscopic cross sections with the results of the two-region EXTERMINATOR-2 problem which was previously described. One parameter which had to be approximated was the microscopic removal cross section for each element. This was done in the following manner. The macroscopic removal cross section may be defined as[57]

$$\Sigma_r = \frac{\overline{\xi\Sigma}_s}{\ln\left[\frac{E_o}{E}\right]} \tag{56}$$

where

$$\overline{\xi\Sigma}_s = \sum_i N_i \xi_i \sigma_i \tag{57}$$

N_i = atom density of the i^{th} isotope in the homogenized cell

ξ_i = average logarithmic energy decrement of the i^{th} isotope

σ_i = microscopic scattering cross section of the i^{th} isotope

E_o = average initial energy of neutrons

E = energy at the bottom of the fast group.

The macroscopic removal cross section and the fast spectrum weighted $\xi_i\sigma_i$ are calculated by FORM; the atom densities N_i are known input parameters. Thus, $\ln E_o/E$, representative of the homogenized cell spectrum was calculated. The microscopic removal cross section for each isotope was calculated as

$$\sigma_i^r = \frac{(\xi_i\sigma_i)}{\ln\left[\frac{E_o}{E}\right]} \tag{58}$$

where both terms on the right hand side are known. To create macroscopic cross sections for the two regions in the heterogeneous cell, the relationship used was[58]

$$\Sigma_r^j = \sum_i N_i^j \sigma_i^r \tag{59}$$

where

N_i^j = atom density of the i^{th} isotope in region j

Σ_r^j = macroscopic removal cross section in region j.

The two sets of fast parameters appear in Table 5.

Lattice Parameters

The lattice parameters were developed using combinations of the cell parameters and EXTERMINATOR-2. The subcritical assembly core was rectangular, so a cylindrical core of equal volume was input into a two-region, two-group, r-z EXTERMINATOR-2 calculation. The central region contained the 0, 40, 50, or 60 percent voided cell parameters depending on which experiment was being duplicated; the outer region contained only the zero percent void parameters. Four experimental void cases were studied: 0, 40, 50, and 60 percent voiding of moderator in the central region; the computer study to be described next relates to these void experiments. Each of the four void situations was represented with the three sets of cell parameters: homogeneous TEMPEST II-homogeneous FORM, heterogeneous TEMPEST II-heterogeneous FORM, and THERMOS-heterogeneous FORM.

The two-region, two-group average fluxes calculated by EXTERMINATOR-2 were used to weight the cell parameters by means of equation (51) to

Table 5. Summary of Fast Group Cell Parameters

Void Fraction	Parameter	FORM Homogeneous	FORM Heterogeneous
0.0	D^f (cm)	1.17947	0.99994
0.0	Σ_r (cm^{-1})	0.02163	0.02142
0.0	Σ_a^f (cm^{-1})	0.01147	0.01168
0.0	$\nu\Sigma_f$ (cm^{-1})	0.00652	0.00664
0.40	D^f	1.46952	1.28158
0.40	Σ_r	0.01115	0.01110
0.40	Σ_a^f	0.01099	0.01110
0.40	$\nu\Sigma_f$	0.00592	0.00587
0.50	D^f	1.56895	1.37884
0.50	Σ_r	0.00856	0.00852
0.50	Σ_a^f	0.01079	0.01087
0.50	$\nu\Sigma_f$	0.00569	0.00573
0.60	D^f	1.68552	1.49206
0.60	Σ_r	0.00601	0.00599
0.60	Σ_a^f	0.01049	0.01055
0.60	$\nu\Sigma_f$	0.00540	0.00543

produce the lattice parameters characteristic of the subcritical assembly. The age to the thermal group, τ, was then calculated from[59]

$$\tau = \frac{D^f}{\Sigma_r + \Sigma_a^f} \tag{60}$$

where

D^f = fast diffusion coefficient

Σ_r = macroscopic removal cross section

Σ_a^f = fast absorption cross section.

In addition, the infinite multiplication factor, k_∞, was obtained from the effective multiplication factor, output by EXTERMINATOR-2, by

$$k_\infty = k_{eff}\left(1 + \frac{\bar{D}B^2}{\bar{\Sigma}_a}\right) \exp(B^2\tau) \ , \tag{61}$$

where

$$B^2 = \left(\frac{\pi}{H+2\epsilon}\right)^2 + \left(\frac{2.405}{R+\epsilon}\right)^2 \tag{62}$$

$\epsilon = 2.1312\ \bar{D}$

H = height of computer model core

R = radius of computer model core

$\bar{D}$ = thermal diffusion coefficient, dependent on void fraction

$\bar{\Sigma}_a$ = thermal macroscopic absorption coefficient of the core

k_{eff} = effective multiplication factor of the model.

The core averaged thermal velocity was determined from

$$\bar{v} = \frac{\bar{\phi}_1 V_1 + \bar{\phi}_2 V_2}{n_1 V_1 + n_2 V_2} \ , \tag{63}$$

where

$\overline{\phi}_i$ = average thermal flux in region i

V_i = volume of region i

n_i = neutron density of region i.

The resulting final lattice parameters pertaining to decay constant prediction appear in Table 6.

Table 6. Pertinent Lattice Parameters of the Subcritical Assembly

Void Fraction	Parameter	TEMPEST/FORM Homogeneous	TEMPEST/FORM Heterogeneous	THERMOS/FORM Heterogeneous
0.0	$\bar{\Sigma}_a$ (cm^{-1})	0.08793	0.07566	0.07035
0.0	$\bar{D}$ (cm)	0.32280	0.27563	0.26679
0.0	k_∞	1.00931	0.97555	0.94691
0.0	τ (cm^2)	35.63	30.21	30.21
0.0	$\bar{v}$ (m/s)	3125.	3125.*	2997.
0.40	$\bar{\Sigma}_a$	0.08266	0.07273	0.06721
0.40	$\bar{D}$	0.38903	0.34303	0.32334
0.40	k_∞	0.94231	0.91242	0.89009
0.40	τ	43.85	37.46	37.41
0.40	$\bar{v}$	3256.	3259.*	3098.
0.50	$\bar{\Sigma}_a$	0.08008	0.07104	0.06564
0.50	$\bar{D}$	0.42142	0.37748	0.35171
0.50	k_∞	0.92844	0.89748	0.87619
0.50	τ	46.96	40.23	40.14
0.50	$\bar{v}$	3342.	3347.*	3159.
0.60	$\bar{\Sigma}_a$	0.07651	0.06850	0.06341
0.60	$\bar{D}$	0.46801	0.42815	0.39309
0.60	k_∞	0.92030	0.88748	0.86674
0.60	τ	50.83	43.68	43.54
0.60	$\bar{v}$	3473.	3483.*	3256.

*This value is the TEMPEST homogeneous $\bar{v}$ weighted with the TEMPEST/FORM heterogeneous flux.

CHAPTER VI

DISCUSSION OF ANALYTICAL AND EXPERIMENTAL RESULTS

The decay constants of the various configurations and void fractions of the subcritical assembly constitute the experimental results and appear in Table 3. The analytical results, consisting of the lattice parameters, were presented in Table 6. To achieve a useful comparison, the lattice parameters were converted to decay constants by means of equation (23) which can be written as

$$\alpha_o(B^2) = \overline{v}\,[\overline{\Sigma}_a + \overline{D}\,B^2 + \overline{\Sigma}_a\,(1-\overline{\beta})\,k_\infty \exp(-B^2\tau)] \qquad (64)$$

where the various parameters are given in Table 6, except for $\overline{\beta}$ which is assumed equal to 0.0065 and B^2 which was determined from

$$B^2 = \left(\frac{\pi}{H+2\epsilon}\right)^2 + \left(\frac{\pi}{W+2\epsilon}\right)^2 + \left(\frac{\pi}{L+2\epsilon}\right)^2 \qquad (65)$$

where H, W, L = height, width, and length of the core, and

$\epsilon = 2.1312\,\overline{D}$.

The predicted decay constants for the non-voided case appear in Table 7; those for the voided cases in Table 8. These values are significantly greater than those in Table 3. The THERMOS/FORM heterogeneous predictions and the experimental results are presented graphically in Figures 34 and 35. The straight lines in these figures show that the decay

Table 7. Decay Constants Predicted for the Non-Voided Cases by Each Model

Core Height (in.)	TEMPEST/FORM Homogeneous B^2 (cm^{-2})	α/v (cm^{-1})	α (sec^{-1})	TEMPEST/FORM Heterogeneous B^2 (cm^{-2})	α/v (cm^{-1})	α (sec^{-1})	THERMOS/FORM Heterogeneous B^2 (cm^{-2})	α/v (cm^{-1})	α (sec^{-1})
16.75	0.013197	0.037095	11592	0.013311	0.030278	9462	0.013332	0.029666	8891
21.00	0.011378	0.032817	10255	0.011468	0.026962	8426	0.011485	0.026635	7983
25.125	0.010403	0.030425	9508	0.010484	0.025126	7852	0.010499	0.024957	7480
29.00	0.009834	0.028995	9061	0.009910	0.024032	7510	0.009924	0.023959	7181
33.50	0.009401	0.027890	8716	0.009473	0.023191	7247	0.009487	0.023191	6950

Table 8. Decay Constants Predicted for the Voided Cases by Each Model

Core Height (in.)	Void Fraction	TEMPEST/FORM Homogeneous B^2 (cm^{-2})	α/v (cm^{-1})	α (sec^{-1})	TEMPEST/FORM Heterogeneous B^2 (cm^{-2})	α/v (cm^{-1})	α (sec^{-1})	THERMOS/FORM Heterogeneous B^2 (cm^{-2})	α/v (cm^{-1})	α (sec^{-1})
16.75	0.50	0.012965	0.045364	15161	0.013068	0.038527	12895	0.013129	0.036522	11537
21.00	0.50	0.011192	0.041127	13745	0.011274	0.035048	11731	0.011323	0.033351	10536
25.125	0.50	0.010238	0.038724	12942	0.010311	0.033094	11077	0.010354	0.031573	9974
29.00	0.50	0.009679	0.037273	12457	0.009747	0.031922	10684	0.009788	0.030507	9637
33.50	0.40	0.009301	0.034810	11334	0.009370	0.029532	9624	0.009400	0.028438	8810
33.50	0.50	0.009253	0.036146	12080	0.009318	0.031015	10381	0.009357	0.029682	9377
33.50	0.60	0.009184	0.036947	12832	0.009243	0.032121	11188	0.009295	0.030635	9975

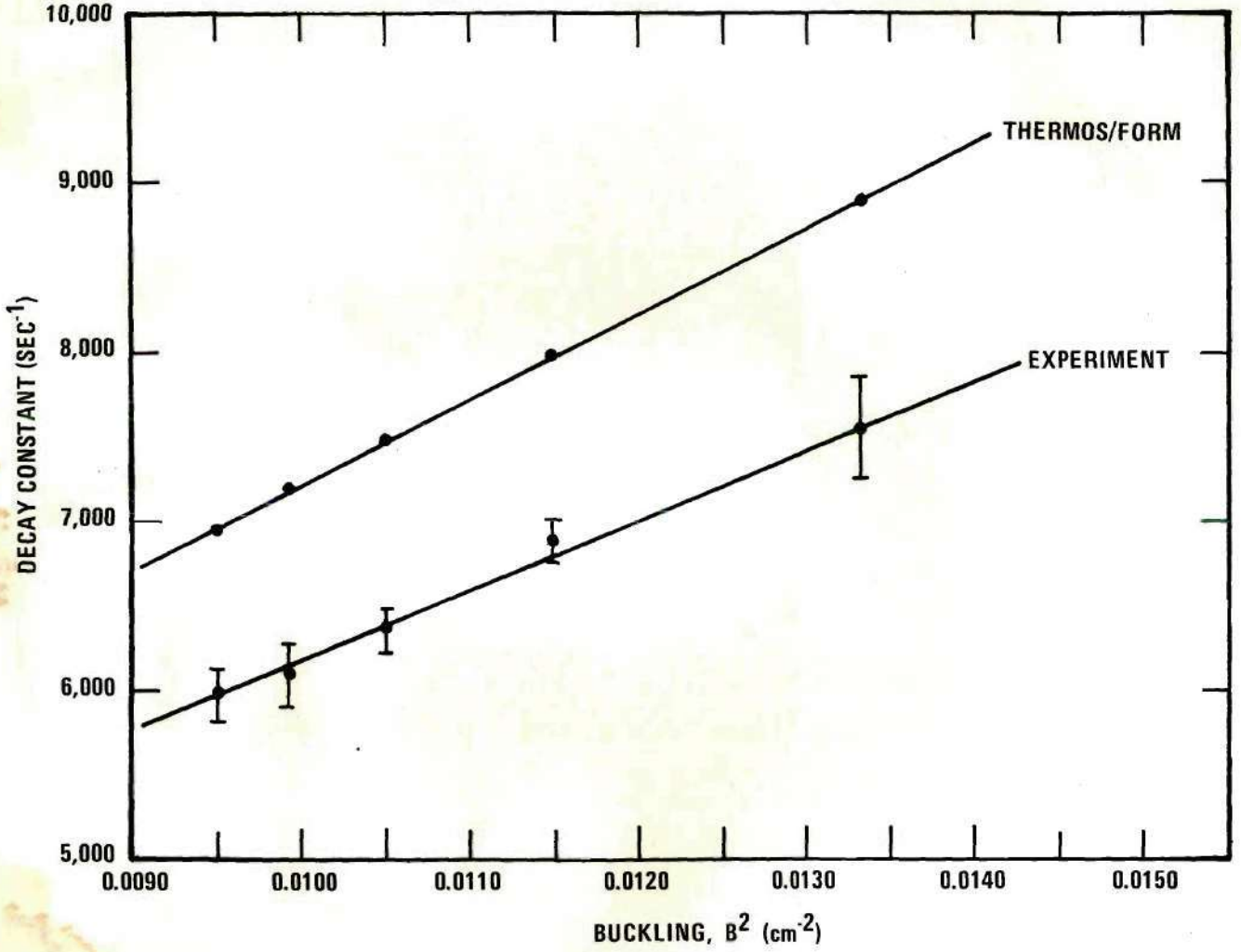

Figure 34. Experimental and THERMOS/FORM Predicted Decay Constants as a Function of Buckling for the Non-Voided Case.

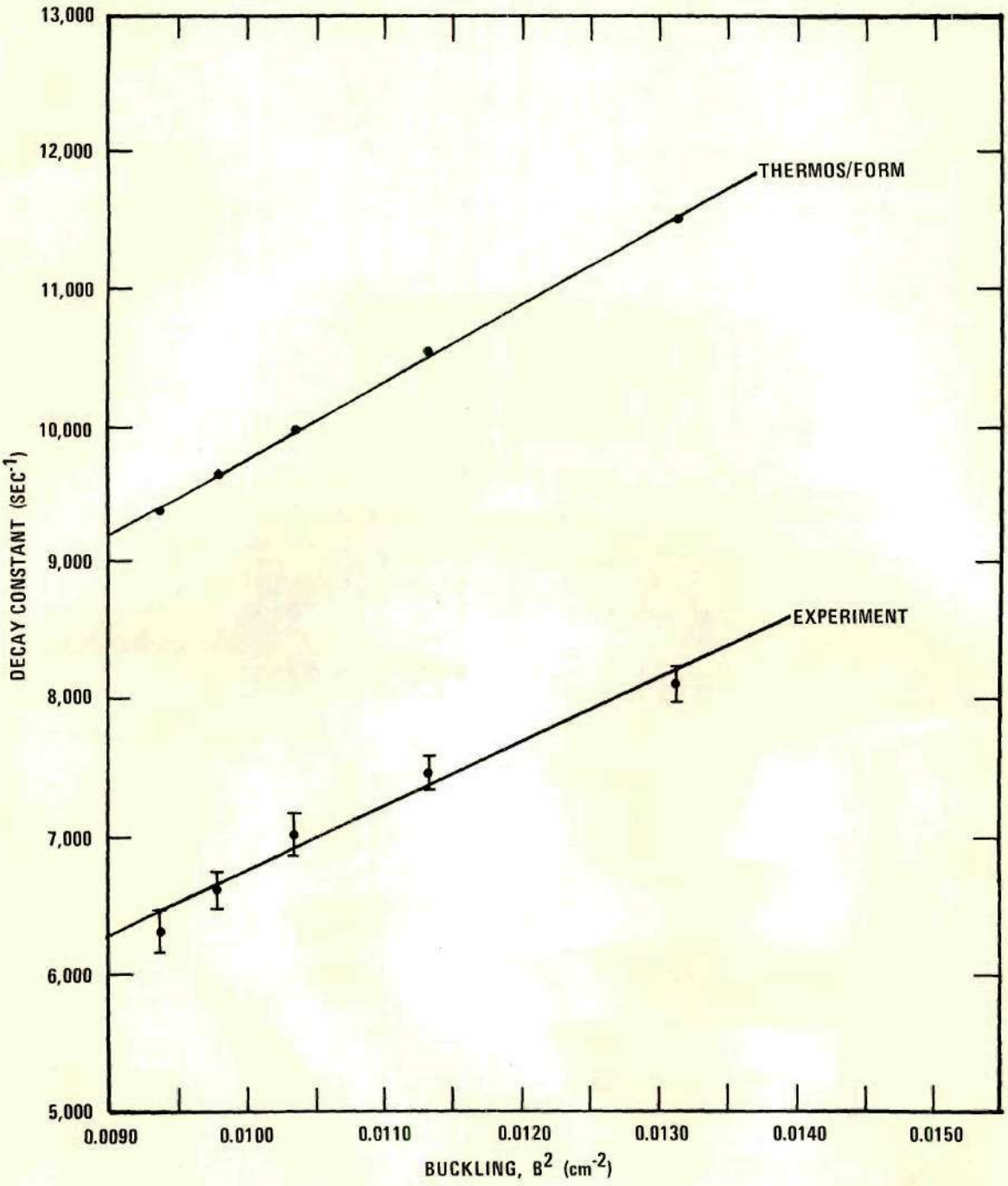

Figure 35. Experimental and THERMOS/FORM Predicted Decay Constants as a Function of Buckling for the 50 Percent Voided Case.

constant for the non-voided case appears to be a linear function of buckling. For the 50 percent void case, the experimental decay constant appears less well-represented by a linear function of buckling. Ideally, the predicted and experimental curves should agree in each case. In the Introduction, it was pointed out that the effect of diffusion cooling is large for pulsed multiplying media. For non-multiplying media this effect is corrected by subtracting the term CB^4 as shown in equation (11). This method was applied to our multiplying media findings as

$$\alpha_{experimental} = \alpha_{predicted} - CB^4 \ . \tag{66}$$

A least squares fit of a straight line was made to the difference between the experimental and THERMOS/FORM heterogeneous decay constants as a function of B^4 for both the non-voided and 50 percent voided cases. The value of C was found to be $9.256 \pm 0.616 \times 10^6$ cm^4/sec for the non-voided case and $2.483 \pm 0.068 \times 10^7$ cm^4/sec for the voided case. The results of applying these corrections are shown in Table 9. The corrected decay constants for the non-voided case are in good agreement with the corresponding measured decay constants; the corrected voided decay constants are not. In order to further improve the agreement between prediction and measurement, a quadratic equation was subtracted from the THERMOS/FORM heterogeneous decay constants and equation (66) became

$$\alpha_{experiment} = \alpha_{predicted} - (a + bB^2 + cB^4) \ . \tag{67}$$

Table 9. Comparison Between Experimental Decay Constants and THERMOS/FORM Predicted Decay Constants Using CB^4 and Quadratic Corrections

	Non-Voided Cases			Voided Cases			
Core Height (in.)	CB^4 Correction $\alpha(sec^{-1})$	Quadratic Correction $\alpha(sec^{-1})$	Experimental Non-Voided $\alpha(sec^{-1})$	Void Fraction	CB^4 Correction $\alpha(sec^{-1})$	Quadratic Correction $\alpha(sec^{-1})$	Experimental Voided $\alpha(sec^{-1})$
16.75	7246	7574	7532 ± 300*	0.50	7258	8097	8101 ± 144*
21.00	6762	6845	6883 ± 127	0.50	7353	7480	7460 ± 121
25.125	6460	6409	6361 ± 144	0.50	7313	6968	7014 ± 155
29.00	6269	6141	6093 ± 183	0.50	7259	6611	6603 ± 140
33.50	6117	5929	5975 ± 158	0.40	6616	5748	6254 ± 125
33.50	6117	5929	5975 ± 158	0.50	7203	6300	6300 ± 152
33.50	6117	5929	5975 ± 158	0.60	7830	6900	6796 ± 147

*The physical significance of the error limits was discussed at the end of Chapter IV.

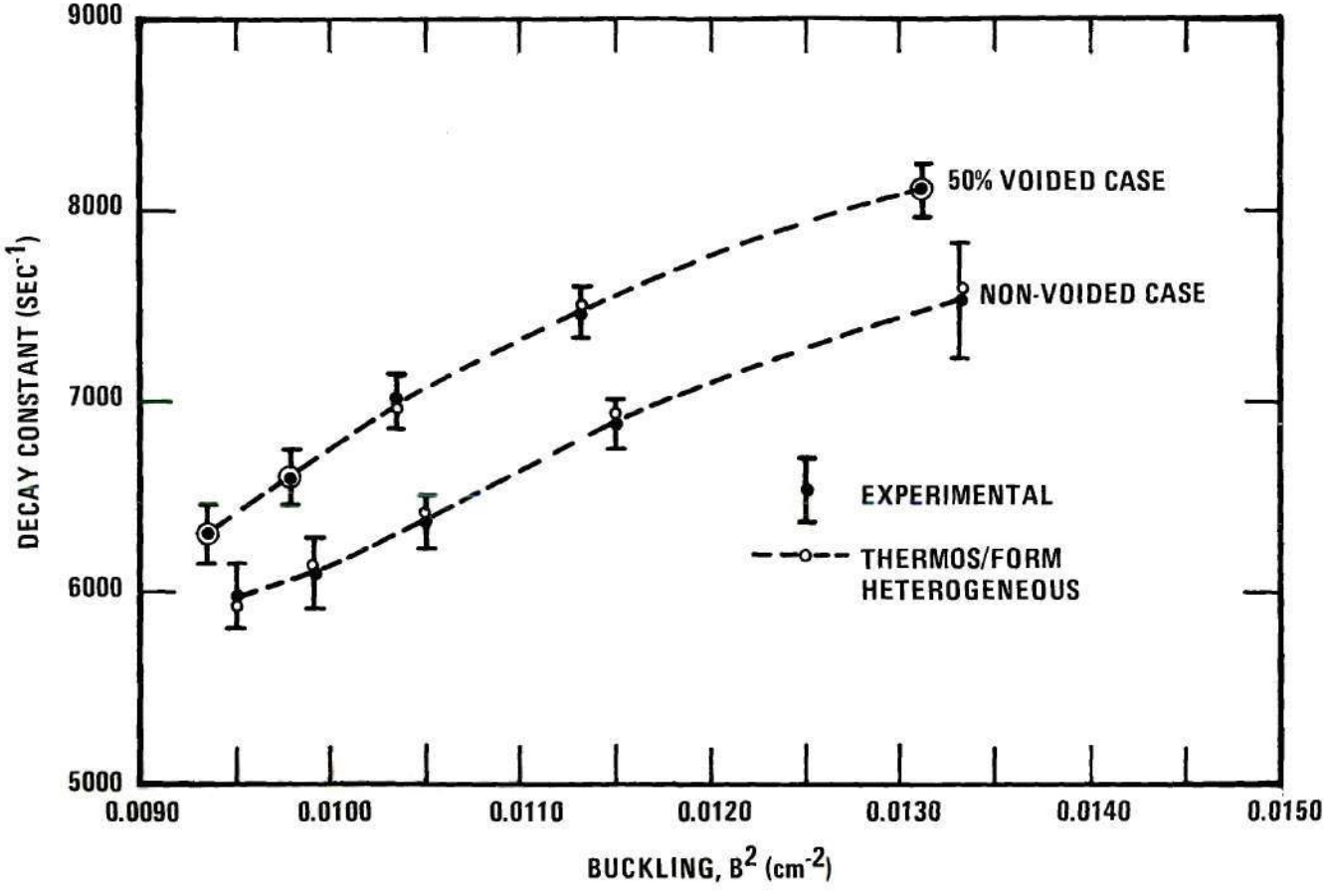

Figure 36. Experimental and THERMOS/FORM Predicted Decay Constants as a Function of Buckling for the Non-Voided and 50 Percent Voided Cases Using the Quadratic Correction.

A least squares fit of a quadratic was made to the difference between the experimental and theoretical decay constants as a function of B^2 for both the non-voided and 50 percent voided cases. The values of the coefficients were found to be $a = 1.535 \times 10^3$ /sec, $b = -1.476 \times 10^5$ cm^2/sec, and $c = 9.843 \times 10^6$ cm^4/sec for the non-voided case and $a = 9.247 \times 10^3$ / sec, $b = -1.202 \times 10^6$ cm^2/sec, and $c = 5.785 \times 10^7$ cm^4/sec for the voided case. The results of applying the quadratic corrections are shown in Table 9. The corrected decay constants are in good agreement with the experimental decay constants for the non-voided and 50 percent voided cases. The 60 percent voided case shows good agreement; the 40 percent voided case fair. The presence of bubbles in the moderator causes neutron streaming. This streaming, along with diffusion cooling, is not accounted for by the nuclear programs when the voids are homogenized with the moderator. It is believed that this causes the decay constant correction to be more complex than $-CB^4$. Figure 36 compares the results of using the THERMOS/FORM heterogeneous parameters corrected by the quadratic equation.

CHAPTER VII

CONCLUSIONS

The decay constants of a light-water-moderated subcritical assembly have been measured for both voided and non-voided systems. These results appear in Table 3. As expected, larger void fractions result in more rapid asymptotic decay. These decay constants have been predicted using lattice parameters determined by three models which were denoted as TEMPEST/FORM homogeneous, TEMPEST/FORM heterogeneous, and THERMOS/FORM heterogeneous. These results appear in Tables 7 and 8. The TEMPEST/FORM heterogeneous and the THERMOS/FORM heterogeneous models provide consistent values. These results also demonstrate the limited ability of the three models to predict the experimentally determined decay constants. The THERMOS/FORM heterogeneous model provides the best agreement with measurement. This model overestimates the decay constants for the non-voided case by approximately 115 percent and the decay constants for the voided case by approximately 140 percent. It is believed that the measured decay constants are well within five percent of their true values. This error arises from the statistical nature of the data. The error associated with the decay constants can effectively be made as small as desired by the continued pulsing of the sample and the collection of large amounts of data. It is felt that the error associated with the decay constants in this work is of a sufficiently small magnitude that the conclusions drawn between experiment and prediction are independent of this

error.

From the data contained in Figures 34 and 35, it is observed that the $\alpha_o(B^2)$ curves generated by the experimental and predicted decay constants differ in absolute magnitude and appear to have different slopes. One then concludes that the measured decay constants were affected by a spectrum cooling. In a pulsed neutron experiment the preferential leakage of higher energy neutrons softens the energy spectrum. The addition of bubbles to a sample amplifies this preferential leakage effect and, in addition, may introduce streaming which favors the leakage of higher energy neutrons, also resulting in spectral softening. It is this spectral cooling effect which is not accounted for by the nuclear analysis programs used in this work. These programs actually show the energy spectrum hardening with increasing void fraction in exact opposition to the conclusion given here. This anomaly is a result of the void as represented in the nuclear analysis programs decreasing the density of the water moderator, making it a less effective thermalizer. As a consequence, the spectrum hardens as the water loses its effectiveness.

The results of the conventional method of treating diffusion cooling, by using $-CB^4$, appear in Table 9. It is seen that this conventional treatment is applicable to the non-voided case, but fails in the 50 percent voided case. This failure is most likely due to effects arising from the neutron streaming. In order to improve the agreement between prediction and measurement, a quadratic equation, equation (67), was used in place of the term $-CB^4$ and these results also appear in Table 9. These findings are graphically compared to experiment in Figure 36 and good

agreement between the measured and predicted decay constants is seen. The complexity of this fitting function indicates that perhaps several of the lattice parameters for the voided case are inaccurate as a result of homogenizing the voids.

The space-, energy-, and time-dependent neutron flux was investigated and the results appear in Chapter III. The asymptotic flux shape along the vertical centerline of the core was found to be asymmetric. This asymmetric flux shape was attributed to the presence of higher space modes of the neutron flux.

CHAPTER VIII

RECOMMENDATIONS

Several extensions of this work, varying in degree of difficulty, could be undertaken. Repeating the experiment using a neutron generator with greater yield, higher allowable pulse rate, and increased neutron production lifetime, would increase the statistical accuracy of the measured decay constants. The experimental portion of this thesis, consisting of the measurement of the decay constants of the voided and non-voided cores, and the investigation of the space-, energy-, and time-dependent neutron flux, required 47,428 neutron generator bursts, a significant fraction of the total yield of the sealed-tube source. The use of two detector systems allowed the decay constants to be determined to within five percent.

If, in addition to increasing accuracy many values of B^2 were used, equation (23) could be least-squares fit to the data by the methods of Bevington.[45] This would permit direct measurement of $\overline{v\Sigma}_a$, $\overline{vD}$, $(1-\bar{\beta})k_\infty$, and τ. Also, a lattice more representative of current power reactor designs might be used, perhaps borrowed from a vendor of pressurized water reactors.

A thorough investigation of the space-, energy-, and time-dependent distribution of neutrons following a burst might lead to an interesting, more completely developed explanation of the behavior of the flux in the lower half of the core.

Another very interesting topic of research along these same lines would be the measurement and prediction of the effects of voids on the anisotropy of the diffusion parameters. This would require the capability of pulsing the core from the side in addition to pulsing from the bottom. The decay constant in this case would take the form:

$$\alpha_o(B_z^2, B_r^2) = \overline{v\Sigma}_a + \overline{vD}_{\parallel} B_z^2 + \overline{vD}_{\perp} B_r^2 - \overline{v\Sigma}_a(1-\bar{\beta}) e^{-B_r^2\tau_{\perp} - B_z^2\tau_{\parallel}} \qquad (68)$$

as detailed in Appendix E, where the subscripts denote neutron transport parallel and perpendicular to the fuel rods. Predictions of the resulting parameters could be based on the works of Behrens[26] and Benoist.[27,31]

A theoretical treatment of the diffusion cooling effect of pulsed multiplying assemblies would be a valuable and much needed contribution to the field of neutron physics.

APPENDICES

APPENDIX A

DETAILS OF DATA REDUCTION

The raw data were corrected for background, dead time, differences in detector efficiency, and sometimes monitor normalization, depending on the particular experiment. Background was defined as the average number of counts in channels 51-75 and was subtracted from each channel used in the analysis of the time dependent neutron decay. The first channel used was the third or fourth channel preceding the channel containing the maximum number of counts and the last channel used was the one containing about twice background. For the preliminary experiments on light-water and on the energy measurements in the reflector, background was always found to be zero.

The dead time correction was then applied to the background corrected data and was

$$DC = \frac{BC}{1 - BC \times \tau_{eff}} \tag{A-1}$$

where

DC = dead time corrected counts per channel

BC = background corrected counts per channel

τ_{eff} = effective dead time.

The effective dead time is

$$\tau_{eff} = \frac{8.2\ \mu sec}{ACW \times NB} \tag{A-2}$$

where

ACW = analyzer channel width (40 μsec)

NB = total number of neutron generator bursts for a given data collection cycle.

Next, the data from the less efficient detector channel were multiplied by the correction factor, whose value as determined by the method described in Chapter II was 1.006.

Lastly, when necessary, the monitor normalization correction was made. The neutron generator output per burst did vary, through variation in gas pressure and target burnup, and the events recorded by the monitor system were directly proportional to the generator output. As a result, by multiplying the data corresponding to the lesser monitor reading by the quotient of the greater monitor reading divided by the lesser, the resulting data were normalized with respect to the larger neutron output. These four corrections yielded what could be considered the "true" number of counts per channel.

One additional calculation made during the data reduction stage was the determination of the time after a neutron generator burst which corresponded to a particular analyzer channel. This relationship was

$$T = ACW \times (DR + CH-2) + ((CH-1) \times 10) + ACW/2 \qquad (A-3)$$

where

T = time to midpoint of channel (μsec)

ACW = analyzer channel width (μsec)

CH = channel number (as on output tape).

APPENDIX B

CURVE FITTING PROCEDURES

The two types of curves fit to the experimental data were the single exponential and the straight line. The methods used to curve fit were adapted from Bevington,[45] who thoroughly develops the theory of curve fitting and error analysis and provides numerous nuclear engineering oriented examples and ready-to-use FORTRAN subroutines.

The single exponential is reduced to an equivalent straight line by taking the natural logarithm of both sides, i.e.,

$$\ln y = \ln [A\, e^{Bt}] \tag{B-1}$$

which reduces to

$$\ln y = \ln A + Bt \ , \tag{B-2}$$

a straight line. Thus, the only curve which need be fitted to exponential or linear data is a straight line. A straight line was fitted to the data by the method of least squares which requires the coefficients of the fitted straight line to minimize the weighted sum of the square of the difference between the experimental "y" value and the fitted "y" value. The coefficients of least squares fitting

$$y = a + bx \tag{B-3}$$

to data of the form (y_i, x_i) are

$$a = \frac{1}{\Delta}\left(\sum \frac{x_i^2}{\sigma_i^2}\sum \frac{y_i}{\sigma_i^2} - \sum \frac{x_i}{\sigma_i^2}\sum \frac{x_i y_i}{\sigma_i^2}\right) \tag{B-4}$$

$$b = \frac{1}{\Delta}\left(\sum \frac{1}{\sigma_i^2}\sum \frac{x_i y_i}{\sigma_i^2} - \sum \frac{x_i}{\sigma_i^2}\sum \frac{y_i}{\sigma_i^2}\right) \tag{B-5}$$

$$\Delta = \sum \frac{1}{\sigma_i^2}\sum \frac{x_i^2}{\sigma_i^2} - \left(\sum \frac{x_i}{\sigma_i^2}\right)^2 \tag{B-6}$$

where σ_i is the standard deviation of the data point y_i. The square of the standard deviations of the coefficients are

$$\sigma_a^2 \simeq \frac{1}{\Delta}\sum \frac{x_i^2}{\sigma_i^2} \tag{B-7}$$

$$\sigma_b^2 \simeq \frac{1}{\Delta}\sum \frac{1}{\sigma_i^2} \, . \tag{B-8}$$

For a counting experiment the standard deviation, σ_i, of the number of counts in channel i, y_i, is $\sqrt{y_i}$. For a straight line fit to the counting data, then,

$$\sigma_i^2 = y_i \, . \tag{B-9}$$

For an exponential fit, however, a transformation was made to obtain a linear equation and this must be taken into account when determining the σ_i of the transformed variable, $\ln y_i$. The transformed standard deviation, σ_i', is related to the standard deviation of the counts in channel i, σ_i,

by

$$\sigma_i' = \frac{d(\ln y_i)}{d y_i} \sigma_i = \frac{\sigma_i}{y_i} = \frac{1}{\sqrt{y_i}} \qquad \text{(B-10)}$$

Thus

$\sigma_i = \sqrt{y_i}$ for a linear fit

$\sigma_i = 1/\sqrt{y_i}$ for an exponential fit.

APPENDIX C

EQUIVALENCE OF PRODUCT OF THE AVERAGE AND AVERAGE OF THE PRODUCT

With the following definitions[60,61]

$$\overline{D} = \frac{\int_0^\infty D(E)\ \phi_M(E)\ dE}{\int_0^\infty \phi_M(E)\ dE} \tag{C-1}$$

and

$$\overline{v} = \frac{\int_0^\infty v n_M(v)\ dv}{\int_0^\infty n_M(v)\ dv}\ , \tag{C-2}$$

where ϕ_M is the Maxwellian flux

n_M is the Maxwellian neutron density,

we have[62]

$$\overline{vD} = \frac{\int_0^\infty D(E)\ \phi_M(E)\ dE}{\int_0^\infty \phi_M(E)\ dE} \cdot \frac{\int_0^\infty v n_M(v)\ dv}{\int_0^\infty n_M(v)\ dv} \tag{C-3}$$

$$= \frac{\int_0^\infty D(E)\ \phi_M(E)\ dE}{\int_0^\infty \phi_M(E)\ dE} \cdot \frac{\int_0^\infty \phi_M(E)\ dE}{\int_0^\infty \frac{1}{v} \cdot v n_M(v)\ dv}$$

(continued)

$$= \frac{\int_o^\infty D(E)\ \phi_M(E)\ dE}{\int_o^\infty \frac{1}{v} \cdot \phi_M(E)\ dE} = \overline{D}_o \ .$$

Also, defining[63]

$$\overline{\Sigma}_a = \frac{\int_o^\infty \Sigma_a(E)\ \phi_M(E)\ dE}{\int_o^\infty \phi_M(E)\ dE} \qquad \text{(C-4)}$$

we have

$$\overline{v\Sigma}_a = \frac{\int_o^\infty v n_M(v)\ dv}{\int_o^\infty n_M(v)\ dv} \cdot \frac{\int_o^\infty \Sigma_a(E)\ \phi_M(E)\ dE}{\int_o^\infty \phi_M(E)\ dE} \qquad \text{(C-5)}$$

$$= \frac{\int_o^\infty \phi_M(E)\ dE}{\int_o^\infty n_M(v)\ dv} \cdot \frac{\int_o^\infty \Sigma_a(E)\ \phi_M(E)\ dE}{\int_o^\infty \phi_M(E)\ dE}$$

$$= \frac{\int_o^\infty v\Sigma_a(E)\ n_M(E)\ dE}{\int_o^\infty n_M(E)\ dE} = \overline{v\Sigma}_a \ .$$

APPENDIX D

DECAY CONSTANT OF MULTIPLYING MEDIUM

The thermal diffusion equation for a bare homogeneous reactor is:

$$\bar{D}\,\nabla^2\phi(\vec{r},t) - \bar{\Sigma}_a\,\phi(\vec{r},t) + S = \frac{1}{\bar{v}}\frac{\partial\phi(\vec{r},t)}{\partial t} \qquad \text{(D-1)}$$

where the source term is

$$S = \nu\Sigma_f \epsilon p_{th}\, L_f(1-\bar{\beta})\,\phi(\vec{r},t)\,. \qquad \text{(D-2)}$$

This is seen as:

$\Sigma_f\phi$ = number of fissions/cm^3-sec in the medium

$\epsilon\nu\Sigma_f\phi$ = number of fission neutrons/cm^3-sec in the medium

$(1-\bar{\beta})\epsilon\nu\Sigma_f\phi$ = number of prompt fission neutrons/cm^3-sec in the medium

$p_{th}L_f(1-\bar{\beta})\epsilon\nu\Sigma_f\phi$ = number of prompt fission neutrons/cm^3-sec which slow to thermal energy escaping fast leakage and resonance capture.

The solution of equation (D-1) incorporates separation of variables:

$$\phi(\vec{r},t) = R(\vec{r})\cdot\phi(t) \qquad \text{(D-3)}$$

where the time equation is (after equation (6) in the main paper):

$$\frac{1}{\phi_{1mn}(t)} \cdot \frac{d\phi_{1mn}(t)}{dt} = - (\overline{vD}\ B^2_{1mn} + \overline{v\Sigma}_a - \bar{v}\ v\Sigma_f\ \epsilon p_{th} L_f(1-\bar{\beta})) \ . \quad \text{(D-4)}$$

Thus,

$$\alpha_o(B^2) = \overline{v\Sigma}_a + \overline{vD}\ B^2 - \bar{v}\ v\Sigma_f\ \epsilon p_{th} L_f(1-\bar{\beta}) \quad \text{(D-5)}$$

or

$$\alpha_o(B^2) = \overline{v\Sigma}^F_a + \overline{v\Sigma}^M_a + \overline{vD}\ B^2 - \overline{v\Sigma}^F_a \eta\ \epsilon p_{th} L_f(1-\bar{\beta}) \quad \text{(D-6)}$$

or

$$\alpha_o(B^2) = \overline{v\Sigma}^M_a + \overline{vD}\ B^2 + \overline{v\Sigma}^F_a\ (1-\eta\epsilon p_{th} L_f(1-\bar{\beta})) \quad \text{(D-7)}$$

which is equation (17) in the main paper.

APPENDIX E

DERIVATION OF THE DECAY CONSTANT EQUATION WITH ANISOTROPIC COEFFICIENTS

The diffusion equation for a heterogeneous non-multiplying medium can be written for cylindrical geometry as

$$\overline{vD}_{\perp} \nabla_r^2 \phi(\vec{r},\vec{z},t) + \overline{vD}_{\parallel} \nabla_z^2 \phi(\vec{r},\vec{z},t) - \overline{v\Sigma}_a \phi(\vec{r},\vec{z},t) \qquad \text{(E-1)}$$

$$= \frac{\partial \phi}{\partial t} (\vec{r},\vec{z},t)$$

where

∇_r^2 = the radial components of the Laplacian operator

∇_z^2 = the axial components of the Laplacian operator

$\overline{D}_{\perp}$ = average radial diffusion coefficient

$\overline{D}_{\parallel}$ = average axial diffusion coefficient.

Assuming space and time independence

$$\phi(\vec{r},\vec{z},t) = R(\vec{r})\ Z(\vec{z})\ T(t) \qquad \text{(E-2)}$$

where $R(\vec{r})$ and $Z(\vec{z})$ are the eigenfunctions satisfying

$$\nabla^2 R + B_r^2 R = 0 \qquad \text{(E-3)}$$

and

$$\nabla^2 Z + B_z^2 Z = 0 \qquad \text{(E-4)}$$

respectively, where

B_r^2 = radial buckling

B_z^2 = axial buckling.

The substitution of equations (E-2), (E-3), and (E-4) into equation (E-1) yields

$$\frac{1}{T}\frac{dT}{dt} = -\left[\overline{vD}_{\perp} B_r^2 + \overline{vD}_{\parallel} B_z^2 + \overline{v\Sigma}_a\right] . \qquad \text{(E-5)}$$

The fundamental decay constant resulting from the integration of equation (E-5) is

$$\alpha_o(B_r^2, B_z^2) = \overline{vD}_{\perp} B_r^2 + \overline{vD}_{\parallel} B_z^2 + \overline{v\Sigma}_a . \qquad \text{(E-6)}$$

In a similar manner, the fundamental decay constant for a multiplying medium may be developed. The neutron age is divided into an axial component, $\tau_{\parallel}$, and a radial component, $\tau_{\perp}$. The resulting equation is

$$\alpha_o(B_r^2, B_z^2) = \overline{v\Sigma}_a + \overline{vD}_{\perp} B_r^2 + \overline{vD}_{\parallel} B^2 - \overline{v\Sigma}_a (1-\beta) . \qquad \text{(E-7)}$$

$$\exp[-B_r^2 \tau_{\perp}] \cdot \exp[-B_z^2 \tau_{\parallel}] .$$

The relationships between the average parameters and the directional parameters are

$$\overline{D} = (1/3)(2\overline{D}_{\perp} + \overline{D}_{\parallel}) \qquad \text{(E-8)}$$

and

$$\tau = (1/3)(2\tau_{\perp} + \tau_{\parallel}) . \qquad \text{(E-9)}$$

APPENDIX F

SCHEMATIC DIAGRAMS OF ELECTRONIC UNITS

The circuits depicted in this appendix were the result of the ingenuity of Mr. Billy D. Statham of the Georgia Tech School of Nuclear Engineering Electronic Shop.

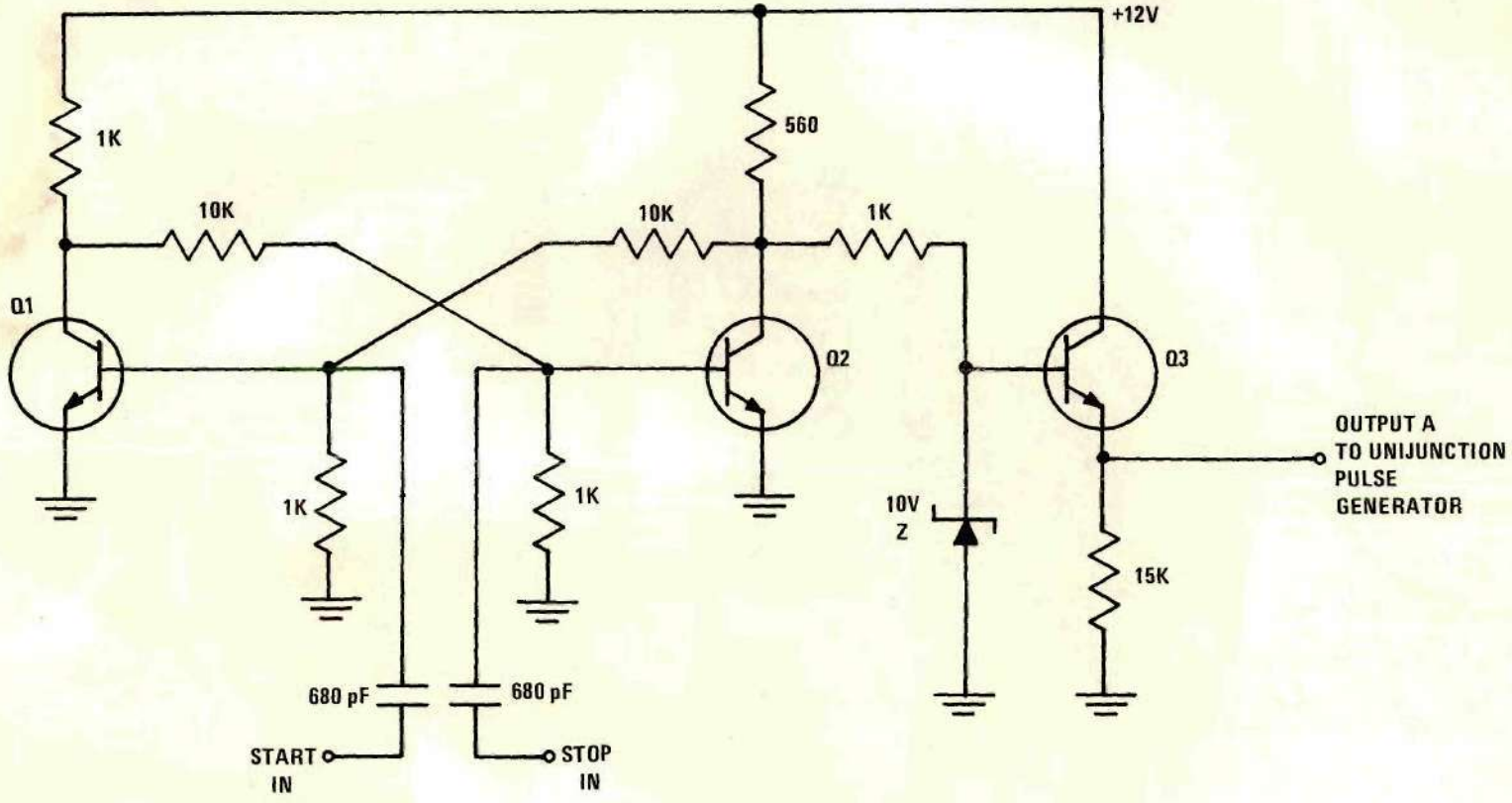

NOTES:

1. PIN A OUTPUT IS +9.35V TO OPERATE UNIJUNCTION PULSE GENERATOR WHEN Q1 IS ON.
2. PIN A OUTPUT IS 0 WHEN Q2 IS ON.
3. ALL TRANSISTORS 2N1613

Figure 37. Schematic Diagram of the Remote-Control Power Supply.

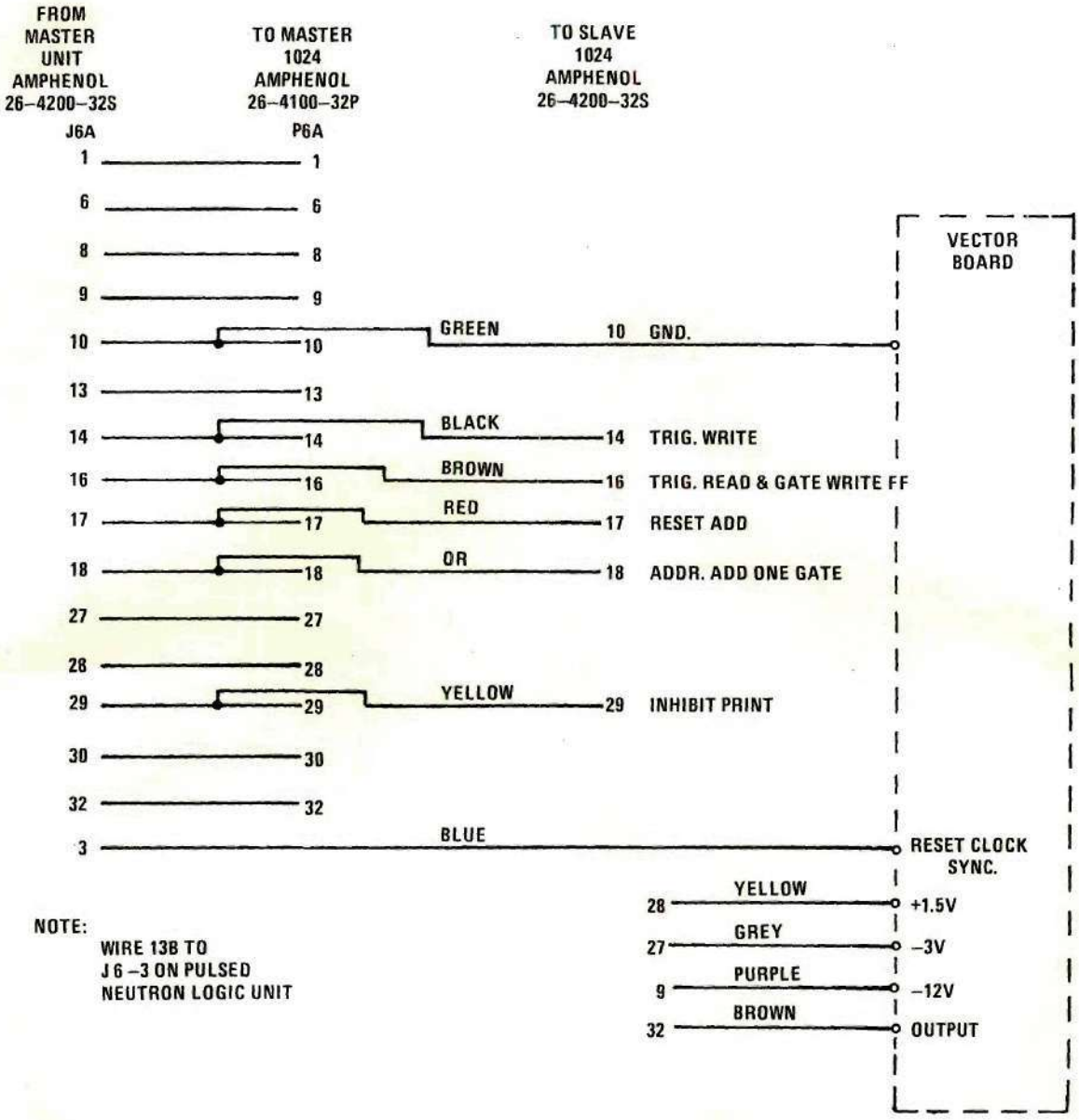

Figure 38. Wiring Interface Between "Master" and "Slave" Analyzers.

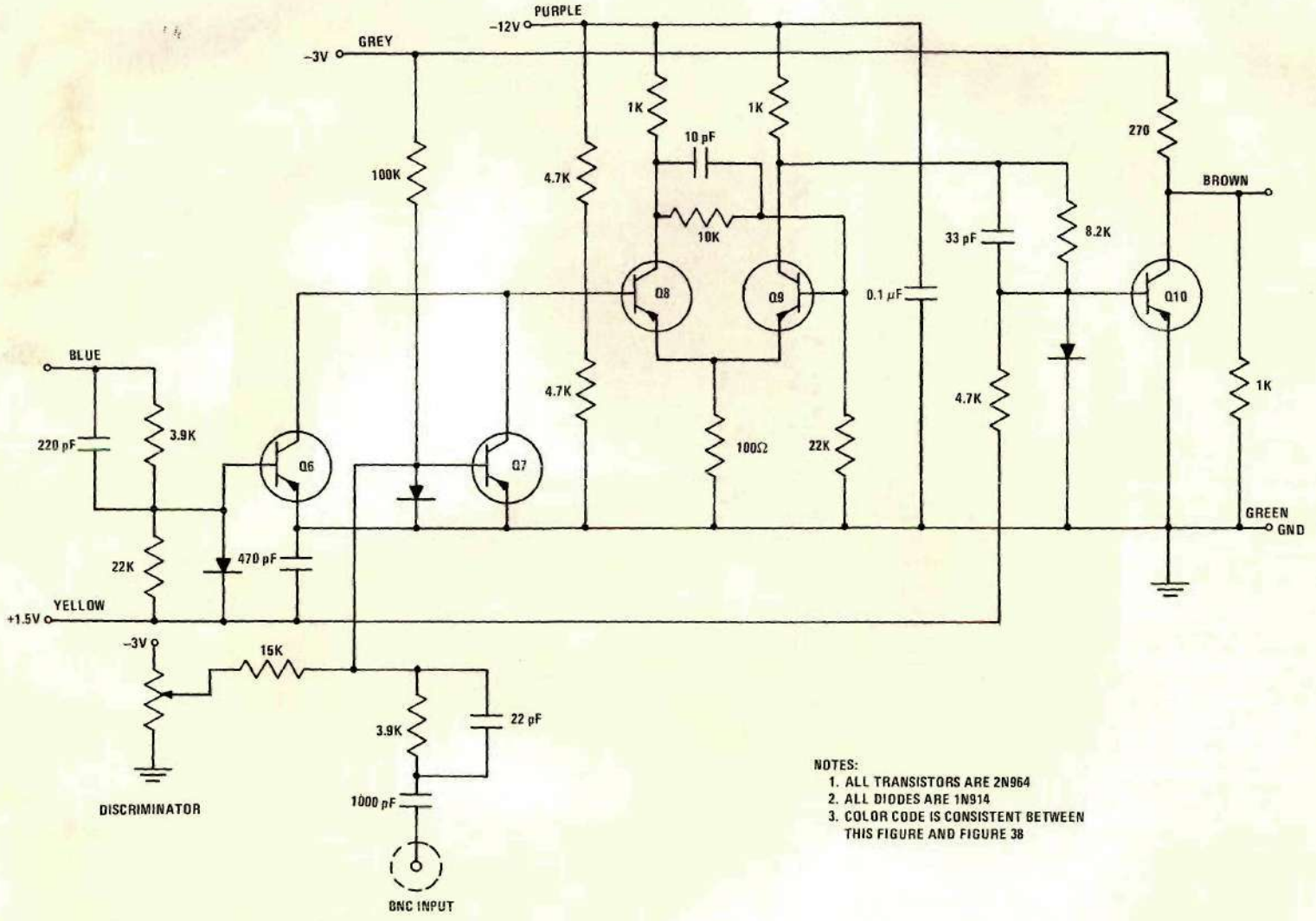

Figure 39. Schematic Diagram of the "Slave" Unit Signal Processing Network.

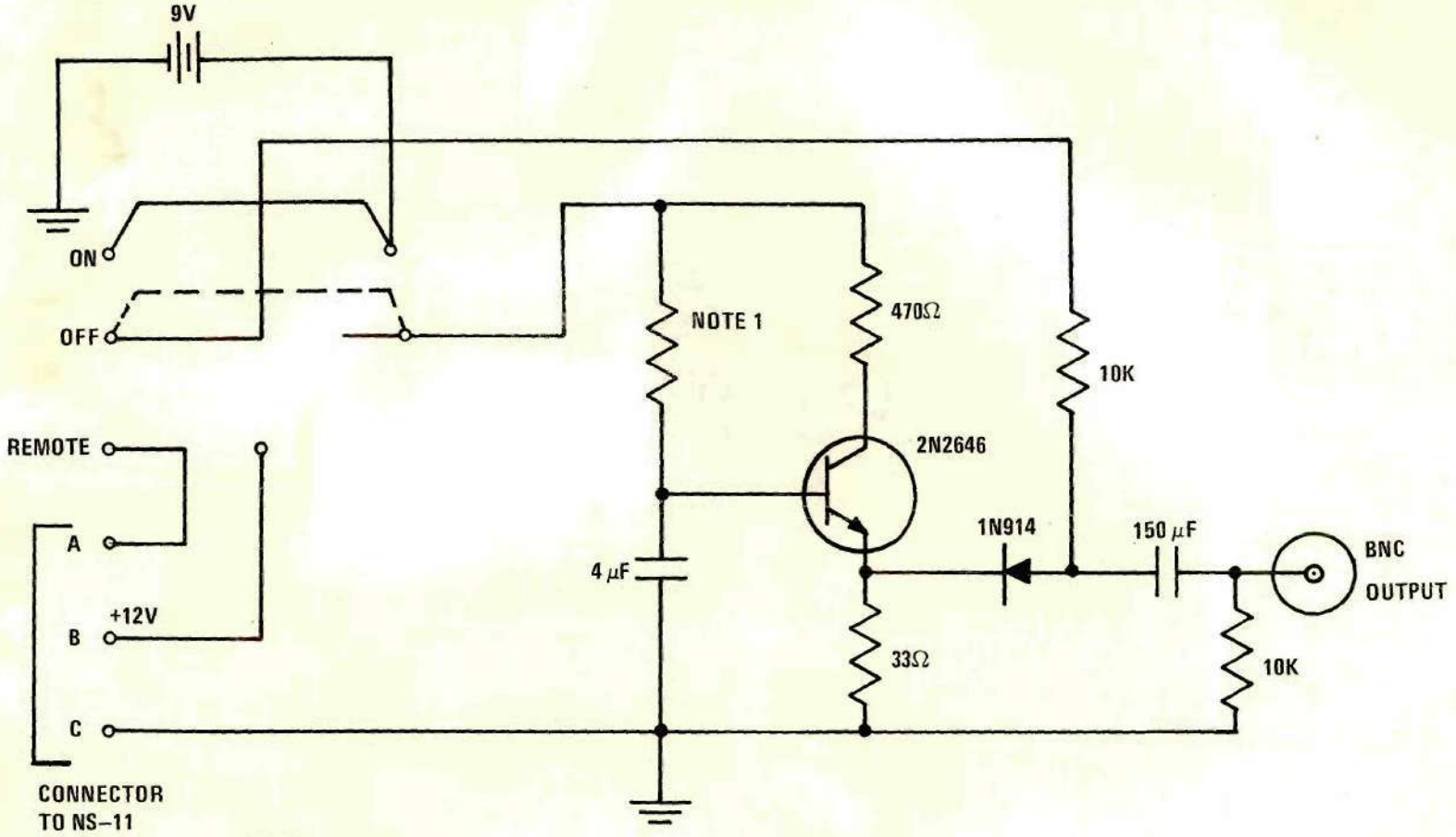

NOTES:

1. RESISTOR VALUES ARE SELECTED BY RANGE SWITCH
2. PIN A HAS +9.35V WHILE NS-11 IS COUNTING

Figure 40. Schematic Diagram of the Unijunction Oscillator.

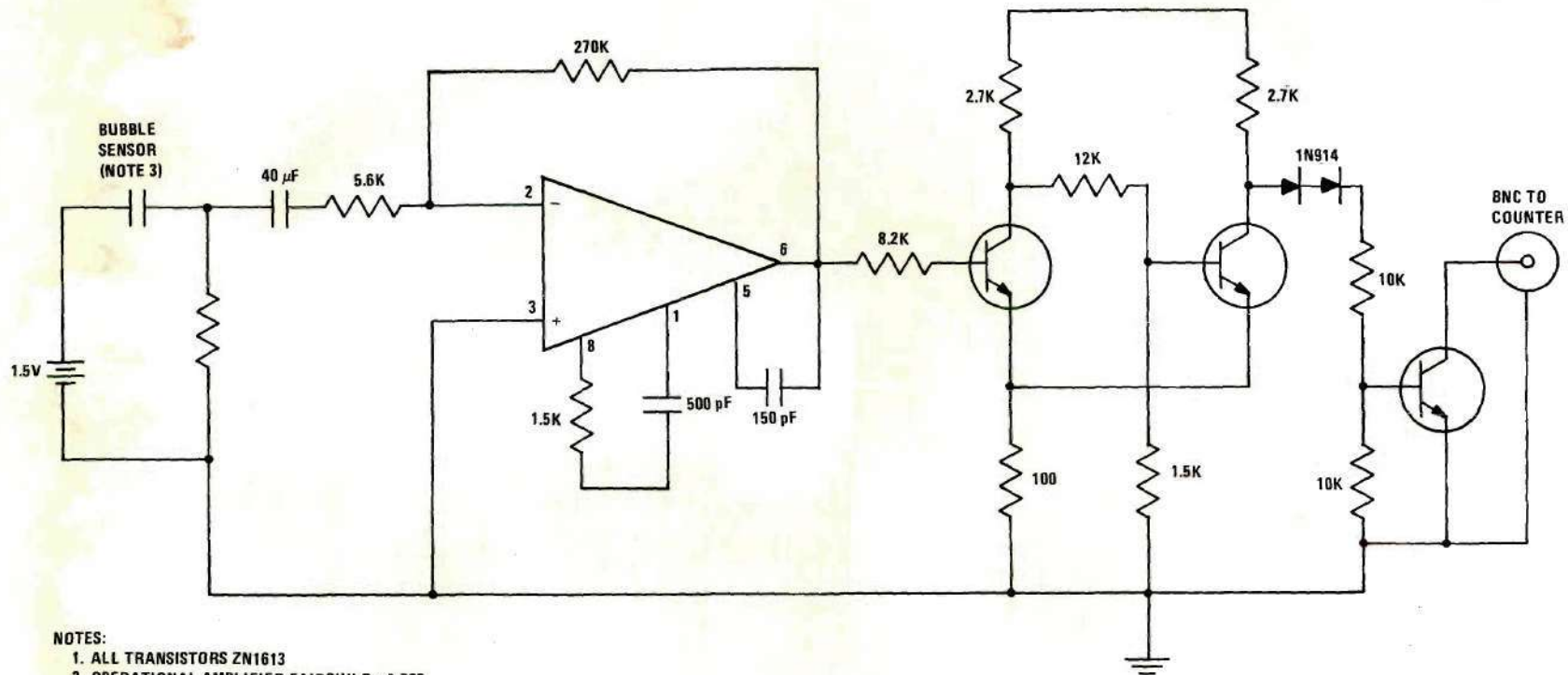

NOTES:

1. ALL TRANSISTORS ZN1613
2. OPERATIONAL AMPLIFIER FAIRCHILD μA 709
3. BUBLE SENSOR IS 2 PARALLEL METAL PLATES 3/8" X 1/2" SPACED 1/8 TO 3/16" APART
4. WHEN BUBBLE IS BETWEEN PLATES RESISTANCE INCREASES AND INPUT GOES NEGATIVE WHILE OUTPUT GOES POSITIVE, FIRING SCHMITT TRIGGER.
5. FOR STOP PULSE CIRCUIT REVERSE POLARITY OF BATTERY.

Figure 41. Schematic Diagram of the Bubble Detector Start Circuit.

BIBLIOGRAPHY

1. L. W. Alvarez, "The Production of Collimated Beams of Monochromatic Neutrons in the Temperature Range 300 -10 K," Physical Review, 54, 609-617 (1938).

2. K. H. Beckurts, "Reactor Physics Research with Pulsed Neutron Sources," Nuclear Instruments and Methods, 11, 144-168 (1961).

3. K. H. Beckurts, "Transient Effects in Space, Time, and Energy," Proceedings of the Brookhaven Conference on Neutron Thermalization Vol. 3, USAEC Report Number BNL-719, RE-1 - RE-62 (1962).

4. F. A. Valente, A Manual of Reactor Physics Experiments, (The Macmillan Company, New York, 1963), Chap. 4.

5. K. H. Beckurts, "A Review of Pulsed Neutron Experiments on Non-Multiplying Media," Pulsed Neutron Research Vol. 1, Proceedings of the Symposium on Pulsed Neutron Research, International Atomic Energy Agency, 3-34 (1965).

6. N. Corngold, "Theoretical Interpretation of Pulsed Neutron Phenomena," Pulsed Neutron Research Vol. 1, IAEA, 199-217 (1965).

7. E. Garelis, "Survey of Pulsed Neutron Source Methods for Multiplying Media," Pulsed Neutron Research Vol. 2, IAEA, 3-23 (1965).

8. G. R. Keepin, "The Pulsed Source Method," Physics of Nuclear Kinetics, (Addison-Wesley Publishing Company, Reading, 1965), 259-281.

9. D. R. Bach, S. I. Bunch, R. J. Cerbone, and R. E. Slovacek, "Prompt Neutron Decay Constants in Multiplying Hydrogenous Media," Nuclear Science and Engineering, 11, 199-210 (1961).

10. A. K. Ghatak and S. Pearlstein, "Approach to Equilibrium of a Neutron Pulse in a Multiplying System," Nuclear Science and Engineering, 22, 182-190 (1965).

11. G. M. Wells, "Pulsed-Neutron Measurements in Far-Subcritical Multiplying Media With and Without Large Reflectors," Transactions of the American Nuclear Society, 9 (1), 170 (1966).

12. B. K. Malaviya, I. Kaplan, T. J. Thompson, and D. D. Lanning, "Studies of Lattice Parameters in Pulsed and Steady-State Experiments on Subcritical Systems," Transactions of the American Nuclear Society, 9 (1), 175 (1966).

13. F. D. Judge and P. B. Daitch, "Time-Dependent Neutron Flux in Pulsed Multiplying Assemblies," Nuclear Science and Engineering, 26, 472-486 (1966).

14. H. E. Bliss, M. J. Driscoll, I. Kaplan, and T. J. Thompson, "Use of the Pulsed-Neutron Source Technique to Determine Values of k_∞ in Subcritical Lattices," Transactions of the American Nuclear Society, 10 (1), 196 (1967).

15. W. G. Flournoy, "Limitations on the Pulsed-Neutron Technique of Measuring Subcritical Parameters," Transactions of the American Nuclear Society, 11 (1), 294 (1968).

16. R. H. Chow and S. R. Bierman, "Pulsed-Neutron Determination of the Effective Multiplying Constant and Neutron Age to Thermal Energy For a Bare Homogeneous Subcritical Assembly of Enriched-Uranyl-Nitrate Salt," Nuclear Science and Engineering, 41, 132-138 (1970).

17. W. E. Graves, H. R. Fike, and G. F. O'Neill, "Experimental Bucklings and Void Effects in Heavy Water Lattices of Natural Uranium Oxide Rod Clusters," Nuclear Science and Engineering, 16, 186-195 (1963).

18. M. Copic, T. Kalin, G. Pregl, and F. Zerdin, "Anisotropy of Diffusion Constant in Media with Empty Channels," Nuclear Science and Engineering, 19, 74-79 (1964).

19. E. Utzinger, W. Heer, and H. R. Lutz, "Pulsed-Source Experiments with Multiplying and Non-Multiplying Heavy Water Systems," Proceedings of the Symposium on Pulsed Neutron Research, loc. cit., 119-136 (1965).

20. L. L. Bennett, "An Experimental Study of the Effect of Empty Channels on the Neutron Diffusion Coefficient in Graphite," Transactions of the American Nuclear Society, 10 (1), 281-282 (1967).

21. R. W. Page, "An Investigation of Neutron Streaming Using the Pulsed Neutron Source Technique," Journal of Nuclear Energy, 21, 403-415 (1967).

22. N. A. Khan and S. M. Kabir, "Effects of Voids on the Diffusion Length and Streaming of Neutrons in Water," Nuclear Science and Engineering, 31, 148-149 (1968).

23. S. R. Bull and T. J. Connolly, "A Pulsed-Source Investigation of the Effect of Cylindrical Void Channels in a Neutron Diffusing Medium," Transactions of the American Nuclear Society, 11 (1), 296-297 (1968).

24. V. Deniz, J. G. Le Ho, and M. Sagot, "Study of Lattices of Graphite with Empty Channels by Means of the Pulsed-Source Technique," Nuclear Science and Engineering, 32, 201-224 (1968).

25. H. Kikuchi, M. Fujii, K. Kiyokawa, T. Ohnishi, and S. Kobayashi, "Physics Studies on BWR Void Simulated Cores, (I)," Journal of Nuclear Science and Technology, 6 (8), 458-465 (1969).

26. D. J. Behrens, "The Effect of Holes in a Reacting Material on the Passage of Neutrons," Proceedings of the Physical Society of London, 62A, 607-616 (1949).

27. P. Benoist, "A General Formulation of the Diffusion Coefficient in a Heterogeneous Medium which May Contain Cavities," UKAEC Report Number AERE-Trans 842, Atomic Energy Research Establishment, Harwell, (1959).

28. N. I. Laletin, "The Effect of a Cylindrical Channel on Neutron Diffusion," Journal of Nuclear Energy, Part A: Reactor Science, 13, 57-64 (1960).

29. C. Carter, "Streaming Due to Holes in a Reactor," Reactor Science and Technology (Journal of Nuclear Energy, Parts A/B), 15, 76-80 (1961).

30. D. C. Leslie, "The Weighting of Diffusion Coefficients in Cell Calculations," Reactor Science and Technology (Journal of Nuclear Energy, Parts A/B), 16, 1-11 (1962).

31. P. Benoist, "Streaming Effects and Collision Probabilities in Lattices," Nuclear Science and Technology, 34, 285-307 (1968).

32. Valente, op. cit., 107.

33. Ibid., 102.

34. Beckurts and Wirtz, op. cit., 224.

35. Keepin, op. cit., 271.

36. Beckurts and Wirtz, op. cit., 221.

37. Ibid., 222.

38. R. V. Meghreblian and D. K. Holmes, Reactor Analysis, (McGraw-Hill Book Company, Inc., New York, 1960), 564.

39. G. R. Keepin, "Pulsed Neutron Techniques," Los Alamos Scientific Laboratory Report LAMS 2215, (1958).

40 W. F. Gilbert and M. Petrovic, "Time and Space Dependence of Neutron Flux Using Pulsed Neutron Techniques," A Manuel of Reactor Laboratory Experiments, Argonne National Laboratories Report ANL 6990, 17.1-17.32 (1965).

41. W. M. Lopez and J. R. Beyster, "Measurement of Neutron Diffusion Parameters in Water by the Pulsed Neutron Method," Nuclear Science and Engineering, 12, 190-202 (1962).

42. E. W. McDaniel and T. A. Elliott, "Design and Uses of a Light-Water-Moderated Subcritical Assembly," American Journal of Physics, 26 (3), 168-174 (1958).

43. S. R. Bierman, K. L. Garlid, and J. D. Clark, "Resolving Time of a Pulsed-Neutron Source Data-Acquisition System," Nuclear Applications, 2, 515-518 (1966).

44. Lopez and Beyster, op. cit., 190.

45. P. R. Bevington, Data Reduction and Error Analysis For the Physical Sciences, (McCraw-Hill Book Company, Inc., New York, 1969), 184.

46. Lopez and Beyster, op. cit., 200.

47. W. W. Clendenin, "Temperature Dependence of Neutron-Pulse Parameters in H_2O," Nuclear Science and Engineering, 18, 355 (1964).

48. "Rotameter Calculations," Variable Area Flowmeter Handbook, Vol. 2, Fischer and Porter Catalog 10A1022, (1969).

49. Judge and Daitch, op. cit., 382-383.

50. R. H. Shudde and J. Dyer, "TEMPEST II - A Neutron Thermalization Code," Atomic International Report AMTD-111 (1962).

51. T. B. Fowler, M. L. Tobias, and D. R. Vondy, "EXTERMINATOR-2: A Fortran IV Code For Solving Multigroup Neutron Diffusion Equations in Two Dimensions," Oak Ridge National Laboratory Report ORNL 4078 (1967).

52. H. C. Honeck, "THERMOS, A Thermalization Transport Theory Code For Reactor Lattices," Brookhaven National Laboratory Report BNL 5826 (1962).

53. D. J. McGoff, "FORM - A Fourier Transform Fast Spectrum Code," Atomics International Report NAA-SR-MEMO 5766 (1960).

54. H. S. Isbin, Introductory Nuclear Reactor Theory, (Reinhold Publishing Corporation, New York, 1963), 459.

55. "Resonance Escape Probability," Nuclear Design Procedure Manual, Westinghouse Report WCAP-1200, section 7 (1960).

56. W. Zernik, "A Simple Theoretical Method For the Calculation of L-Factors," Westinghouse Report RD-RPM-M-8, 18 (1961).

57. Isbin, op. cit., 136.

58. A. Radkowsky (Ed.), Selected Basic Techniques, Naval Reactors Physics Handbook, Vol. 1, U. S. Atomic Energy Commission, 321, (1964).

59. Ibid., 231.

60. Beckurts and Wirtz, op. cit., 102.

61. Ibid., 98.

62. Ibid., 221.

63. Ibid., 102.

VITA

Robert John Lord, Jr. was born on May 22, 1943 in Jackson Heights, New York. Upon graduation from Massapequa High School, Massapequa, New York in 1961, he attended the Georgia Institute of Technology where he completed the requirements for the degree of Bachelor of Science in Physics in 1965.

Mr. Lord continued his education in graduate school at Georgia Tech and received a Master of Science in Nuclear Engineering degree in 1967. He was supported during his doctoral studies by the National Science Foundation, the National Defense Education Act, and by the School of Nuclear Engineering.

Mr. Lord is a member of the American Nuclear Society and Sigma Xi.